Design and Implementation of a Regenerative Shock Absorber

by

Amir Maravandi

M.Sc., University of Guilan, 2005

B.Sc., University of Yazd, 2002

Thesis Submitted in Partial Fulfillment
of the Requirements for the Degree of

Doctor of Philosophy

in the
School of Mechatronic Systems Engineering
Faculty of Applied Sciences

SIMON FRASER UNIVERSITY
Spring 2015

APPROVAL

Name: Amir Maravandi

Degree: Doctor of Philosophy

Title of Thesis: Design and Implementation of a Regenerative Shock Absorber

Examining Committee: Dr. Woo Soo Kim, P.Eng.
Chair
Assistant Professor, School of Mechatronic Systems Engineering

---

Dr. Mehrdad Moallem, P.Eng.
Senior Supervisor
Professor, School of Mechatronic Systems Engineering

Dr. Farid Golnaraghi, P.Eng.
Supervisor
Professor, School of Mechatronic Systems Engineering

Dr. Siamak Arzanpour, P.Eng.
Supervisor
Associate Professor, School of Mechatronic Systems Engineering

---

Dr. Flavio Firmani, P.Eng.
Internal Examiner
Lecturer, School of Mechatronic Systems Engineering

Dr. Reza Fotouhi, P.Eng.
External Examiner
Professor, Department of Mechanical Engineering

Date Approved: April 14, 2015

Partial Copyright Licence

Abstract

In this thesis, the development of a novel regenerative shock absorber sized for a passenger car suspension system is studied. In the first phase, DC and AC rotary machines along with charging circuits, to be used in the energy conversion stage of the proposed shock absorber are analyzed. In this analysis, the rotary damping coefficients provided by these systems are obtained following by experimental results.

In the second phase, the development of a novel regenerative shock absorber in a proof of concept setting is presented. This system consists of a new linear-to-rotary conversion mechanism called algebraic screw, a gearhead, and a rotary machine. The design and analysis of this system is presented. The linear damping coefficient provided by this shock absorber is obtained. Experimental results are presented that evaluate performance of the proposed system on a small-scale suspension system.

In the third phase, the development of a novel regenerative shock absorber sized for a passenger car is presented. The shock absorber includes a simple and highly efficient motion converter stage called "two-leg mechanism", a planetary gearhead, and a brushless three-phase rotary machine. The design and analysis of the regenerative shock absorber is presented by considering the linear damping coefficient and efficiency of the electromechanical device. The performance of the regenerative shock absorber is evaluated under sinusoidal excitation inputs for typical amplitudes and frequencies in a vehicular suspension system.

In the fourth phase, the effect of nonlinear terms of the shock absorber on linear damping coefficient provided by this system is studied. Next, the idea of using a variable external resistance, provided by the charging circuit, to compensate the nonlinear terms is presented.

Keywords : Regenerative shock absorber; motion converter; linear damping; efficiency

Acknowledgments

I would like to thank my senior supervisor, Dr. Mehrdad Moallem, for his support, guidance, and insightful discussions throughout this research. It was a privilege for me to work with him and learn from his experience.

I would also like to thank Dr. Farid Golnaraghi and Dr. Siamak Arzanpour, members of my Ph.D. supervisory committee, for providing valuable comments that helped me to improve this work; specially, Dr. Golnaraghi for providing me with the experimental setup for a part of this project.

Many thanks go to my colleges and lab mates at the Motion and Power Electronic Control Lab. Their helps, comments, and assistance played an important role in the development of this dissertation. In particular, I want to thank Ali Mootab for his help on the electrical engineering issues of my project.

I would also like to acknowledge funding by the Natural Sciences and Engineering Research Council of Canada (NSERC), and the Canadian Networks of Centres of Excellence under the Auto 21 program.

My special thanks go to my family in Iran for their love, patience, support, and encouragement.

Contents

List of Tables

List of Figures

Chapter 1

Introduction

1.1 Motivation for the Research

Transportation accounts for 25% and 28% of the total energy consumption in Canada and the United States, respectively [1]-[3]. Considering that passenger travel accounts for 54% and freight for 42% of transportation demand [2], it can be concluded that any improvement in fuel efficiency of the vehicles, has a significant effect on decreasing the energy consumption and emission.

In a combined city/highway driving, only about 14%-30% of the energy from the fuel is used to overcome resistance from road friction and air drag, depending on the drive cycle. The rest of the energy is lost to engine and inefficiencies, or used to power accessories, as depicted in Figure 1.1. Therefore, the potential to improve fuel efficiency with advanced technologies is enormous [4].

One of the advanced technologies to improve vehicle fuel efficiency is regenerative systems. Among the two popular regenerative systems, i.e., regenerative braking and regenerative suspension, regenerative braking has been studied in the literature [5]-[15], and has achieved great commercialization success. Regenerative braking is currently utilized in different brands of cars [16]-[18]. However, regenerative suspension, which is the subject of this thesis, has not put into practice.

The main functionality of a vehicle suspension is to reduce the vibration disturbance from road roughness, acceleration, deceleration, and cornering to the chassis for better ride comfort and to maintain good tireground contact force for better vehicle handling and mobility. To this end, traditional suspension systems consist of springs and viscous shock absorbers. Viscous

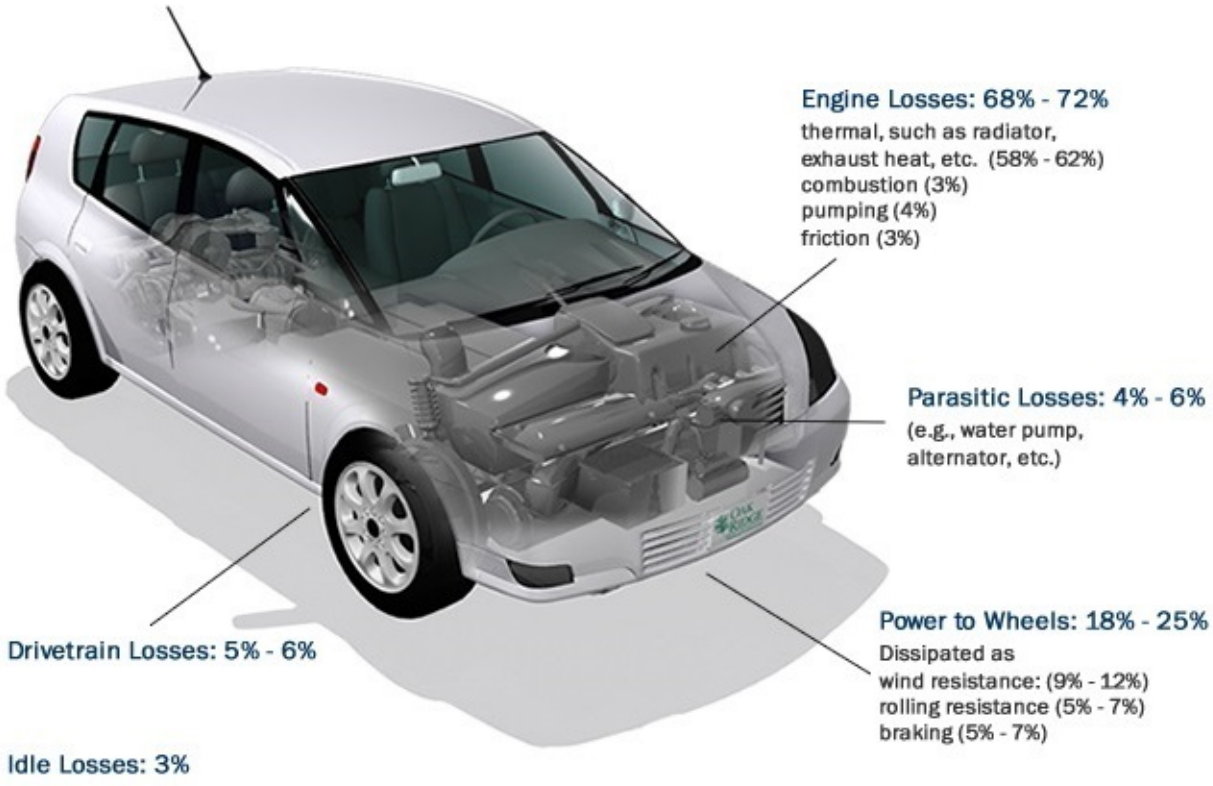

Figure 1.1: Energy requirements for combined city/highway driving [4].

shock absorbers dissipate the vibration energy into waste heat to achieve ride comfort and road handling.

While a conventional shock absorber dissipates mechanical energy into heat with a fixed damping coefficient, a regenerative shock absorber converts the mechanical vibration energy into battery charge via an appropriate charging circuit. In addition, this type of shock absorber can provide a variable damping coefficient through proper control.

In the process of studying regenerative shock absorbers, a fundamental question must be answered: How much is the fuel efficiency improved by utilizing a regenerative shock absorber? To answer this question, first we should study the potential for harvesting power from a shock absorber of a typical vehicle.

Energy dissipated by conventional shock absorbers has been presented in different works [19]-[27]. Segel and Pei analyzed the influence of highway pavement roughness on the vehicular

resistance to motion due to tire and suspension damping. They indicated that approximately 200W of power is dissipated by dampers of a passenger car at 30 mph [19]. Hsu looked into the electrical active suspension and estimated that up to 400W of energy is recoverable at a highway driving speed of 100km/hr [21]. Abouelnour and Hammad looked into the concept of energy and electro-mechanic suspension. Their simulation studies based on a quarter car model predicts that 150W of energy dissipated by shock absorbers can be converted into electrical power at 100km/hr [22]. Kawamoto et al. modeled a ball-screw type electromagnetic damper. Their experiments show that a 15.3W energy recovery from one shock absorber of a vehicle on Class C road traveling at 80km/hr can be achieved, mainly from vibration above 2 Hz [24]. Zhang et al. tested a regenerative suspension with a ball screw and a three-phase motor on a vibration test rig and obtained 11.7W for each shock absorber [25]. A main work in this area was presented by Zuo and Zhang [27]. They performed a comprehensive assessment about the available power in a vehicle suspension system, including analysis, simulation, and experiment. They concluded that 100 – 400W of power is available from the shock absorbers of a typical middle-sized passenger car traveling at 100km/hr on the good and average roads.

By considering the car engine efficiency of about 30% [28], [29], an alternator efficiency of about 50% [28], and fuel energy density about 30 Mj/L [30], the fuel consumption saving due to regenerative shock absorbers is obtained about 2%-6% [31]. Comparing the amount of fuel saved by regenerative shock absorbers, with the amount of fuel saving due to regenerative braking (4%-8%), we can conclude that, there is a potential for regenerative shock absorbers commercialization [4], [12].

1.2 Background and Overview of the Present State of Technology

Regenerative shock absorbers have been studied for about two decades to recover the vibration energy dissipated by traditional shock absorbers in suspension systems. Many researchers explored different principles and designs of regenerative shock absorbers. Based on the energy conversion stage mechanism, above systems can be classified into two main categories as follows.

1.2.1 Regenerative shock absorber using a linear generator

The simplest design presented in the literature for regenerative shock absorbers is the linear one. This type of regenerative shock absorber consists of a magnet assembly and a coil assembly, mounted to two sides of the shock absorber. Any shock applied to the vehicle is directly transmitted to the regenerative shock absorber; and causes a relative displacement between the magnets and the coils. This relative displacement cuts the magnetic lines and generates electric energy. The resulting counter electromotive force generated by the linear generator provides the damping force [32]-[43].

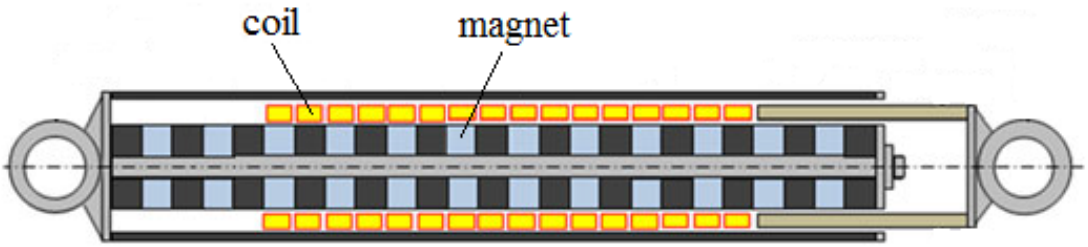

Figure 1.2: Linear regenerative shock absorber.

Linear regenerative shock absorbers can be easily and reliably integrated into car suspension systems. However, all of them presented in the literature are either too large for retrofit or unable to provide enough damping force. For instance, the shock absorber presented in [32] has reasonable dimensions to be retrofit in the suspension system of a passenger car but it can only provide a damping coefficient of 940 $N.s/m$ in short circuit condition. Another example is the shock absorber presented in [33]. This system provides a damping coefficient of 1350 $N.s/m$, but its dimensions are almost twice as big as a conventional shock absorber.

Use of magnet arrays were studied for the applications involving eddy current shock absorbers. Although this type of shock absorber can provide passive damping, the energy harvesting capability is not possible using such approach [44]-[47].

Application of linear machines in active and semi–active shock absorbers has been presented in the literature [48]-[54]. However the objective of these systems is improving the ride comfort. Furthermore, they not only cannot regenerate energy but also consume more energy to provide better ride comfort.

1.2.2 Regenerative shock absorber using a rotary generator

Compared to a linear machine, a brushless rotary machine is more cost-effective and is smaller in size. For instance, the 1 kW cylindrical linear machine for a marine wave energy converter presented in [55] has a mass of about 1800 kg with dimensions $3.3m \times 1.3m$, whereas a 1 kW rotary machine equipped with a high-ratio gearing (see e.g., [56]) is in the order of 1%, in volume and mass, when compared to the linear machine reported in [55]. Therefore utilizing a rotary machine as the energy conversion device in regenerative shock absorbers could help us to design a regenerative shock absorber that can meet the damping force and size criteria, simultaneously. As the motion profile due to road roughness is a linear reciprocating signal, any rotary regenerative shock absorber would need a mechanism to convert the linear motion into a rotary one. Based on the utilized linear-to-rotary converter, the rotary regenerative shock absorbers presented in the literature are categorized into three groups as follows:

1- Rotary regenerative shock absorber using hydraulic system

In this type of regenerative shock absorber, the vehicle shock causes the hydraulic piston of the shock absorber to move up and down, making a hydraulic flux. After passing through some hydraulic equipment, the hydraulic flux rotates hydraulic motor, which drives the rotary generator. The counter electromotive force produced by the generator provides the system with the required damping force. This type of regenerative shock absorber has drawbacks such as low efficiency, large response time, and high cost due to the need for precision sealing, oil tank, and pipelines. [57]-[62].

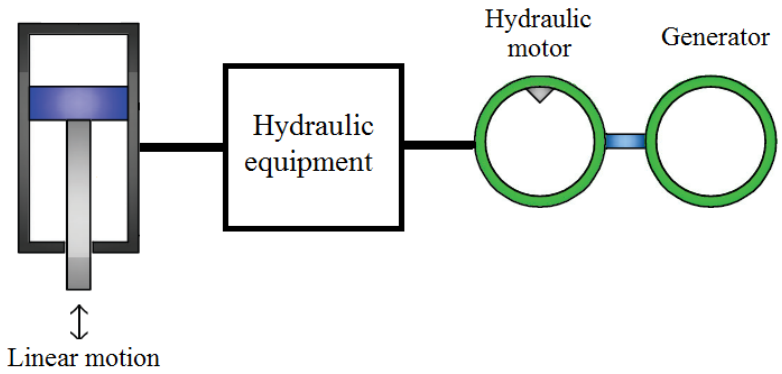

Figure 1.3: Regenerative shock absorber using hydraulic system.

2- Rotary regenerative shock absorber using a ball screw-nut

In this type of regenerative shock absorber, a nut is connected to the casting of the shock absorber and has translational motion due to the shocks applied to the vehicle. This translational motion is converted into a rotary motion via a ball screw system which rotates the screw. Since the screw is connected to the shaft of a rotary generator, the generator rotates simultaneously. In this system, the damping force is produced by the generator connected to an external load. This type of shock absorber does not perform well at high frequencies and has considerable friction in low frequencies [63]-[70].

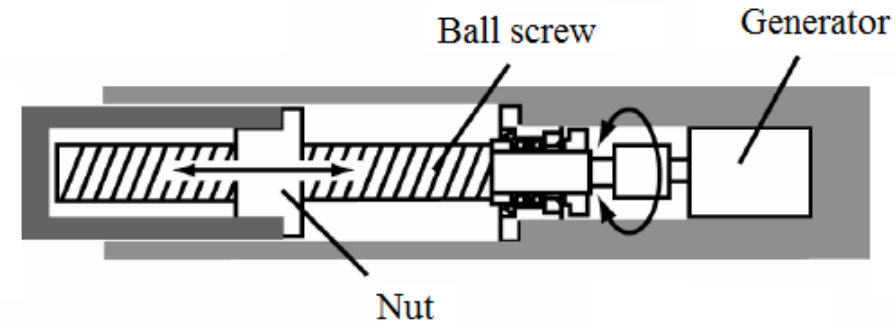

Figure 1.4: Regenerative shock absorber using ball screw-nut.

Since a roller screw mechanism is similar but more precise compared to a ball screw mechanism, use of this system as a motion converter was studied. The problem with this mechanism is poor performance at high frequencies. In addition due to complexity, this system is not cost effective [71],[72].

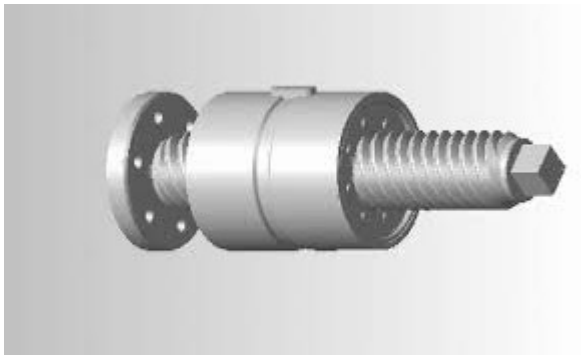

Figure 1.5: Roller screw.

3- Rotary regenerative shock absorber using a rack-pinion

The principle of this type of regenerative shock absorber is shown in Figure 1.6. This system is composed of a rackpinion, bevel gears, gearhead, and a generator. The generator is mounted on the inner casting, and the outer casting is used to enclose the system. The rack is connected to the end of the outer casting and drives the pinion when there is a relative motion between two ends of the shock absorbers. Through bevel gears, the rotational motion of the pinion is transferred by 90° to the rotational motion of the generator. The gearhead is used to magnify the motion, and the generator connected to an external load provides damping for the system.

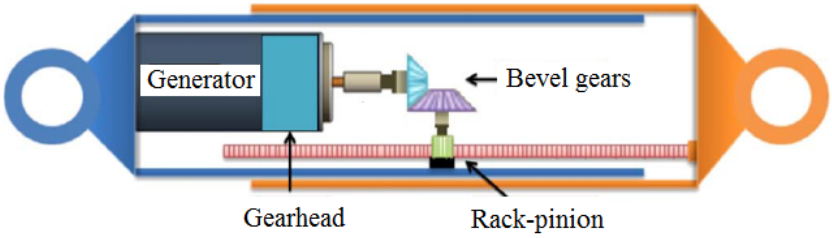

Figure 1.6: Regenerative shock absorber using rack-pinion.

Figure 1.7 shows a motion conversion mechanism of this type of shock absorber providing unidirectional rotary motion. The key components of this system are two roller clutches which transmit rotation only in one direction. As a result, the shaft of the rotary machine always rotates in one direction. Backlash between gears, high friction, and use of several parts for motion conversion are disadvantages of this type of regenerative shock absorber. [73]-[77].

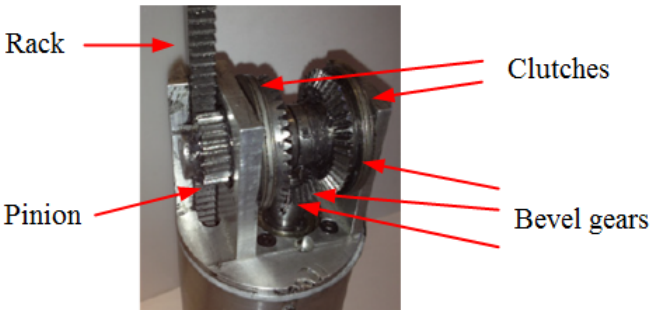

Figure 1.7: Unidirectional motion conversion mechanism.

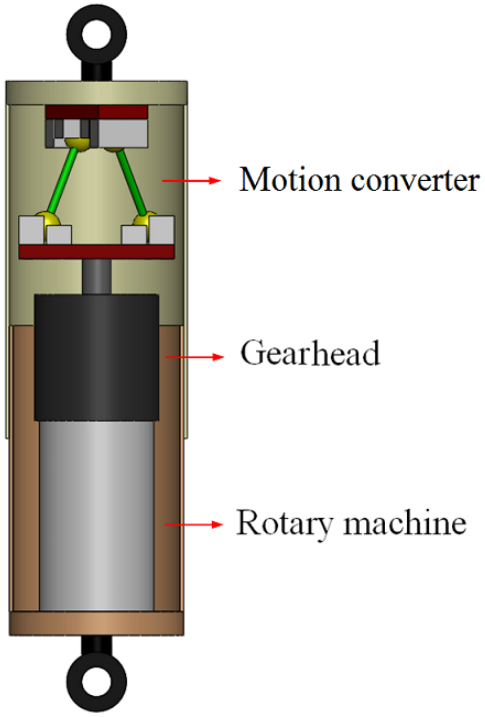

Figure 1.8: Presented regenerative shock absorber.

1.3 Summary of Contributions and Outline of Dissertation

To alleviate the aforementioned problems, this thesis presents a novel regenerative shock absorber which meets three main criteria needed for a practical regenerative shock absorber i.e., linear damping coefficient, appropriate size, and mechanical efficiency, simultaneously. As shown in Figure 1.8, this system consists of a simple and highly efficient motion converter called two-leg mechanism, a gearhead, and a brushless permanent magnet rotary machine. From the energy regeneration perspective, the motion converter converts translational motion due to road roughness into rotary motion. Then, the planetary gearhead increases the rotary motion amplitude, resulting in a higher voltage at the output of the generator. Finally, the generator and charging circuit perform energy conversion. From the damping perspective, the rotary machine connected to a charging circuit provides rotary damping which is amplified through the gearhead. The motion converter then converts the rotary damping into a linear one.

The contributions of this thesis are summarized as follows:

1.3.1 Chapter 2

This chapter presents an analysis about DC and AC rotary machines to be used as the energy conversion stage of the regenerative shock absorber. First, a DC rotary machine connected to an external resistor (to simulate a single phase charging circuit) is studied in electrical and mechanical domains and the rotary damping coefficient provided by the system is calculated. The above analysis is extended to an AC rotary machine and the rotary damping coefficient provided by this machine connected to three external resistors (to simulate a three phase charging circuit) is presented by an analytical expression. Considering that the system including the AC machine, provides a higher rotary damping coefficient, this system is chosen to be used in the presented regenerative shock absorber. Experiments are conducted to verify analytical results.

1.3.2 Chapter 3

In this chapter, the design of a novel regenerative shock absorber is studied. To this end, the first step is studying the motion converter, referred to as algebraic screw. An analytical expression describing the relationship between translational and rotational motions of the converter is derived and the collision angle between legs is obtained. Then a regenerative shock absorber using an algebraic screw mechanism, as a part of a car suspension system, is studied and an analytical expression describing the linear damping coefficient provided by this system is derived. Furthermore, the functionality of a quarter car using the presented shock absorber is studied through simulations. Experimental results are presented in which a prototype of the proposed shock absorber is used to verify the theoretical results.

1.3.3 Chapter 4

This chapter presents the design and implementation of a novel regenerative shock absorber for a passenger-sized car. In this procedure, the results obtained in Chapter 2 and Chapter 3 are used, modified, and extended as follows. First, a novel motion converter, referred to as a "two-leg mechanism", is introduced and analyzed. This mechanism is simpler and smaller than the algebraic screw mechanism presented in Chapter 2. Then a regenerative shock absorber using the two-leg mechanism is presented and studied in terms of linear damping coefficient and efficiency. Considering two main criteria, (i.e., linear damping coefficient and efficiency), a prototype shock absorber is designed and manufactured which satisfies the size limits. The performance of the prototype in terms of damping and efficiency is evaluated on a test-bench

under sinusoidal displacement.

1.3.4 Chapter 5

In this chapter, the effect of nonlinear terms of the two-leg mechanism, on the linear damping coefficient of the proposed regenerative shock absorber is studied. In this work we use variable external resistances, provided by the charging circuit, to compensate the two-leg mechanism nonlinear terms. Experimental results are presented to evaluate analytical studies.

1.3.5 Chapter 6

The research accomplished in this thesis is summarized in this chapter. Based on the theoretical, simulation, and experimental studies, general conclusions concerning the outcome of this thesis are provided along with suggestions for future work.

Chapter 2

Damping Analysis of Rotary Machines

2.1 Introduction

The source of linear damping provided by the proposed regenerative shock absorber is the damping provided by the rotary machine connected to the charging circuit. In other words, any change in rotary damping coefficient provided by the rotary machine connected to a charging circuit affects the functionality of the regenerative shock absorber in terms of damping coefficient and efficiency. This chapter analyzes rotary machines connected to charging circuits and the effect of parameters of these systems on the rotary damping coefficient. The organization of this chapter is as follows.

In Section 2.2, a DC permanent magnet rotary machine connected to a single phase charging circuit is studied. By comparing the results of electrical and mechanical domains, the rotary damping coefficient provided by this system is obtained. In Section 2.3, the above procedure is extended to an AC permanent magnet rotary machine connected to a three phase charging circuit. Experimental results to evaluate the accuracy of the derived formula are presented in this section.

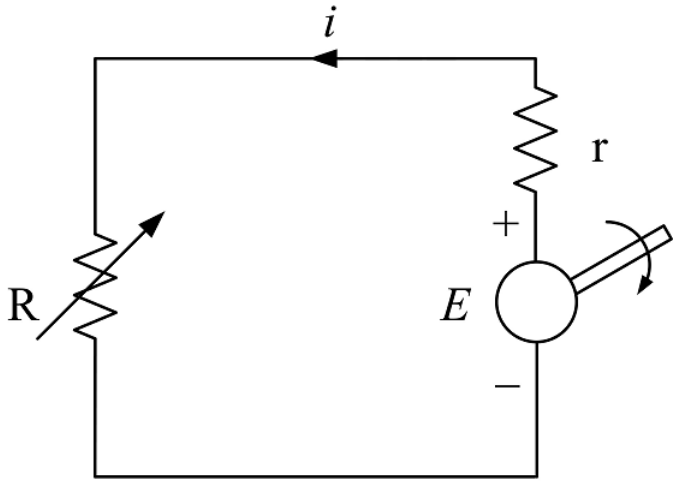

Figure 2.1: Single phase rotary generator connected to a simulated charging circuit (resistor R).

2.2 Analysis of a DC Permanent Magnet Rotary Machine Connected to a Charging Circuit

A permanent magnet DC motor is used as a generator in this study. This machine along with a single phase charging circuit provides rotary damping for the regenerative shock absorber. Meanwhile, this system captures energy originated from road vibrations and saves the energy into a battery. The single phase charging circuit is modeled as a pure controllable external resistor in this study [78]-[79]. To derive the formula describing the rotary damping coefficient provided by a DC generator along with a charging circuit, this system should be studied in both electrical and mechanical domains.

First let us study the system in the electrical domain. To this end, by considering that the charging circuit is modeled as a pure controllable external resistor, the electric circuit of the rotary generator connected to a charging circuit is modeled as shown in Figure 2.1. Referring to Figure 2.1, we have

$$E = i(R + r) \tag{2.1}$$

where E is the induced voltage of the generator, i is the current of the circuit, r is the internal resistance of the generator, and R is the controllable external resistor.

Rearranging (2.1) results in

$$i = \frac{E}{R+r}. \tag{2.2}$$

The total instantaneous electrical power, including the part captured in the charging circuit and the part lost in the internal resistance of the generator, can be expressed as follows

$$P_E = P_{captured(R)} + P_{lost(r)} = Ri^2 + ri^2. \tag{2.3}$$

Substituting (4.39) in (2.3) and performing some algebraic manipulations yield

$$P_E = P_{captured(R)} + P_{lost(r)} = \frac{E^2}{R+r}. \tag{2.4}$$

The relationship between the generator shaft rotary speed, $\dot{\gamma}$, and induced voltage is as follows

$$E = k_t\dot{\gamma} \tag{2.5}$$

where k_t is the torque constant of the generator. Substituting (2.5) in (2.4) yields

$$P_E = \frac{{k_t}^2\dot{\gamma}^2}{R+r}. \tag{2.6}$$

Equation 2.6 describes the total instantaneous electrical power, including the part captured in the charging circuit and the part lost in the internal resistance of the generator, in the electrical domain.

let us consider this system in the mechanical domain. The relationship between the generator shaft rotary speed and torque applied to the shaft by the magnetic field of the generator, τ_E, is as follows

$$\tau_E = B_R\dot{\gamma} \tag{2.7}$$

where B_R is the rotary damping coefficient of the generator connected to the charging circuit. The summation of power lost and captured in the generator along with the charging circuit can be calculated as follows

$$P_E = \tau_E\dot{\gamma}. \tag{2.8}$$

Substituting (2.7) in (2.8) results in

$$P_E = B_R\dot{\gamma}^2. \tag{2.9}$$

Equation 2.9 describes the total instantaneous electrical power, including the part captured in the charging circuit and the part lost in the internal resistance of the generator, in the mechanical domain. Comparing (2.6) and (2.9) results in

$$B_R = \frac{{k_t}^2}{R + r}. \tag{2.10}$$

Equation 2.10 describes the rotary damping coefficient provided by a DC generator connected to a charging circuit based on the parameters of the generator (k_t, r) and charging circuit (R).

2.3 Analysis of an AC Permanent Magnet Rotary Machine Connected to a Charging Circuit

Let us consider a brushless permanent magnet AC motor to be used as a rotary generator. This machine along with a three phase charging circuit provides rotary damping and saves energy in a battery. Similar to the previous section, the charging circuit of the AC machine is simplified. Since the AC machine has three phases, the charging circuit is modeled as three pure controllable external resistors [80]-[81]. To analyze the system in the electrical domain and by considering the charging circuit as three controllable external resistors, the electric circuit of the system is modeled as shown in Figure 2.2.

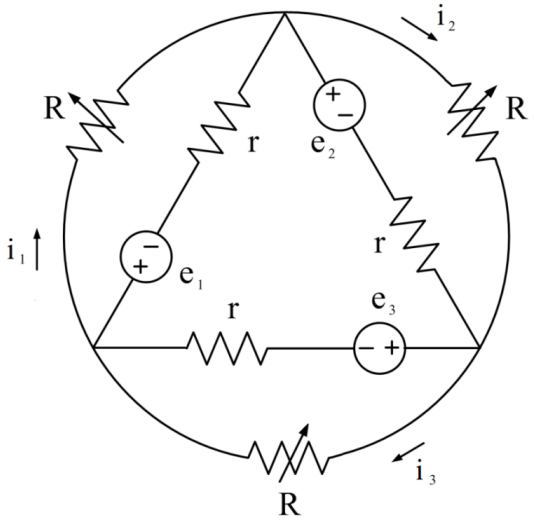

Figure 2.2: Three phase rotary generator connected to a simulated charging circuit (resistors R).

Referring to Figure 2.2, we have

$$\begin{aligned} e_1 &= i_1(R+r) \\ e_2 &= i_2(R+r) \\ e_3 &= i_3(R+r) \end{aligned} \tag{2.11}$$

where e_n $(n = 1, 2, 3)$ is the induced voltage of the generator in each phase, i_n $(n = 1, 2, 3)$ is the current of each loop, r is the internal resistance of each phase of the generator, and R is the controllable external resistor. Rearranging (2.11) results in

$$\begin{aligned} i_1 &= \frac{e_1}{(R+r)} \\ i_2 &= \frac{e_2}{(R+r)} \\ i_3 &= \frac{e_3}{(R+r)} \end{aligned} \tag{2.12}$$

The total instantaneous electrical power, including the part captured in the charging circuit and the part lost in the internal resistances of the generator, can be expressed as follows

$$P_E = P_{captured(R)} + P_{lost(r)} = R({i_1}^2 + {i_2}^2 + {i_3}^2) + r({i_1}^2 + {i_2}^2 + {i_3}^2). \tag{2.13}$$

Substituting (2.12) in (2.13) and performing some algebraic manipulations yield

$$P_E = P_{captured(R)} + P_{lost(r)} = \frac{{e_1}^2}{R+r} + \frac{{e_2}^2}{R+r} + \frac{{e_3}^2}{R+r}. \tag{2.14}$$

Referring to Figure 2.2, we have

$$\begin{aligned} e_1 &= E_m \cos(\omega_e t - 120) \\ e_2 &= E_m \cos(\omega_e t) \\ e_3 &= E_m \cos(\omega_e t + 120) \end{aligned} \tag{2.15}$$

where E_m and ω_e are the amplitude and angular frequency of the induced voltage of the generator, respectively. Substituting (2.15) in (2.14) and performing some algebraic manipulations yield

$$P_E = \frac{1.5 \times {E_m}^2}{R+r}. \tag{2.16}$$

The relationship between the generator shaft rotary speed, $\dot{\gamma}$, and amplitude of the induced voltage is as follows

$$E_m = k_t \dot{\gamma} \tag{2.17}$$

where k_t is the torque constant of the generator. Substituting (2.17) in (2.16) results in

$$P_E = \frac{1.5 \times {k_t}^2 \dot{\gamma}^2}{R + r}. \tag{2.18}$$

Equation 2.18 describes the total instantaneous electrical power, including the part captured in the charging circuit and the part lost in the internal resistances of the generator, in the electrical domain.

Let us consider this system in the mechanical domain. The relationship between the generator shaft rotary speed and torque applied to the shaft by the magnetic field of the generator, τ_E, is as follows

$$\tau_E = B_R \dot{\gamma} \tag{2.19}$$

where B_R is the rotary damping coefficient of the generator connected to the charging circuit. The summation of power lost and captured in the generator along with the charging circuit can be calculated as follows

$$P_E = \tau \dot{\gamma}. \tag{2.20}$$

Substituting (2.19) in (2.20) results in

$$P_E = B_R \dot{\gamma}^2. \tag{2.21}$$

Equation 2.21 describes the total instantaneous electrical power, including the part captured in the charging circuit and the part lost in the internal resistances of the generator, in mechanical domain. Comparing (2.18) and (2.21) results in

$$B_R = \frac{1.5 \times {k_t}^2}{R + r}. \tag{2.22}$$

Equation 2.22 describes the rotary damping coefficient of an AC generator connected to a charging circuit based on parameters of the generator (k_t, r) and charging circuit (R).

Comparing (2.10) and (2.22) shows that for the same parameters of rotary generators (k_t, r), the rotary damping coefficient provided by an AC generator is 50% higher than the one provided by a DC generator. The higher rotary damping coefficient provided by the rotary generator along with the charging circuit helps to use a gearhead with smaller gearing ratio; and smaller gearing ratio causes higher mechanical efficiency in the gearhead [82]. Since mechanical efficiency of the regenerative shock absorber has a direct relationship with the mechanical efficiency of the

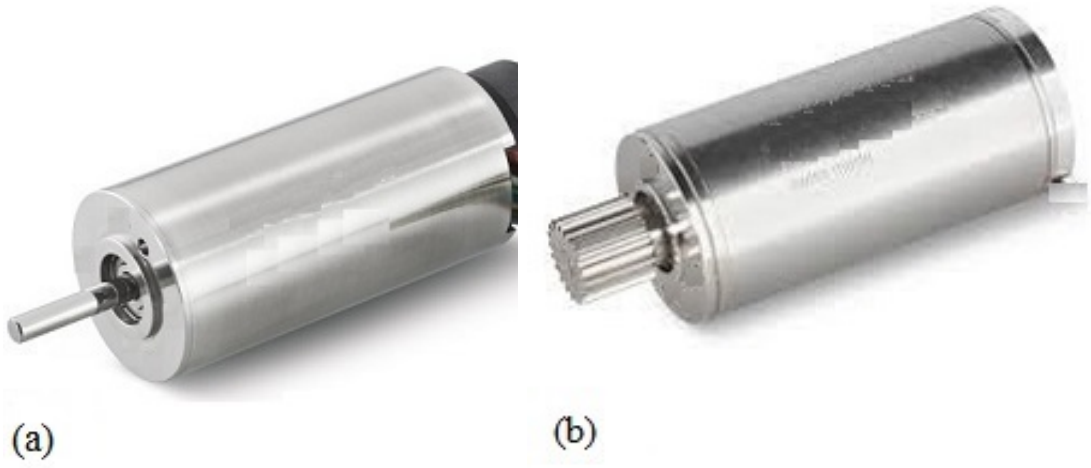

Figure 2.3: Utilized AC rotary machine (a) Without pinion (b) With pinion.

gearhead, it can be concluded that using an AC rotary generator results in higher mechanical efficiency for the regenerative shock absorber. In addition, AC rotary generators can take advantage of brushless technology. In this technology the rotary generator loses the brushes which causes lower friction and offers higher mechanical efficiency [83]-[85]. Similar to the efficiency effect of the gearhead, higher mechanical efficiency of the rotary generator results in a higher mechanical efficiency in the regenerative shock absorber. To summarize, it can be said that, using a brushless AC rotary generator results in higher efficiency because of taking advantage of brushless technology and reduction in gearing ratio of the gearhead. Therefore, in this work a brushless AC rotary generator is utilized. It should be noted that the mechanical efficiency of the suggested regenerative shock absorber and its relationship with the mechanical efficiencies of different parts of the system will be discussed in details in Section 4.4.

To avoid complexity in the system in terms of connecting the generator shaft to the gearhead, the AC rotary generator is picked such that it is capable of being connected to a planetary gearhead via a pinion attached to its shaft. Figure 2.3 shows the utilized AC rotary machine with and without the pinion.

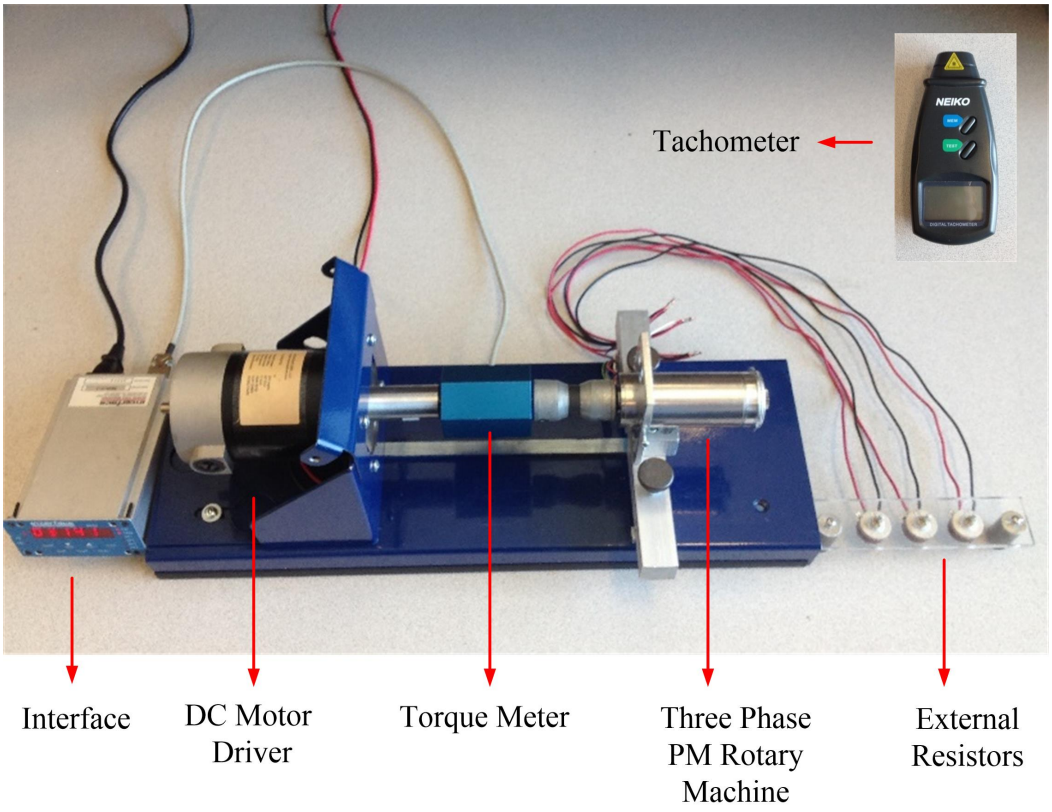

Figure 2.4: Dynamo experimental setup.

2.3.1 Experimental Results

In this section, accuracy of Equation 2.22 describing the rotary damping coefficient of an AC generator connected to a charging circuit was verified experimentally. In these experiments a dynamo setup shown in Figure 2.4 was used. In this setup, a DC motor driver (MOTOR-SOLVER, LLC, 250 watts), powered by a power supply, was used to provide different torques. The shaft of the driver was connected to the shaft of the utilized AC permanent magnet rotary machine (Maxon ECmax 40-283873) via a torque meter (Interface T8-2-A7A). Therefore, any torque provided by the driver was transfered to the shaft of the rotary machine and measured by the torque meter. The measured torques were shown via the indicator (Interface 9834) connected to the torque meter. Another parameter to study the rotary damping coefficient, is the rotary speed of the rotary machine shaft. To measure this parameter, a laser photo tachometer (Neiko 20713A) shown in Figure 2.4 was used and different rotary speeds corresponds to different torques were measured .

Table 2.1: Parameters of the used rotary machine (Maxon ECmax 40-283873).

Parameter	**Value**
Phase to phase terminal resistance, r_p	7.19 Ohm
Torque constant of the rotary machine, k_t	0.126 Nm/A

Before analyzing the experimental results and comparing them with theoretical results, one issue about the rotary machine must be clarified as follows. Referring to Equation 2.22, parameters of the rotary machine affecting the rotary damping coefficient are torque constant, k_t, and internal resistance of each phase, r. But referring to data sheet of the utilized rotary machine, provided parameters are torque constant, k_t, and phase to phase terminal resistance, r_p, shown in Table 2.1. Therefore by utilizing the phase to phase terminal resistance of the machine, r_p, internal resistance of each phase of the machine, r, should be calculated. To this end and by considering that the winding of the machine is Δ, the internal circuit of the machine is modeled as shown in Figure 2.5.

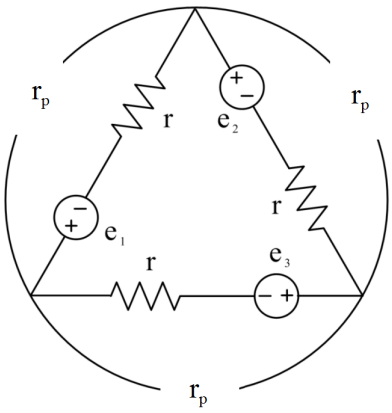

Figure 2.5: Rotary machine winding.

Referring to Figure 2.5 and utilizing parallel and series rules of resistances, we have

$$r_p = \frac{(r+r)\times r}{(r+r)+r}. \tag{2.23}$$

Rearranging (2.23) results in

$$r = 1.5 \times r_p. \tag{2.24}$$

Equation 2.24 shows the relationship between phase to phase terminal resistance, r_p, and internal resistance of each phase, r, of the rotary machine.

•Rotary Damping Coefficient for External Resistors of R = 5 Ω

For the first set of experiments, the utilized rotary machine (Maxon ECmax 40-283873) was connected to three external resistors of R = 5 Ω similar to the pattern shown in Figure 2.2. Using Equation 2.22, Equation 2.24, and Table 2.1 the rotary damping coefficient provided by this system is calculated as follows

$$B_{RT(R=5)} = \frac{1.5 \times 0.126^2}{7.19 \times 1.5 + 5} = 1.51 \times 10^{-3} N.m.s$$

Then, using the set up shown in Figure 2.4, ten experiments for different rotary speeds were conducted. The results of the experiments provided in Table 2.2 show three different torques for each rotary speed.

Table 2.2: Experimental results for external resistors of R = 5 Ω.

	$\dot{\gamma}$ (rad/s)	τ_f $(N.m)$	τ_{f+E} $(N.m)$	τ_E $(N.m)$
1	11.1	0.03	0.048	0.018
2	20.3	0.03	0.063	0.033
3	29.1	0.03	0.076	0.046
4	33.3	0.03	0.083	0.053
5	45.8	0.03	0.105	0.075
6	50.9	0.03	0.112	0.082
7	60.3	0.03	0.127	0.097
8	69.7	0.03	0.144	0.114
9	81.1	0.03	0.159	0.129
10	83.2	0.03	0.166	0.133

In the first experiment, τ_f, is related to open circuit condition in which the external resistors are disconnected from the rotary machine. In this case, the measured torque is the torque due to friction in different parts of the rotary machine. As it can be seen in Table 2.2, the torque due to friction is constant for different rotary speeds. This observation is in agreement with the theory indicating the independency of friction to the speed. The second one, τ_{f+E}, is related to the condition that the external resistors were connected to the rotary machine. In this case the measured torque, τ_{f+E}, is the summation of the torque due to friction, τ_f, and the torque due to magnetic field of the generator, τ_E. Therefore, τ_E, which is the torque due to magnetic

field of the generator is calculated as follows

$$\tau_E = \tau_{f+E} - \tau_f \tag{2.25}$$

By applying regression method on the experimental results of shaft rotary speed, $\dot{\gamma}$, and torque due to magnetic field, τ_E, the rotary damping coefficient is obtained as shown in Figure 2.6.

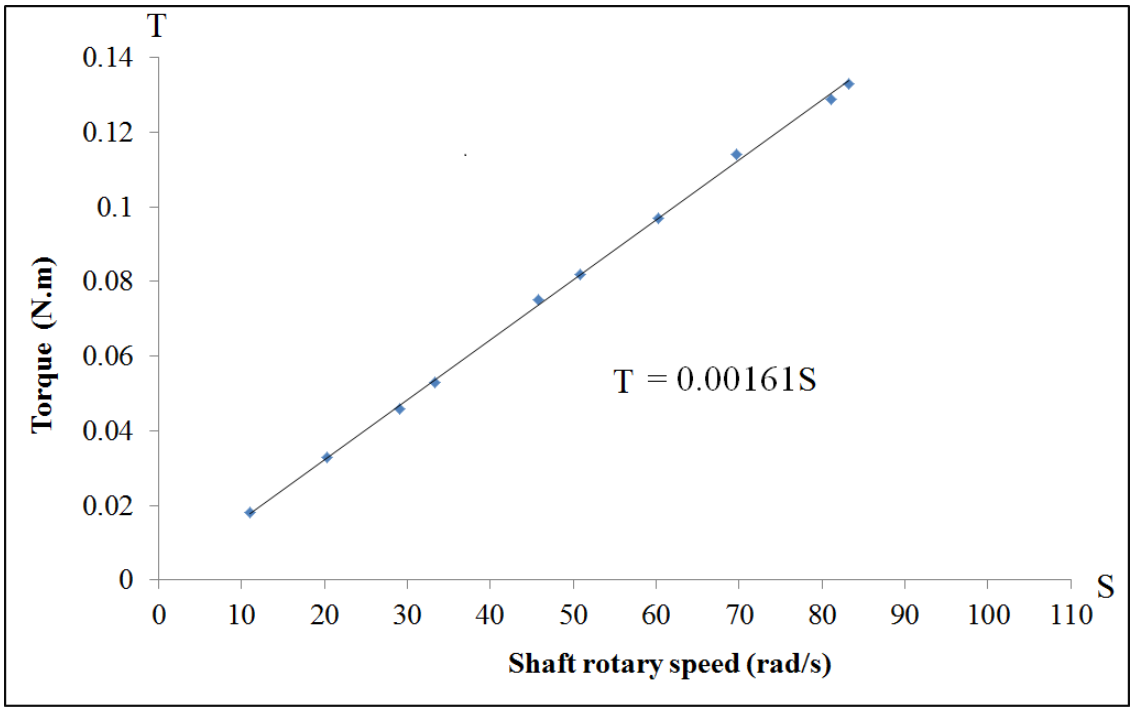

Figure 2.6: Experimental results showing the rotary damping coefficient for R = 5 Ω.

Referring to Figure 2.6 we have

$$B_{RE(R=5)} = 1.61 \times 10^{-3} N.m.s$$

Error between theoretical and experimental results is calculated as follows

$$Error_{(R=5)} = \left(\frac{1.61 \times 10^{-3} - 1.51 \times 10^{-3}}{1.61 \times 10^{-3}}\right) \times 100 = 6.2\%$$

The previous set of experiments was repeated for external resistors of R = 10 Ω, R = 15 Ω, and R = 20 Ω. The following are the results of these sets of experiments.

•Rotary Damping Coefficient for External Resistors of R = 10 Ω

$$B_{RT(R=10)} = \frac{1.5 \times 0.126^2}{7.19 \times 1.5 + 10} = 1.15 \times 10^{-3} N.m.s$$

Table 2.3: Experimental results for external resistors of R = 10 Ω.

	$\dot{\gamma}$ (rad/s)	τ_f $(N.m)$	τ_{f+E} $(N.m)$	τ_E $(N.m)$
1	21	0.03	0.056	0.026
2	28.6	0.03	0.066	0.036
3	41.6	0.03	0.082	0.052
4	46.3	0.03	0.088	0.058
5	55.6	0.03	0.099	0.069
6	62.1	0.03	0.108	0.078
7	75.9	0.03	0.125	0.095
8	79	0.03	0.128	0.098
9	95.3	0.03	0.149	0.119
10	100.5	0.03	0.156	0.126

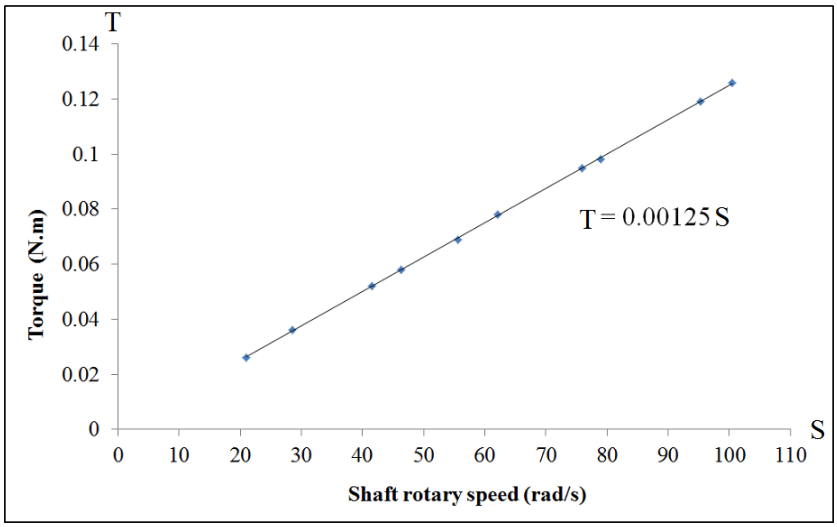

Figure 2.7: Experimental results showing the rotary damping coefficient for R = 10 Ω.

$$B_{RE(R=10)} = 1.25 \times 10^{-3} N.m.s$$

$$Error_{(R=10)} = (\frac{1.25 \times 10^{-3} - 1.15 \times 10^{-3}}{1.5 \times 10^{-3}}) \times 100 = 8.7\%$$

•Rotary Damping Coefficient for External Resistors of R =15 Ω

$$B_{RT(R=15)} = \frac{1.5 \times 0.126^2}{7.19 \times 1.5 + 15} = 0.923 \times 10^{-3} N.m.s$$

Table 2.4: Experimental results for external resistors of R = 15 Ω.

	$\dot{\gamma}$ (rad/s)	τ_f $(N.m)$	τ_{f+E} $(N.m)$	τ_E $(N.m)$
1	26	0.03	0.055	0.025
2	29.6	0.03	0.059	0.029
3	40.6	0.03	0.069	0.039
4	41.6	0.03	0.070	0.040
5	57.2	0.03	0.085	0.055
6	65.5	0.03	0.095	0.065
7	72.8	0.03	0.101	0.071
8	84.2	0.03	0.111	0.081
9	90.5	0.03	0.116	0.086
10	94.6	0.03	0.120	0.090

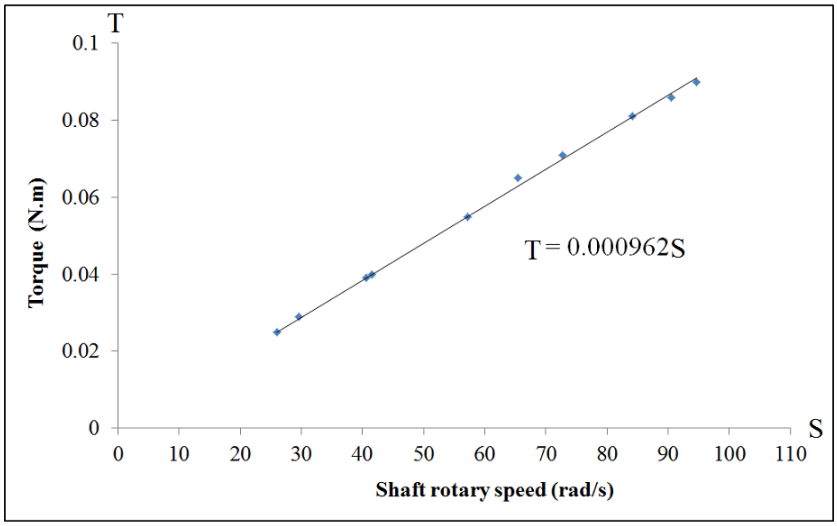

Figure 2.8: Experimental results showing the rotary damping coefficient for R = 15 Ω.

$$B_{RE(R=15)} = 0.962 \times 10^{-3} N.m.s$$

$$Error_{(R=15)} = (\frac{0.962 \times 10^{-3} - 0.923 \times 10^{-3}}{0.923 \times 10^{-3}}) \times 100 = 4.2\%$$

•Rotary Damping Coefficient for External Resistors of R = 20 Ω

$$B_{RT(R=20)} = \frac{1.5 \times 0.126^2}{7.19 \times 1.5 + 20} = 0.735 \times 10^{-3} N.m.s$$

Table 2.5: Experimental results for external resistors of R = 20 Ω.

	$\dot{\gamma}$ (rad/s)	τ_f $(N.m)$	τ_{f+E} $(N.m)$	τ_E $(N.m)$
1	31.6	0.03	0.055	0.025
2	44	0.03	0.065	0.035
3	53.8	0.03	0.073	0.043
4	62.4	0.03	0.080	0.050
5	67.8	0.03	0.083	0.053
6	75.6	0.03	0.09	0.06
7	78.4	0.03	0.093	0.063
8	82	0.03	0.096	0.066
9	88.9	0.03	0.101	0.071
10	101.5	0.03	0.110	0.08

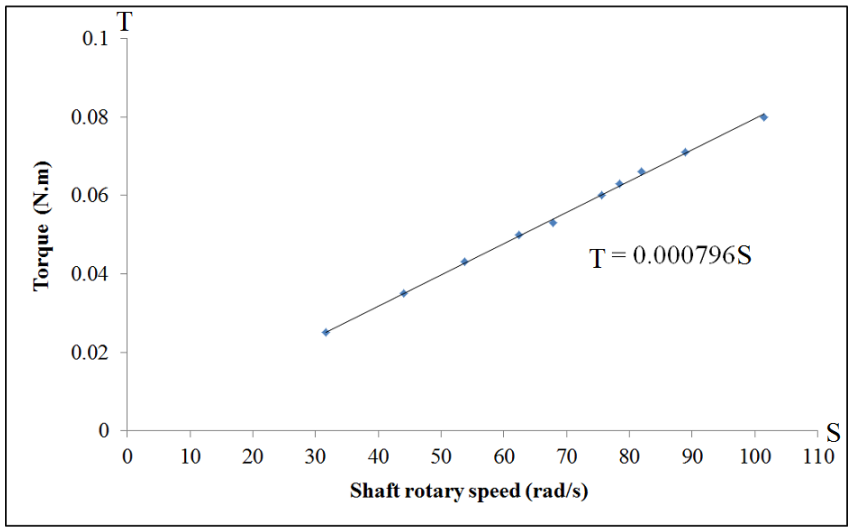

Figure 2.9: Experimental results showing the rotary damping coefficient for R = 20 Ω.

$$B_{RE(R=20)} = 0.796 \times 10^{-3} N.m.s$$

$$Error_{(R=20)} = (\frac{0.796 \times 10^{-3} - 0.735 \times 10^{-3}}{0.735 \times 10^{-3}}) \times 100 = 8.3\%$$

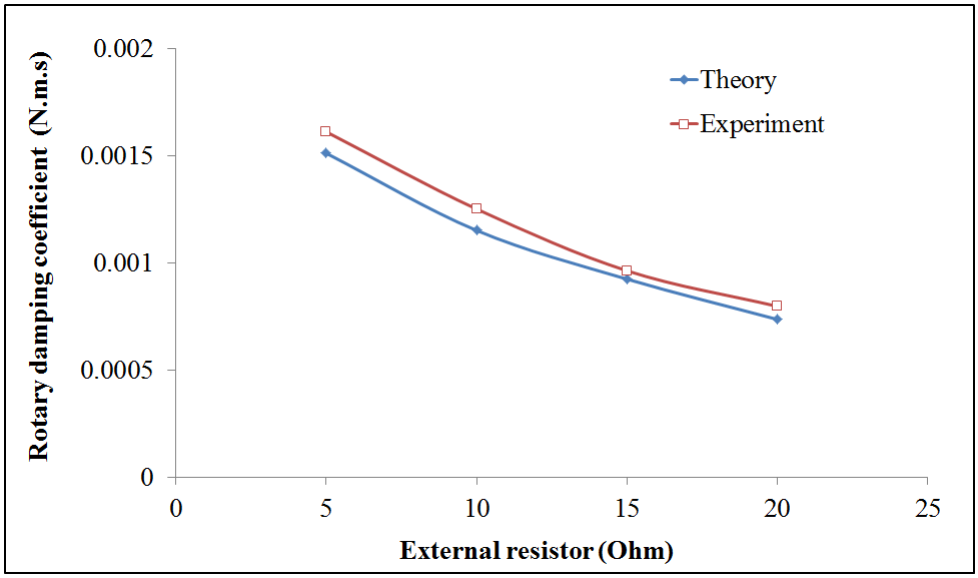

Figure 2.10: Experimental and theoretical results of rotary damping coefficient, B_R, versus external resistor, R.

Figure 2.10 shows the experimental and theoretical results of the rotary damping coefficient provided by the rotary machine connected to different external resistors. Referring to this figure, there is a good match between results obtained from theory and experiment proving accuracy of Equation 2.22. The sources of small errors between experimental and theoretical results are measurements by the mentioned torque meter and tachometer. By using more precise measuring tools the errors can be decreased.

2.4 Summary and Conclusions

In this chapter, analytical expressions describing the rotary damping coefficients provided by DC and AC rotary machines connected to charging circuits were derived. Then considering that the rotary damping provided by the AC rotary machine is 50% higher; and AC rotary machines have higher efficiencies, this type of rotary machine was chosen for this work. Furthermore, validity of the equation describing the rotary damping coefficient of an AC rotary machine connected to a charging circuit was examined. The results demonstrated the accuracy of this equation.

Chapter 3

Regenerative Shock Absorber Using an Algebraic Screw

3.1 Introduction

This chapter presents the development of a novel regenerative shock absorber. This system consists of a simple and highly efficient linear-to-rotary conversion mechanism called, algebraic screw, a gearhead, and an AC rotary machine connected to three external resistors (to simulate the effect of a three phase charging circuit). In this system, the rotary machine is connected to three external resistors which provides rotary damping. The resulting rotary damping is then increased by using a gearhead. Finally, the algebraic screw converts the rotary damping into a linear one. It should be noted that, the objective of this chapter is to study linear damping; and the regenerative shock absorber for a passenger– scale car will be studied in the next chapter.

The organization of this chapter is as follows. The algebraic screw mechanism is introduced and studied in Section 3.2. In Section 3.3 dynamics of the suggested regenerative shock absorber is analyzed by utilizing a one-degree-of-freedom model of a quarter car, and the analytical expression describing the linear damping coefficient provided by the shock absorber is derived. Section 3.4 presents simulation results to verify the accuracy of the analysis conducted in Section 3.3. In Section 3.5 the performance of the shock absorber is evaluated experimentally. Finally, summary and conclusions are presented in Section 3.6.

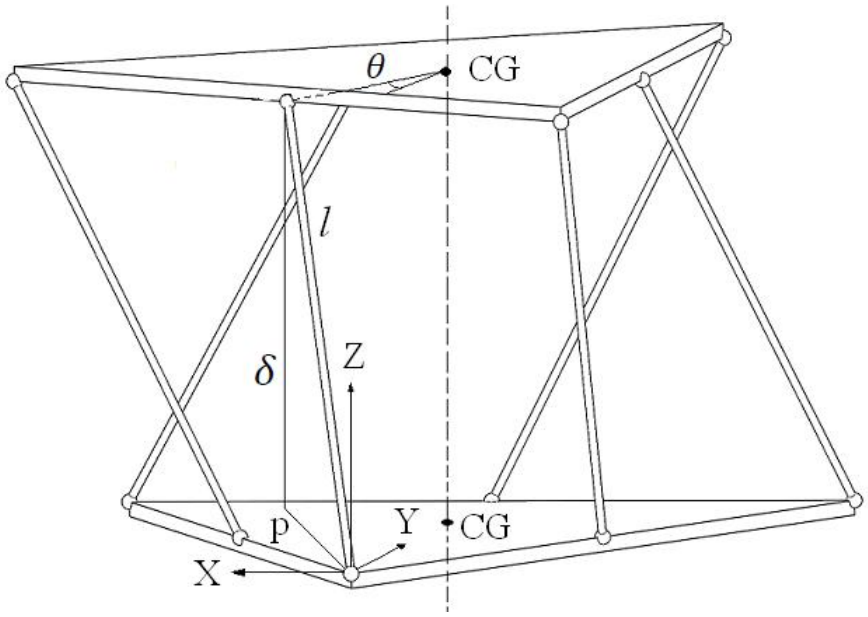

Figure 3.1: Schematic diagram of the algebraic screw

3.2 Kinematic Analysis of the Algebraic Screw Mechanism

The algebraic screw mechanism was first introduced and used as a robotic joint [86]-[90]. This kinematic mechanism consists of two equilateral triangular plates connected to each other via six legs. As depicted in Figure 3.1, each leg of the algebraic screw has two ball-joint anchor points: The first one is located on the vertex of each triangular plate and the second one is located on the midpoint edge of the other plate.

The algebraic screw mechanism reported in the literature, has two disadvantages as follows. First, the formula describing the separation of the algebraic screw plates as a function of the rotation angle between plates is correct only for a specific geometry of the algebraic screw. This specific geometry, which is a constraint in algebraic screw design, states that the length of each leg must be equal to the height of the triangles. This constraint leads to bigger dimensions in the size of the algebraic screw. By removing this constraint, a smaller algebraic screw can be designed for a specific stroke of the shock absorber and less space is needed to fit this mechanism in a suspension system. The second disadvantage of the previous works is the lack of study about collision between legs. In these works collision was not considered and there is not any prediction about the angle in which legs collide each other.

In this work, the constraint between length of each leg and height of the triangles has been

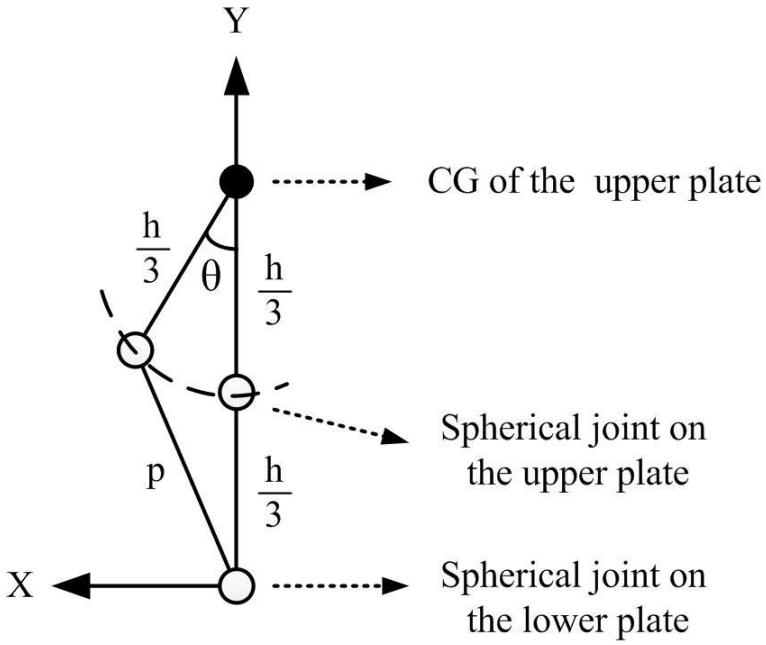

Figure 3.2: Projections of p on X and Y axes

removed and a comprehensive formula describing the separation of the algebraic screw plates as a function of the rotation angle between plates is presented. In addition, the collision between legs is studied and the collision angle is obtained.

Referring to Figure 3.1, let us obtain a formula describing the separation of plates, δ, as a function of the rotation angle θ. To this end, considering Figure 3.1 we have

$$l^2 = \delta^2 + p^2 \tag{3.1}$$

where δ is the projection of l on the Z axis and p is the projection of l on the XY plane. Referring to Figure 3.2, the projection of p on the X and Y axes, as a function of the triangle height, h, and θ, respectively, are given by

$$p_X = \frac{h}{3} sin\theta, \quad p_Y = \frac{2h}{3} - \frac{h}{3} cos\theta\cdot \tag{3.2}$$

Utilizing the geometrical relationships $p^2 = p_X^2 + p_Y^2$ and $h = a\frac{\sqrt{3}}{2}$, where a is the length of the triangle side, and (4.2) results in

$$p^2 = \frac{a^2}{12}(5 - 4\cos\theta)\cdot \tag{3.3}$$

Substituting (4.3) in (4.1) yields

$$\delta = \sqrt{l^2 - \frac{a^2}{12}(5 - 4cos\theta)}\cdot \tag{3.4}$$

Equation 3.4 describes the separation of the algebraic screw plates, δ, as a function of the rotation angle between plates, θ, without any constraint in the geometry of the algebraic screw. From (3.4), when $\theta = 0$, the algebraic screw is fully extended and δ reaches its maximum value.

Since the force applied by a linear shock absorber is proportional to the speed between two sides of the shock absorber, and the algebraic screw is used as a linear-to-rotary converter in the suggested regenerative shock absorber, it is necessary to obtain the relationship between the translation and rotary speeds of the two plates of the algebraic screw. This relationship will be used in Section 3.3 and explained in details. To this end, taking a derivative of (3.4) and performing some algebraic manipulations, yield

$$\dot{\delta} = -\frac{a^2 sin\theta}{6\sqrt{l^2 - \frac{a^2}{12}(5 - 4cos\theta)}}\dot{\theta}\cdot \tag{3.5}$$

Equation 3.5 describes a nonlinear kinematic relationship between the translation and rotary speeds of the two plates of the algebraic screw. Let us define the relative linear and rotary motions by $\tilde{\delta}$ and $\tilde{\theta}$, respectively, as follows

$$\delta - \delta_0 = \tilde{\delta} \tag{3.6}$$

$$\theta - \theta_0 = \tilde{\theta} \tag{3.7}$$

where δ_0 and θ_0 are the static equilibrium points of δ and θ, respectively. Substituting (3.6) and (3.7) into (3.4), linearization about θ_0, and taking a derivative result in

$$\dot{\tilde{\delta}} = -c\dot{\theta} \tag{3.8}$$

where c is the slope of the nonlinear relationship between $\dot{\delta}$ and $\dot{\theta}$ given by

$$c = \frac{a^2 sin\theta_0}{6\delta_0}\cdot \tag{3.9}$$

The process of linearization and taking derivative of (3.4) is presented in Appendix A.

Equations 3.5 and 3.8 will be utilized in Section 3.3 to obtain the formula describing the linear damping coefficient provided by the regenerative shock absorber.

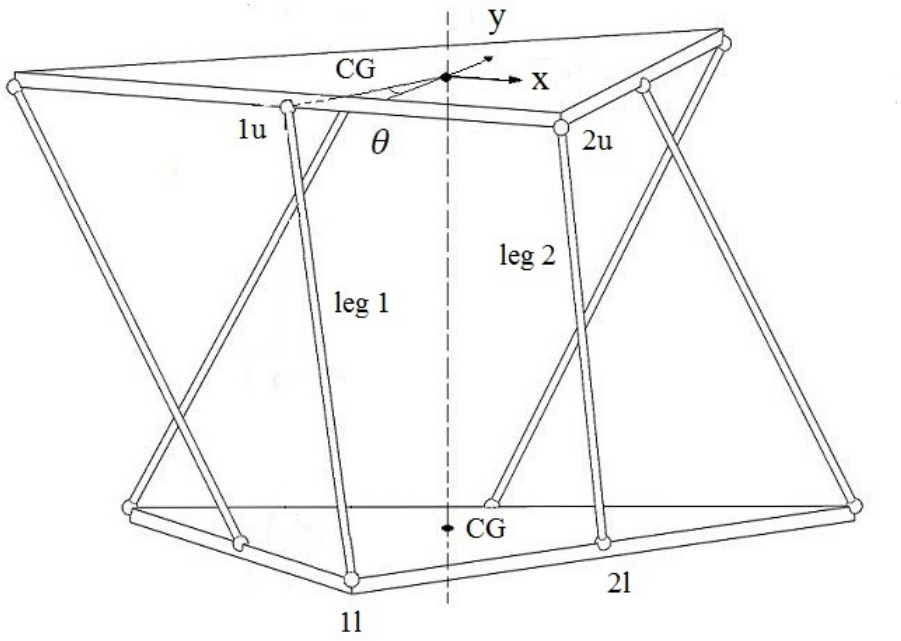

Figure 3.3: Schematic diagram of the algebraic screw to analyze collision.

3.2.1 Collision between legs of algebraic screw

Since both triangular plates rotate around same axis, which passes through the centroids of them [88], [89], there is symmetry in rotation of the algebraic screw plates. Therefore to study the collision between legs, any two adjacent legs can be considered. To find the collision angle, a coordinate system is attached to the centroid of the upper plate as shown in Figure 3.3, then the coordinates of midpoints of two adjacent legs are obtained in this coordinate system, the angle in which these two midpoints become coincident is the collision angle, θ_c.

In Figure 3.3, two adjacent legs and their spherical joints are shown. The notations used in this figure and their meanings are as follows:

1u : Spherical joint of the leg **1** on the **upper** plate
1l : Spherical joint of the leg **1** on the **lower** plate
2u : Spherical joint of the leg **2** on the **upper** plate
2l : Spherical joint of the leg **2** on the **lower** plate

Projection of leg 1 on xy plane, and its relationship with the height of the triangular plates

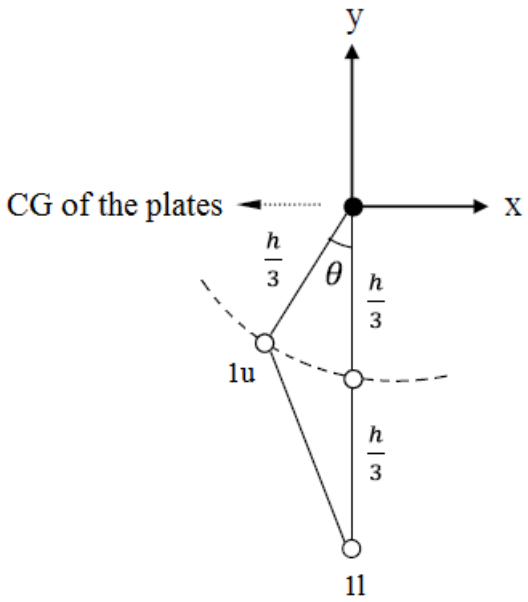

Figure 3.4: Projection of leg 1 on xy plane, and its relationship with the height of the triangular plates and rotation angle.

and rotation angle are shown in Figure 3.4. Considering Figure 3.3 and Figure 3.4, for the spherical joints 1l and 1u we have

$$\begin{aligned} x_{1l} &= 0 \\ y_{1l} &= -\frac{2h}{3} \\ z_{1l} &= -\delta \end{aligned}$$

$$\begin{aligned} x_{1u} &= -\frac{h}{3} sin\theta \\ y_{1u} &= -\frac{h}{3} cos\theta \\ z_{1u} &= 0 \end{aligned}$$

Then, the coordinate of the midpoint of leg 1 is calculated as follows

$$\begin{aligned} x_{1m} &= \frac{x_{1l} + x_{1u}}{2} = -\frac{h}{6} sin\theta \\ y_{1m} &= \frac{y_{1l} + y_{1u}}{2} = -\frac{h}{3} - \frac{h}{6} cos\theta \\ z_{1m} &= \frac{z_{1l} + z_{1u}}{2} = -\frac{\delta}{2} \end{aligned}$$

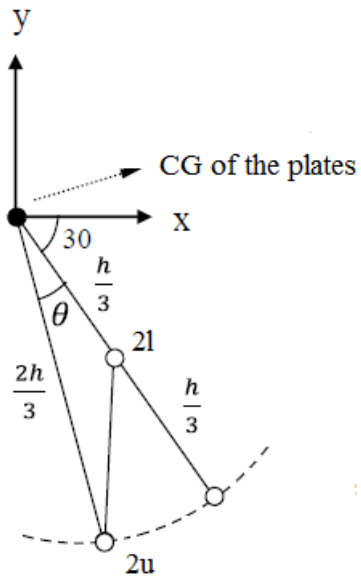

Figure 3.5: Projection of leg 2 on xy plane, and its relationship with height of the triangular plates and rotation angle.

Projection of leg 2 on xy plane, and its relationship with the height of the triangular plates and rotation angle, are shown in Figure 3.5. Considering Figure 3.3 and Figure 3.5, for the spherical joints 2l and 2u we have

$$x_{2l} = \frac{h}{3}cos30$$
$$y_{2l} = -\frac{h}{3}sin30$$
$$z_{2l} = -\delta$$

$$x_{2u} = \frac{2h}{3}cos(\theta + 30)$$
$$y_{2u} = -\frac{2h}{3}sin(\theta + 30)$$
$$z_{2u} = 0$$

Then, the coordinate of the midpoint of leg 2 is calculated as follows

$$x_{2m} = \frac{x_{2l} + x_{2u}}{2} = \frac{h}{6}cos30 + \frac{h}{3}cos(\theta + 30)$$
$$y_{2m} = \frac{y_{2l} + y_{2u}}{2} = -\frac{h}{6}sin30 - \frac{h}{3}sin(\theta + 30)$$
$$z_{2m} = \frac{z_{2l} + z_{2u}}{2} = -\frac{\delta}{2}$$

Finally, by equalizing the coordinates of the midpoints of leg 1 and leg 2, the collision angle is obtained as follows

$$x_{1m} = x_{2m} \Rightarrow \theta_c = 120$$
$$y_{1m} = y_{2m} \Rightarrow \theta_c = 120$$
$$z_{1m} = z_{2m} \Rightarrow \theta_c = anyangle$$

As it can be seen, the collision angle is $\theta_c = 120$. It should be noted that, in our analysis, to calculate the collision angle, the diameter of legs was assumed to be zero. Therefore the obtained collision angle, $\theta_c = 120$, is theoretical estimates. To avoid collision between legs in practical applications of the algebraic screw, the theoretical collision angle should be used as the criterion. Then, by considering the diameter of legs and manufacturing limits, practical value of the collision angle can be obtained.

3.3 Modeling of the Regenerative Shock Absorber Using an Algebraic Screw

To analyze the regenerative shock absorber using the algebraic screw mechanism, the system is studied as a part of suspension system of a quarter car. A one-degree-of-freedom (1-DOF) model of a quarter car is shown in Figure 3.6. The equation of motion for the model is obtained by using the Lagrangian formulation as follows

$$\frac{d}{dt}(\frac{\partial T}{\partial \dot{z}}) - (\frac{\partial T}{\partial z}) + \frac{\partial U}{\partial z} + \frac{\partial R_D}{\partial \dot{z}} = F \tag{3.10}$$

where $z = x - y$ is the relative displacement between the absolute displacement x and base excitation y; $F = 0$ due to zero external forces; and T, U, R_D are the energies due to kinetic, potential, and damping effects, respectively. The term T is given by

$$T = \frac{1}{2}m_m\dot{x}^2 + \frac{1}{2}m_t\dot{x}^2 + \frac{1}{2}I_t\dot{\theta}^2 + \frac{1}{2}I_g\dot{\theta}^2 + \frac{1}{2}I_r\dot{\gamma}^2 \tag{3.11}$$

where m_m is the mass of the upper body shown in Figure 3.6 representing a quarter of the sprung mass of a vehicle body; m_t and I_t are the mass and moment of inertia of the algebraic screw plates, respectively; and I_g, I_r are the moments of inertia of the gearhead and the rotary machine, respectively; and $\dot{\gamma}$ is given by

$$\dot{\gamma} = n\dot{\theta} \tag{3.12}$$

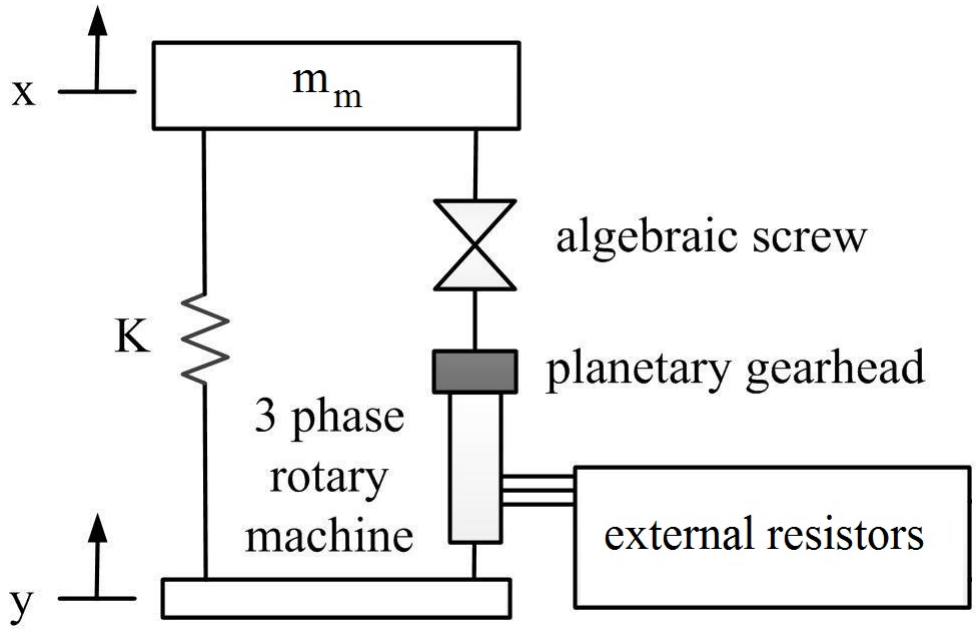

Figure 3.6: One-degree-of-freedom model of the quarter car.

where n is the gearing ratio of the planetary gearhead. Substituting (3.12) in (3.11) results in

$$T = \frac{1}{2}m_m\dot{x}^2 + \frac{1}{2}m_t\dot{x}^2 + \frac{1}{2}I_t\dot{\theta}^2 + \frac{1}{2}I_g\dot{\theta}^2 + \frac{1}{2}I_r n^2\dot{\theta}^2. \tag{3.13}$$

The potential energy U is given by

$$U = \frac{1}{2}K(x-y)^2 = \frac{1}{2}Kz^2 \tag{3.14}$$

where K is the stiffness coefficient, representing the stiffness of the mechanical parts of the suspension system. Furthermore, the damping effect R_D is given by

$$R_D = \frac{1}{2}B_R\dot{\gamma}^2 + \frac{1}{2}B_f\dot{z}^2 \tag{3.15}$$

where B_R is the rotary damping due to the rotary machine connected to external resistors (discussed in Section 2.3), and B_f is the equivalent viscous-damping coefficient due to friction in different parts of the system[91], [92]. Substituting (3.12) in (3.15) results in

$$R_D = \frac{1}{2}B_R n^2\dot{\theta}^2 + \frac{1}{2}B_f\dot{z}^2. \tag{3.16}$$

Since the absolute displacement x and base excitation y are measured from static equilibrium level, we have

$$z = \delta - \delta_0. \tag{3.17}$$

Differentiating (3.17) with respect to time results in

$$\dot{z} = \dot{\delta}\cdot \tag{3.18}$$

Substituting (3.5) into (3.18) yields

$$\dot{z} = -\frac{a^2 sin\theta}{6\sqrt{l^2 - \frac{a^2}{12}(5 - 4\cos\theta)}}\dot{\theta}\cdot \tag{3.19}$$

Hence, rearranging (3.19) and substituting in (3.13) results in

$$T = \frac{1}{2}(m_m + m_t)\dot{x}^2 + (I_t + I_g + n^2 I_r)\frac{18[l^2 - \frac{a^2}{12}(5 - 4\cos\theta)]}{a^4 sin^2\theta}\dot{z}^2. \tag{3.20}$$

From (3.19) and (3.16) we have

$$R_D = (\frac{18[l^2 - \frac{a^2}{12}(5 - 4\cos\theta)]n^2 B_R}{a^4 sin^2\theta} + \frac{B_f}{2})\dot{z}^2. \tag{3.21}$$

Now, substituting (3.14), (3.20), and (3.21) into (3.10) and performing some algebraic manipulations yield

$$\begin{aligned}&(m_m + m_t + (I_t + I_g + n^2 I_r)\frac{36[l^2 - \frac{a^2}{12}(5 - 4\cos\theta)]}{a^4 sin^2\theta})\ddot{z}\\ &+(\frac{36[l^2 - \frac{a^2}{12}(5 - 4\cos\theta)]n^2 B_R}{a^4 sin^2\theta} + B_f)\dot{z} + Kz = -(m_m + m_t)\ddot{y}.\end{aligned} \tag{3.22}$$

Using the linear approximation given by (3.8) results in

$$(m_m + m_t + \frac{I_t + I_g + n^2 I_r}{c^2})\ddot{z} + (\frac{n^2 B_R}{c^2} + B_f)\dot{z} + Kz = -(m_m + m_t)\ddot{y}. \tag{3.23}$$

Let us define M, B_{EP}, B, and m as follows

$$M = m_m + m_t + \frac{I_t + I_g + n^2 I_r}{c^2} \tag{3.24}$$

$$B_{EP} = \frac{n^2 B_R}{c^2} \tag{3.25}$$

$$B = B_{EP} + B_f \tag{3.26}$$

$$m = m_m + m_t \tag{3.27}$$

Substituting (3.24), (3.25), (3.26), and (3.27) into (3.23) yields

$$M\ddot{z} + B\dot{z} + Kz = -m\ddot{y} \tag{3.28}$$

In (3.26), the total linear damping coefficient B consists of B_{EP} and B_f. B_{EP} is the linear damping coefficient originated from electrical part of the rotary machine connected to the external resistors (discussed in Section 2.3), and B_f is the linear damping coefficient due to friction in different parts of the system. Substituting (2.22) into (3.25) results in

$$B_{EP} = \frac{1.5 \times n^2 {k_t}^2}{c^2(R+r)}. \tag{3.29}$$

Equation 3.29 describes the linear damping coefficient originated from electrical part of the rotary machine connected to the external resistors based on the effect of different components. According to (3.29), c is the parameter related to the algebraic screw mechanism; n is the effect of gearhead; k_t and r are related to the generator; and R is the effect of the external resistors (simulated charging circuit).

As a simple model, road roughness profile can be described by a sinusoidal function [73], which means in Figure 3.6, the base excitation can be given by

$$y = Y \sin(\omega t) \tag{3.30}$$

where Y and ω represent the amplitude and frequency of the base excitation, respectively. Substituting (3.30) into (3.28) and solving (3.28) yields [91], [92]

$$z = Z \sin(\omega t - \phi_z) \tag{3.31}$$

where ϕ_z is the phase difference between the base excitation and relative displacement, and Z is the amplitude of the relative displacement given by

$$Z = \frac{mY\omega^2}{\sqrt{M^2(\omega_n^2 - \omega^2)^2 + B^2\omega^2}} \tag{3.32}$$

and $\omega_n = \sqrt{\frac{K}{M}}$.

Solving (3.32) in terms of B results in

$$B = \sqrt{\frac{m^2Y^2\omega^4 - M^2Z^2(\omega_n^2 - \omega^2)^2}{Z^2\omega^2}}. \tag{3.33}$$

If $\omega = \omega_n$, (3.33) is changed to

$$B = \frac{m\omega Y}{Z}. \tag{3.34}$$

Thus, knowledge of the base excitation profile and the amplitude of relative displacement can be utilized to calculate the damping coefficient by using (3.33) or (3.34) .

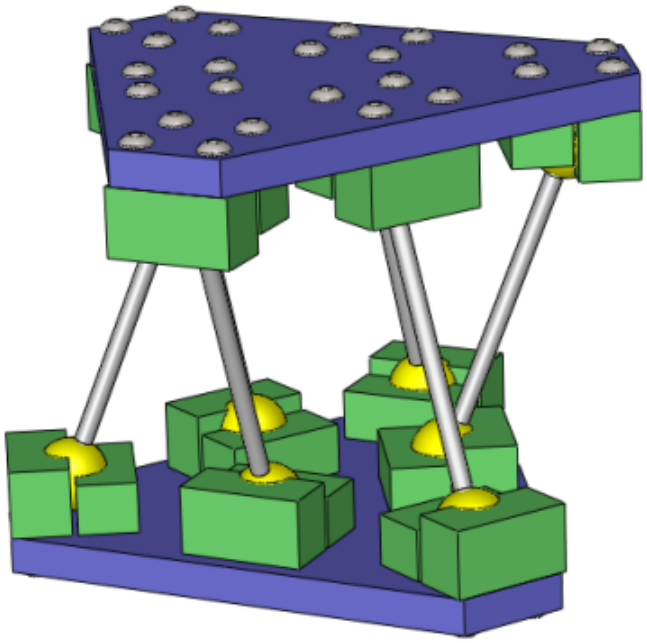

Figure 3.7: Designed prototype of the algebraic screw.

3.4 Simulation Results

Using the SimMechanics toolbox of MATLAB, a Simulink model of a quarter car shown in Figure 3.6 was developed and used for two objectives : Evaluate the accuracy of Equation 3.29 describing the linear damping coefficient provided by the shock absorber, and evaluating the effect of algebraic screw nonlinear terms on relative displacement described by Equation 3.32. The procedure of developing the Simulink model and used dimensions are as follows.

First, to have reasonable dimensions for the Simulink model, a Solidworks model of the algebraic screw shown in Figure 3.7 is designed. To design the Solidworks model, the limits of rotation angle and translational motion are considered as follows.

To avoid collision between legs, by utilizing the theoretical collision angle of 120 degrees (discussed in Section 3.2.1), and considering the manufacturing limits and diameter of each leg, the practical rotation angle between the algebraic screw plates is obtained to be 105 degrees.

Based on published literature [27], [73], [95], the usual stroke of the shock absorber for a regular road is between 0.5 cm and 1 cm, rarely increasing to 1.5 cm. In this work, a stroke between 0.5 and 1 cm is called working area and the stroke between 1 cm and 1.5 cm is called safety area.

Table 3.1: Dimensions of the designed algebraic screw.

Parameter	Value
Algebraic screw leg length, l	5.9178 cm
Length of the triangle side of the algebraic screw , a	7.56 cm

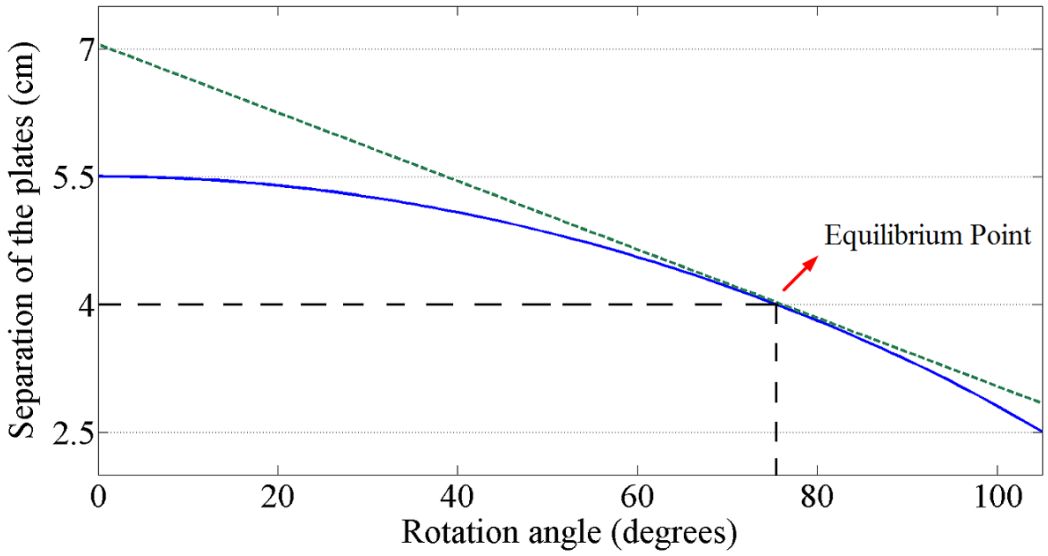

Figure 3.8: Nonlinear and linear mapping around the operating point describing the separation of the algebraic screw plates, δ, versus rotation angle, θ.

By utilizing Equation 3.4, and considering the working and safety areas, the algebraic screw mechanism is designed to convert 3 cm of peak-to-peak translational motion (2×1.5 cm of stroke) into 105 degrees of rotation, providing a motion range of $\delta_1 = 2.5$ cm to $\delta_2 = 5.5$ cm. Table 3.1 shows the dimensions of the designed algebraic screw mechanism.

For the motion range of algebraic screw, the static operating point is calculated as $\delta_0 = \frac{2.5+5.5}{2} = 4$ cm. By using Equation 3.4, the corresponding rotation angle to the static operating point is calculated equal to $\theta_0 = 75$ degrees. Figure 3.8 illustrates the nonlinear mapping and its linearized approximation around the operating point in the working and safety areas of the device.

By substituting parameters of the algebraic screw shown in Table 3.1, and information on the static equilibrium point of the algebraic screw in Equation B.9, the slope of the nonlinear

relationship between $\dot{\delta}$ and $\dot{\theta}$ is calculated as follows

$$c = \frac{a^2 sin\theta_0}{6\delta_0} = \frac{0.0756^2 \times sin75}{6 \times 0.04} = 0.023m.$$

This parameter will be used to calculate the linear damping coefficient provided by the shock absorber.

By utilizing the dimensions of the designed algebraic screw provided in Table 3.1, a Simulink model of this device was developed. To complete the Simulink model of the regenerative shock absorber, a gearhead with a gearing ratio of 4.3:1 and a rotary damper with rotary damping coefficient of $B_R = 0.00281N.m.s$ (instead of the rotary machine connected to the charging circuit discussed in Section 2.3) was added to the model. Using Equation 3.25 the linear damping coefficient provided by the Simulink model is calculated as follows

$$B_{EP} = \frac{n^2 B_R}{c^2} = \frac{4.3^2 \times 0.00281}{0.023^2} = 100N.s/m$$

It should be noted that in (3.25), the linear approximation given by (3.8) was used, therefore the calculated linear damping coefficient is a fixed number ($B_{EP} = 100N.s/m$) which is accurate as long as the regenerative shock absorber works around the operating point. However, because of the nonlinear terms of the algebraic screw, the linear damping coefficient provided by the Simulink model is variable, fluctuating about $B_{EP} = 100N.s/m$. The suggested regenerative shock absorber is always used as a part of the suspension system. The main functionality of a suspension system is the vibration control of the relative displacement, z, between car seats, x, and wheels, y. Therefore, in simulation results, our main focus would be on the relative displacement.

To complete the Simulink model of the quarter shown in Figure 3.6, stiffness coefficient, K, and mass of a quarter car, m_m, must be chosen appropriately. To this end, let us consider Table 3.2 showing the parameters of a real quarter car. By comparing the linear damping coefficients of a real quarter car (1500 N.s/m) and Simulink model (100 N.s/m) it can be noticed that the other parameters should be scaled down by the factor of 15. Table 3.3 shows the parameters of the Simulink model of the quarter car.

To simplify the Simulink model, friction, mass, and moment of inertia of the algebraic screw plates, inertia of the gearhead, and inertia of the rotary machine, was ignored in this model. By considering the values of these parameters equal to zero in formulations provided in Section 3.3, we have $M = m = m_m$ and $B = B_{EP}$.

Table 3.2: Parameters of a real quarter car.

Parameter	**Value**
Mass, m_m	450 Kg
Stiffness coefficient, K	30000 N/m
Damping coefficient, B	1500 N.s/m

Table 3.3: Parameters of the Simulink model of the quarter car.

Parameter	**Value**
Mass, m_m	30 Kg
Stiffness coefficient, K	2000 N/m
Damping coefficient, B	100 N.s/m

Applying different base excitation profiles, the Simulink model was evaluated in working and safety areas and the results are shown in Figures 3.9 to Figure 3.12. In these figures, modeling refers to a quarter car system in which a linear shock absorber with a fixed damping coefficient of $B = 100N.s/m$ was used and simulation refers to the explained Simulink model of the quarter car in which the suggested regenerative shock absorber was used. As it can be seen in Figures 3.9 and 3.10, modeling and simulation results of force-displacement loops do not match, which is due to nonlinearity of the algebraic screw. However, as explained before, our main focus would be on the results of relative displacement. Using Figures 3.11 and 3.12, accuracy of Equation 3.25, and effect of algebraic screw nonlinear terms on relative displacement can be evaluated as follows:

Figure 3.11 (a) shows that the modeling and simulation results completely agree. In addition, in both systems mass, stiffness coefficient, and base excitation profile are the same. Therefore it can be concluded that the linear damping coefficient provided by the suggested regenerative shock absorber around the equilibrium point (up to 5 mm of stroke) is equal to the linear damping coefficient provided by a linear shock absorber. This fact proves accuracy of Equation 3.25, in which parameter c which is the slope of the nonlinear relationship between $\dot{\delta}$ and $\dot{\theta}$, was used. Moreover, this fact can be confirmed by Figure 3.8 showing that nonlinear and linear mappings match up to 5 mm of displacement from equilibrium point.

Figures 3.11 (b) and (c) show that by increasing the relative displacement up to 10 mm, no big difference between simulation and modeling results can be seen. This fact proves that

despite the existence of nonlinear terms in algebraic screw, the suggested regenerative shock absorber can work properly in working area.

By considering Figure 3.12, showing the system in the safety area, it can be noticed that simulation results show smaller relative displacements compared to the modeling results for the positive stroke. Regarding this difference, one should consider two points: First, the Simulink model of the regenerative shock absorber utilizing the designed prototype, shown in Figure 3.7, includes nonlinearity of the algebraic screw but the modeling is based on the linear approximation provided by Equation B.9. Hence, the difference between simulation and modeling results is due to the difference between nonlinear and linear mappings shown in Figure 3.8. Secondly, this differences means error=$\frac{12.5-11.2}{12.5} \times 100 = 10\%$ for the stroke of 12.5 mm and error=$\frac{15-13}{15} \times 100 = 13\%$ for the stroke of 15 mm; considering that a shock absorber rarely works in safety area and these errors are small enough, they can be ignored for the application of usual passenger cars. It should be noted that, by utilizing a more linear mechanism, e.g. two-leg mechanism which will be introduced in the next chapter, the error between modeling and simulation results can be decreased.

Regarding the simulation results, two points should be elaborated: First, in the simulation model, all of the parameters of the quarter car were scaled down by the same factor. Thus, the obtained results for the proof of concept scale are applicable for a real quarter car. Secondly, in the quarter car, the shock absorber works along with a mass and a spring. Since the mass and spring are linear, they eliminate some of the nonlinear terms of the damping force originated from the algebraic screw. Thus the obtained results are correct only for the combination of mass, stiffness coefficient and damping coefficient shown in Table 3.2 and Table 3.3. For any other combination simulation should be repeated.

3.5 Experimental Results

To evaluate the performance of the system experimentally, the algebraic screw shown in Figure 3.7 was fabricated. The physical model of the algebraic screw is shown in Figure 3.13. Then a proof of concept regenerative shock absorber including the built algebraic screw, a 4.3:1 planetary gearhead (Maxon GP52C 223081), and a rotary permanent-magnet machine (Maxon EC-max 40-283873) connected to three external resistors was developed. Table 3.4 shows the parameter values of the developed prototype of the shock absorber.

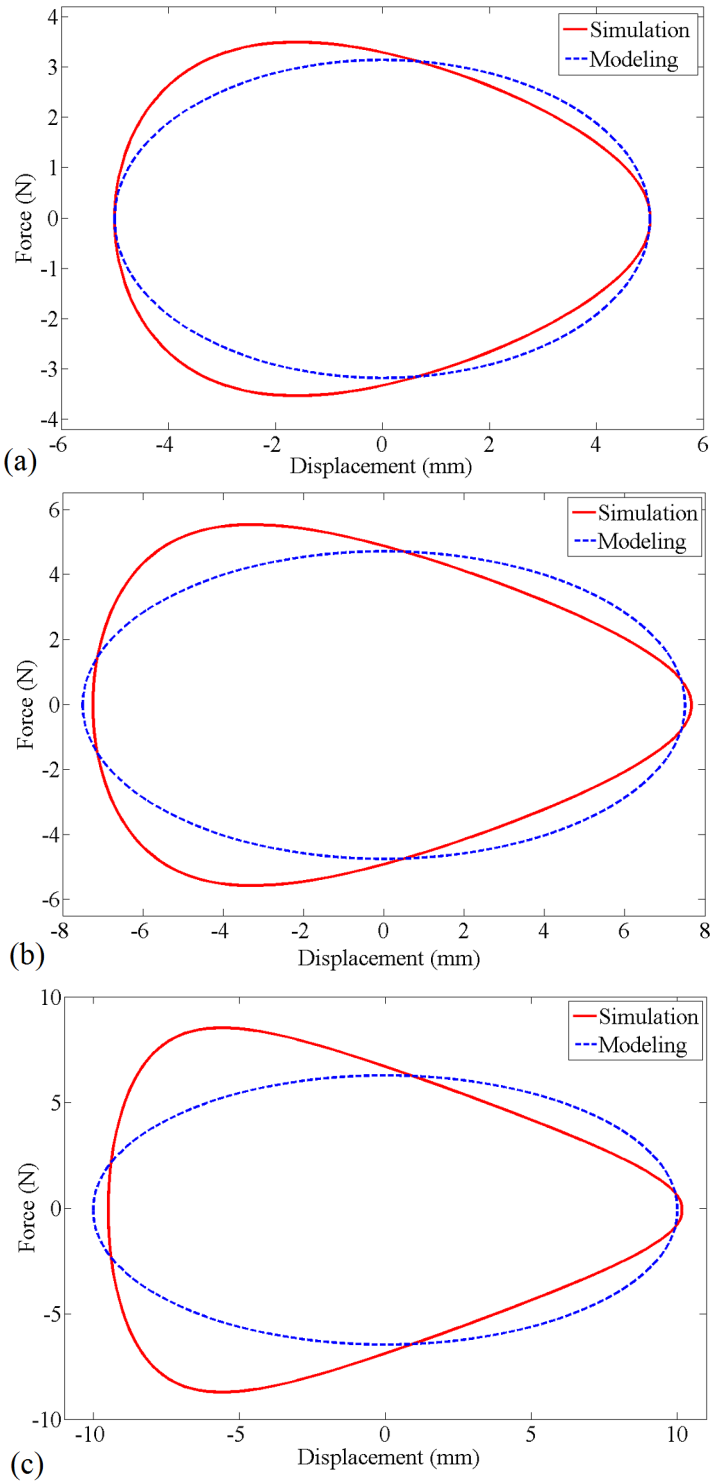

Figure 3.9: Simulation and modeling results of the force-displacement loops for the amplitude of (a) 5 mm, (b) 7.5 mm, (c) 10 mm.

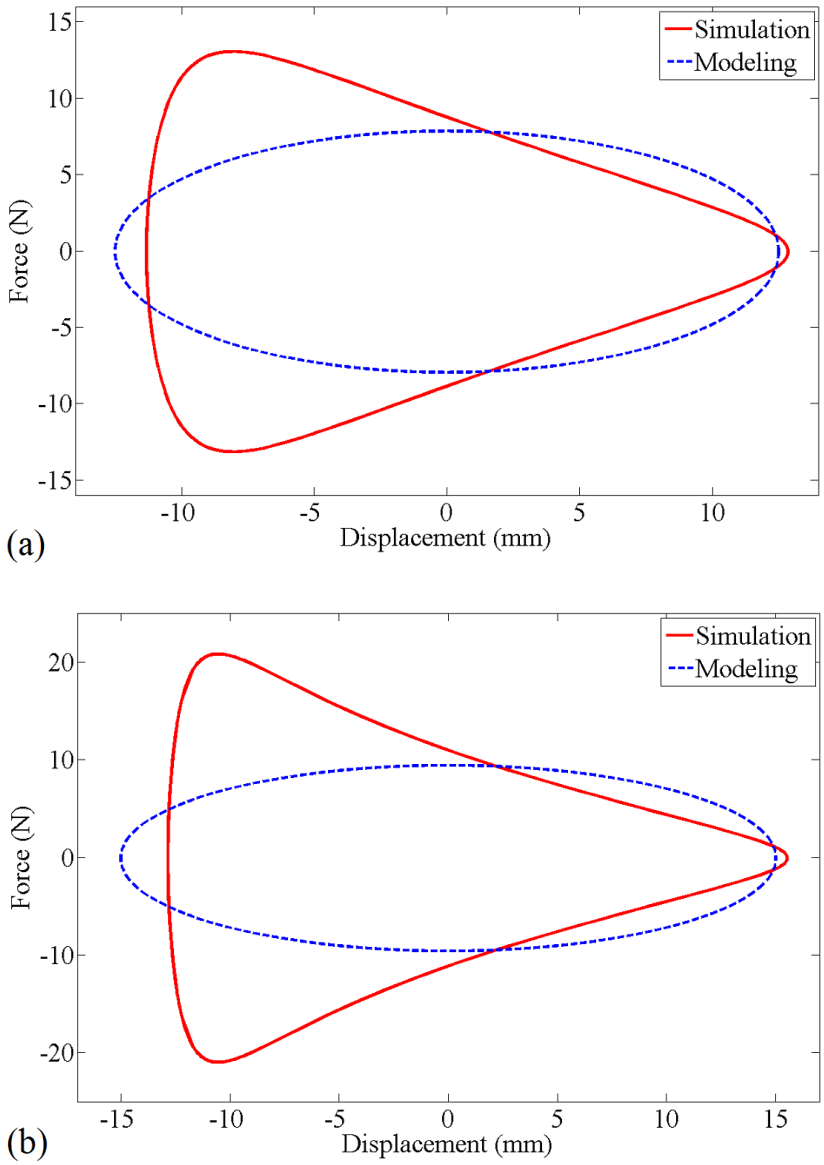

Figure 3.10: Simulation and modeling results of the force-displacement loops for the amplitude of (a) 12.5 mm, (b) 15 mm.

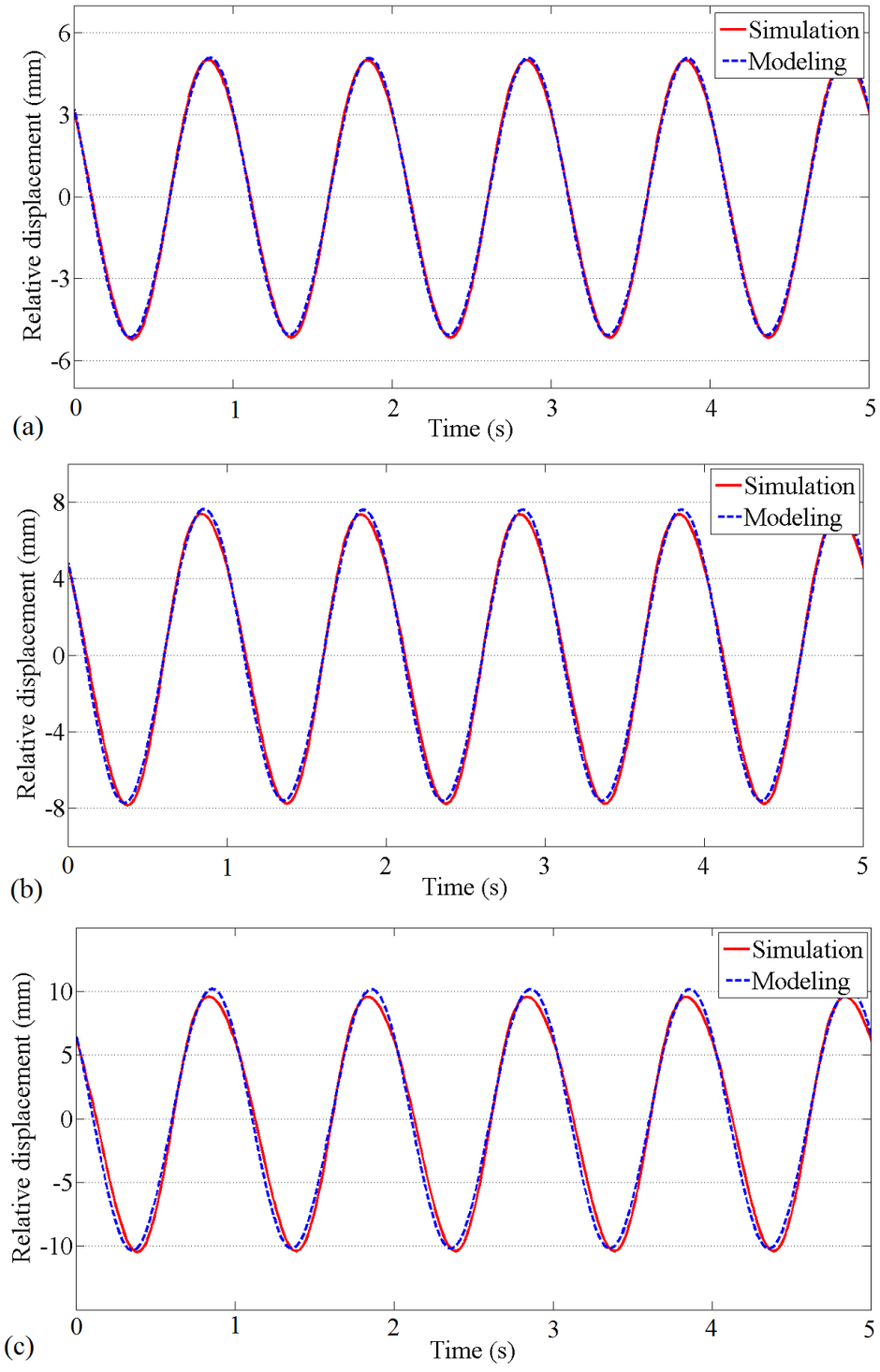

Figure 3.11: Simulation and modeling results in working area for the relative displacement of (a) 5 mm, (b) 7.5 mm, (c) 10 mm.

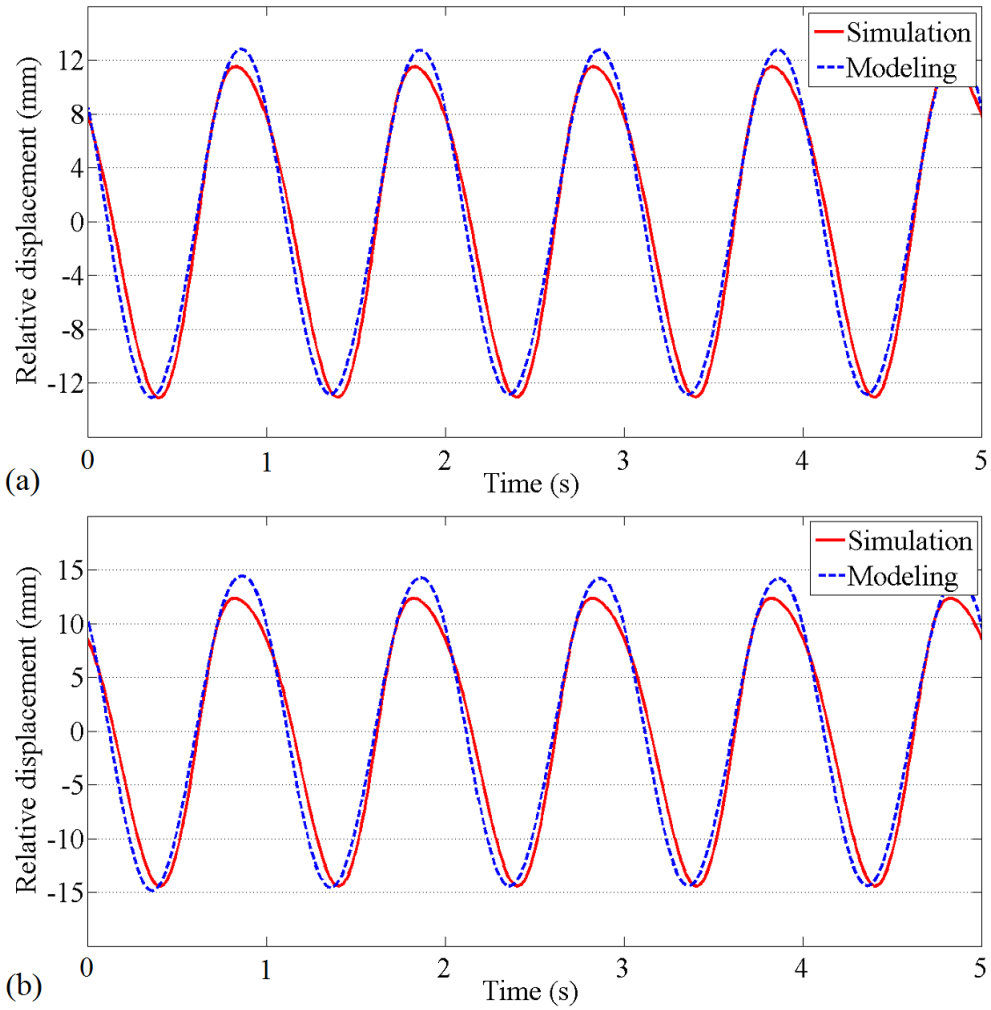

Figure 3.12: Simulation and modeling results in safety area for the relative displacement of (a) 12.5 mm, (b) 15 mm.

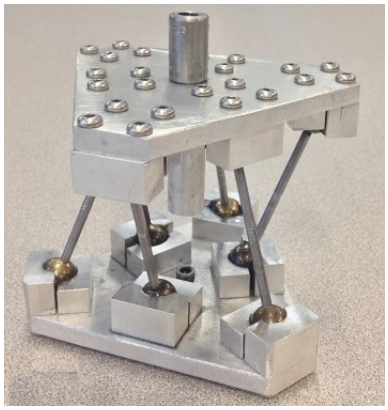

Figure 3.13: Physical model of the algebraic screw.

Table 3.4: Parameter values of the developed prototype.

Parameter	**Value**
Phase to phase resistance of the rotary machine, r	7.19 Ohm
Torque constant of the rotary machine, k_t	0.126 Nm/A
Rotor inertia of the rotary machine, I_r	$101 \times 10^{-7} kg.m^2$
Gearing ratio of the gearhead, n	4.3
Inertia of the gearhead, I_g	$12 \times 10^{-7} kg.m^2$
Algebraic screw leg length, l	5.9178 cm
Length of the triangle side of the algebraic screw , a	7.56 cm
Inertia of the algebraic screw plate, I_t	$0.6 \times 10^{-4} kg.m^2$
Mass of the algebraic screw plate, m_t	0.25 kg

Furthermore, the prototype of the regenerative shock absorber was tested using a mass-spring experimental setup shown in Figure 3.14. The experimental setup includes a sprung mass ($m_m = 6.3kg$), four parallel springs ($K = 6800N/m$) and a base connected to a hexapod. In the experimental setup, the hexapod (Mikrolar P2000) was used to shake the system, the displacement signal was measured by a displacement sensor (MLT Series 101.6 mm from Honeywell), and a dSPACE 1104 real-time board along with a host computer system was used for data acquisition and analysis. The main purpose of conducting experiments is to verify Equation 3.29. All of the parameters of Equation 3.29 are shown in Table 3.4 except c and R; as calculated in the previous section $c = 0.023m$, and R was changed for different sets of experiments as follows.

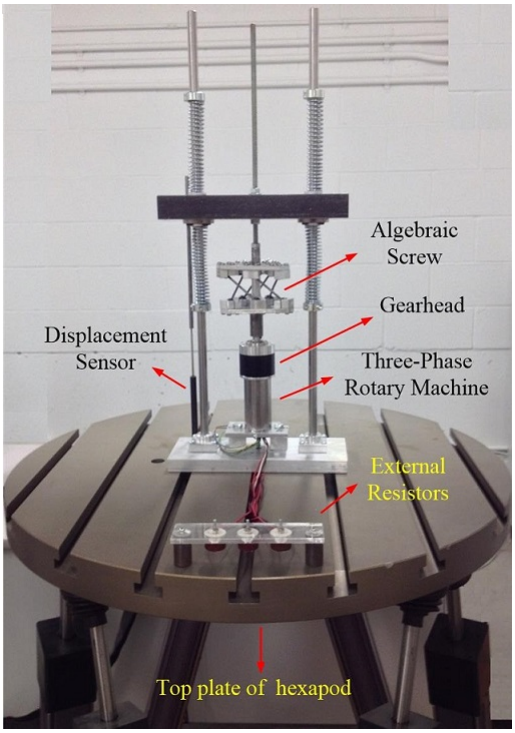

Figure 3.14: Mass-spring setup connected to the hexapod and the prototype.

•Linear Damping Coefficient for External Resistors of R = 5 Ω

Using Equation 3.29, the linear damping coefficient for R = 5 Ω is calculated as follows

$$B_{EPt(R=5)} = \frac{1.5 \times 4.3^2 \times 0.126^2}{0.023^2 \times (1.5 \times 7.19 + 5)} = 53N.s/m$$

By utilizing the setup shown in Figure 3.14, the linear damping coefficient will be obtained from experimental results. Since Equation 3.29 shows only the damping due to the electrical part of the shock absorber (not friction), the effect of friction should be excluded from experimental results. To this end, the experiments were conducted in three steps.

In the first step, the base was oscillated at a frequency of ω and an amplitude of Y_f in open circuit condition and amplitude of relative displacement, Z, was measured. Since the circuit is open, the only force that affects the system is friction and the obtained linear damping coefficient is due to friction. The frequency of the oscillation is 29.83 rad/s which is equal to the natural frequency of the system and the oscillation amplitude $Y_f = 0.9mm$ and corresponding

amplitude of relative displacement $Z = 4.6mm$ are shown in the first and second columns of Table 3.5. Using Equation 3.34 the linear damping coefficient due to friction, B_f, is calculated as follows and shown in the third column of Table 3.5.

$$B_f = \frac{m\omega Y_f}{Z} = \frac{6.55 \times 29.83 \times 0.0009}{0.0046} = 38N.s/m$$

Table 3.5: Experimental results for R=5 Ω corresponds to B_{EP}=53 N.s/m.

Y_f **(mm)**	Z **(mm)**	B_f **(N.s/m)**	Y_{f+EP} **(mm)**	B **(N.s/m)**	B_{EP} **(N.s/m)**
0.9	4.6	38	2.2	93	55
0.95	5.5	34	2.5	89	55
1	6.4	30.5	2.85	87	56.5

Equation 3.35 shows the equivalent viscous-damping coefficient due to friction

$$B_f = \frac{4\beta}{\pi\omega Z} \tag{3.35}$$

where β is the hysteretic damping constant [91], [92]. Referring to this equation, linear damping coefficient due to friction depends on excitation frequency, ω, and relative displacement, Z. This fact should be considered in the second step of the experiments.

In the second step, the external resistors were connected to the rotary machine and the previous procedure repeated. Therefore, the obtained linear damping coefficient, B, is due to friction and electrical part of the system. It should be noted that since the linear damping coefficient due to friction depends on excitation frequency and relative displacement, in this step the excitation frequency was kept equal to the excitation frequency of the first step (ω= 29.83 rad/s) and the base excitation amplitude, Y_{f+EP}, was increased such that the relative displacement did not change. The base excitation amplitude $Y_{f+EP} = 2.2mm$ is shown in the forth column of Table 3.5. Using Equation 3.34 the linear damping coefficient due to friction and electrical part of the system, B, is calculated as follows and shown in the fifth column of the table.

$$B_{f+EP} = \frac{m\omega Y_{f+EP}}{Z} = \frac{6.55 \times 29.83 \times 0.0022}{0.0046} = 93N.s/m$$

In the final step, first by rearranging Equation 3.26 we have

$$B_{EP} = B - B_f \tag{3.36}$$

Then, by using Equation 3.36, the linear damping coefficient due to electrical part of the system is calculated as follows and shown in the sixth column of the Table 3.5.

$$B_{EP} = 93 - 38 = 55 N.s/m$$

To decrease the error of the results, the mentioned experiment was repeated for $Y_f = 0.95$ mm and $Y_f = 1$ mm and the obtained results are shown in the third and forth rows of the Table 3.5. The average of the calculated linear damping coefficients due to electrical part, B_{EP}, was calculated and used to verify the theory.

$$B_{EPe(R=5)} = \frac{55 + 55 + 56.5}{3} = 55.5 N.s/m$$

Error between theoretical and experimental results is calculated as follows

$$Error_{(R=5)} = (\frac{55.5 - 53}{53}) \times 100 = 2.5\%$$

The relative displacement, Z, in open circuit condition and for the case that the rotary machine is connected to the external resistors are shown in Figure 3.15.

The previous set of experiments was repeated for external resistors of R = 10 Ω, R = 15 Ω, and R = 20 Ω. The following are the results of these sets of experiments.

•Linear Damping Coefficient for External Resistors of R = 10 Ω

$$B_{EPt(R=10)} = \frac{1.5 \times 4.3^2 \times 0.126^2}{0.023^2(1.5 \times 7.19 + 10)} = 40 N.s/m$$

Table 3.6: Experimental results for R=10 Ω corresponds to B_{EP}=40 N.s/m.

Y_f **(mm)**	Z **(mm)**	B_f **(N.s/m)**	Y_{f+EP} **(mm)**	B **(N.s/m)**	B_{EP} **(N.s/m)**
0.9	4.6	38	1.88	80	42
0.95	5.5	24	2.15	76	42
1	6.4	30.5	2.4	73	42.5

$$B_{EPe(R=10)} = \frac{42 + 42 + 42.5}{3} = 42.2 N.s/m$$

$$Error_{(R=10)} = (\frac{42.2 - 40}{40}) \times 100 = 5.5\%$$

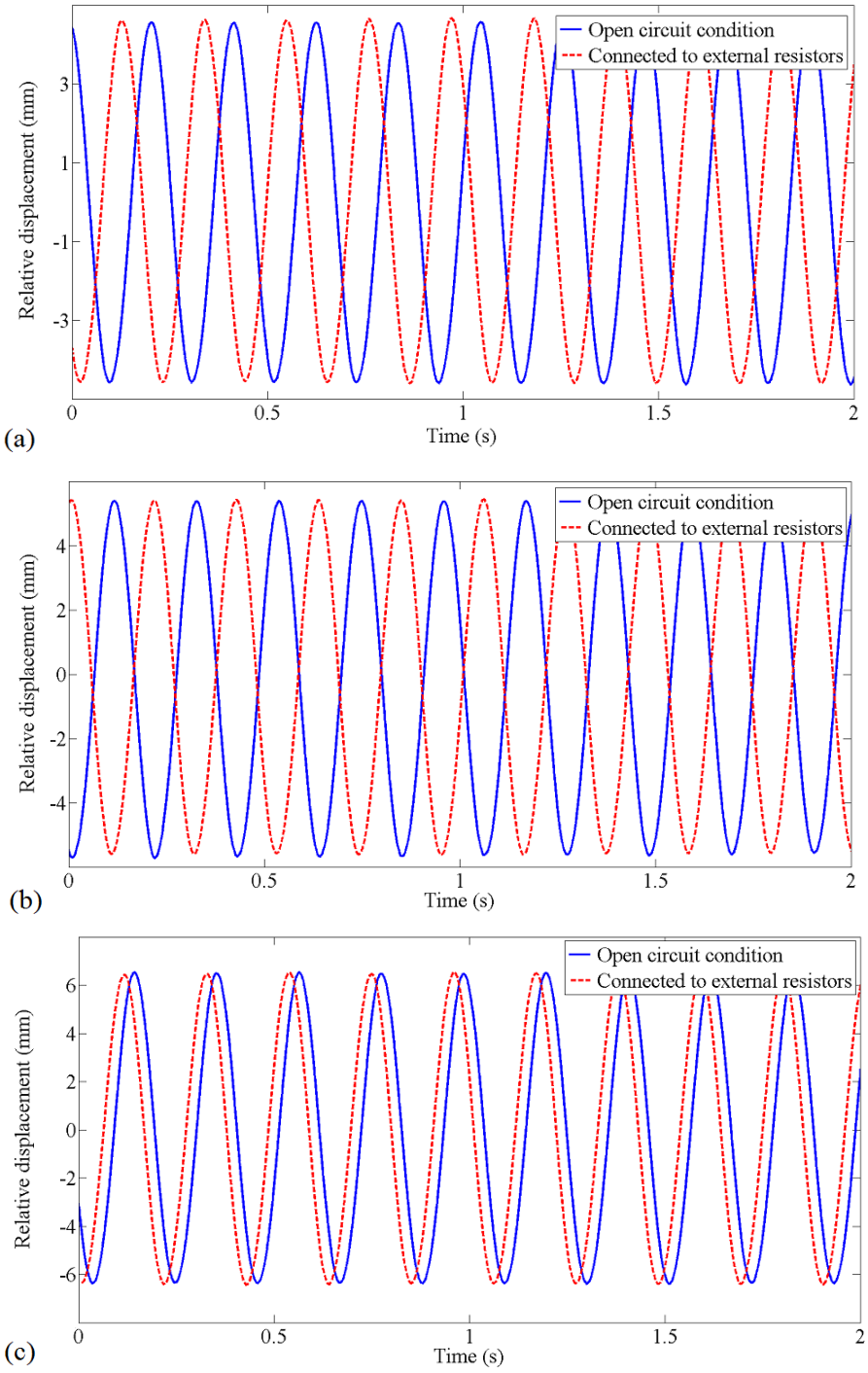

Figure 3.15: Relative displacement corresponding to (a) $Y_f = 0.9$ mm, (b) $Y_f = 0.95$ mm ,(c) $Y_f = 1$ mm in open circuit condition, and (a) $Y_{f+EP} = 2.2$ mm, (b) $Y_{f+EP} = 2.5$ mm ,(c) $Y_{f+EP} = 2.85$ mm for the case that the rotary machine is connected to external resistors of R=5Ω.

•Linear Damping Coefficient for External Resistors of R = 15 Ω

$$B_{EPt(R=15)} = \frac{1.5 \times 4.3^2 \times 0.126^2}{0.023^2(1.5 \times 7.19 + 15)} = 32N.s/m$$

Table 3.7: Experimental results for R=15 Ω corresponds to B_{EP}=32 N.s/m.

Y_f **(mm)**	Z **(mm)**	B_f **(N.s/m)**	Y_{f+EP} **(mm)**	B **(N.s/m)**	B_{EP} **(N.s/m)**
0.9	4.6	38	1.68	71	33
0.95	5.5	34	1.92	68	34
1	6.4	30.5	2.1	64	33.5

$$B_{EPe(R=15)} = \frac{33 + 34 + 33.5}{3} = 33.5N.s/m$$

$$Error_{(R=15)} = (\frac{33.5 - 32}{32}) \times 100 = 5\%$$

•Linear Damping Coefficient for External Resistors of R = 20 Ω

$$B_{EPt(R=20)} = \frac{1.5 \times 4.3^2 \times 0.126^2}{0.023^2(1.5 \times 7.19 + 20)} = 27N.s/m$$

Table 3.8: Experimental results for R=20 Ω corresponds to B_{EP}=27 N.s/m.

Y_f **(mm)**	Z **(mm)**	B_f **(N.s/m)**	Y_{f+EP} **(mm)**	B **(N.s/m)**	B_{EP} **(N.s/m)**
0.9	4.6	38	1.56	66	28
0.95	5.5	34	1.78	63	29
1	6.4	30.5	1.95	59.5	29

$$B_{EPe(R=20)} = \frac{28 + 29 + 29}{3} = 28.7N.s/m$$

$$Error_{(R=20)} = (\frac{28.7 - 27}{27}) \times 100 = 6\%$$

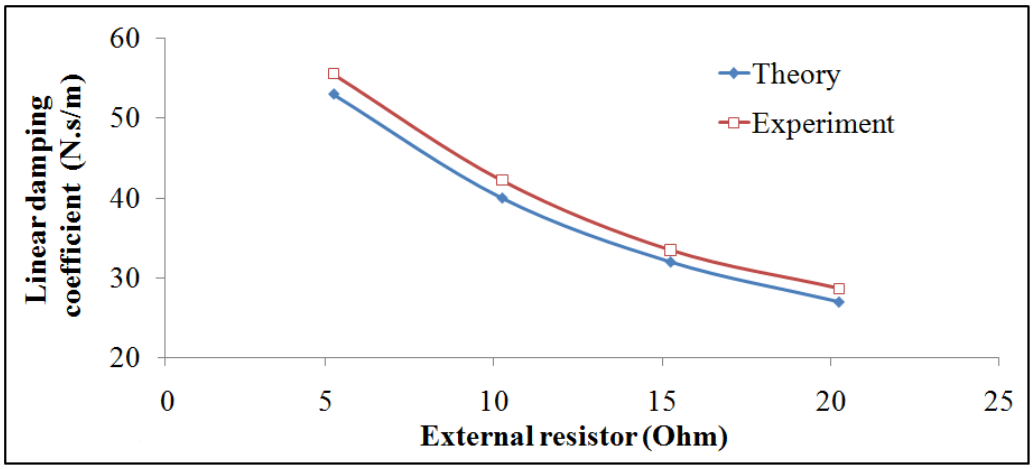

Figure 3.16: Experimental and theoretical results of the linear damping coefficient, B_{EP}, versus external resistor, R.

Figure 3.16 shows the experimental and theoretical results of the linear damping coefficient due to electrical part of the regenerative shock absorber.

Referring to Figure 3.16 there is a good match between experimental and theoretical results proving accuracy of Equation 3.29. The sources of small errors between experimental and theoretical results are as follows: measurements by the displacement sensor and data acquisition system, data reading, and lack of ability to recognize the exact natural frequency .These errors could be taken care of by using more precise devices and more developed softwares.

3.6 Summary and Conclusions

In this chapter, first the algebraic screw mechanism was introduced and a comprehensive formula describing the separation of the algebraic screw plates as a function of the rotation angle was derived. In addition collision between legs of the algebraic screw was studied. Then a proof of concept regenerative shock absorber using algebraic screw was studied; and the formula describing the linear damping coefficient provided by this system was derived. Furthermore, the accuracy of the model was evaluated by simulation and experimental results. Both results show good agreement with the analytical results.

Chapter 4

Regenerative Shock Absorber Using a Two-Leg Mechanism

4.1 Introduction

This chapter presents analysis, modeling, simulation and experimental results of a novel regenerative shock absorber, sized for a passenger car suspension system in terms of physical dimension and damping coefficient. This system consists of a simple and high efficient linear-to-rotary conversion mechanism called two-leg mechanism, a gearhead, and an AC rotary machine connected to three external resistors (to simulate the effect of a three phase charging circuit). There are three main differences between the work presented in this chapter and the proof of concept regenerative shock absorber using an algebraic screw, presented in the previous chapter. First, in this chapter a two-leg mechanism is used as the motion converter device which is simpler, has smaller dimensions, and bigger collision angle compared to the algebraic screw mechanism. Secondly, in this chapter the regenerative shock absorber is designed for a passenger car suspension system in terms of size and damping coefficient, while in the previous chapter size was not considered and the provided damping coefficient was small. Third, in this chapter the efficiency of the shock absorber is analyzed and evaluated through experiments.

The regenerative shock absorber presented in this chapter is shown in Figure 4.1. It consists of three main parts: a two-leg mechanism, a gearhead, and an AC brushless permanent magnet rotary machine. The performance of each of these parts can be explained from two perspectives: energy regeneration and damping. From energy regeneration perspective, the two-leg

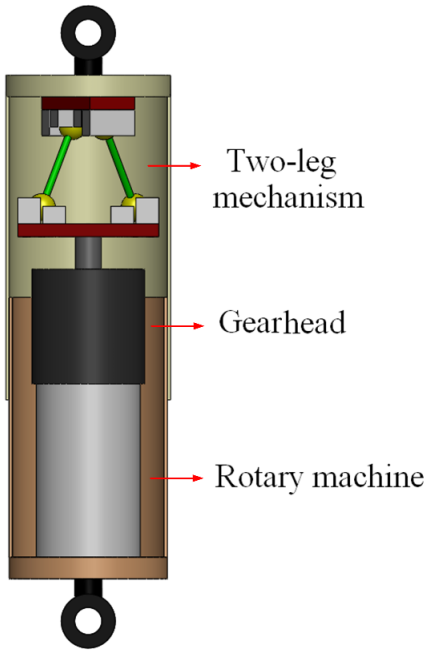

Figure 4.1: Designed regenerative shock absorber.

mechanism converts translational motion due to road roughness into rotary motion. Then the planetary gearhead increases the rotary motion amplitude, resulting in a higher voltage at the output of the generator. Finally, the generator and charging circuit perform energy conversion and save energy in a battery. From the damping perspective, the rotary machine connected to a charging circuit provides rotary damping, then this damping is increased through the gearhead, and at the end the two-leg mechanism converts the rotary damping to linear one needed for the suspension system.

The organization of this chapter is as follows. Section 4.2 describes the kinematic design of the linear-to-rotary motion converter, referred to as the two-leg mechanism. The dynamics of the regenerative shock absorber is studied in Section 4.3. Section 4.4 provides an analysis of the power and efficiency of the proposed system. Simulation results are provided in Section 4.5. Experimental results about the linear damping coefficient and efficiency of the shock absorber are presented in Section 4.6. Summery and conclusions are presented in Section 4.7.

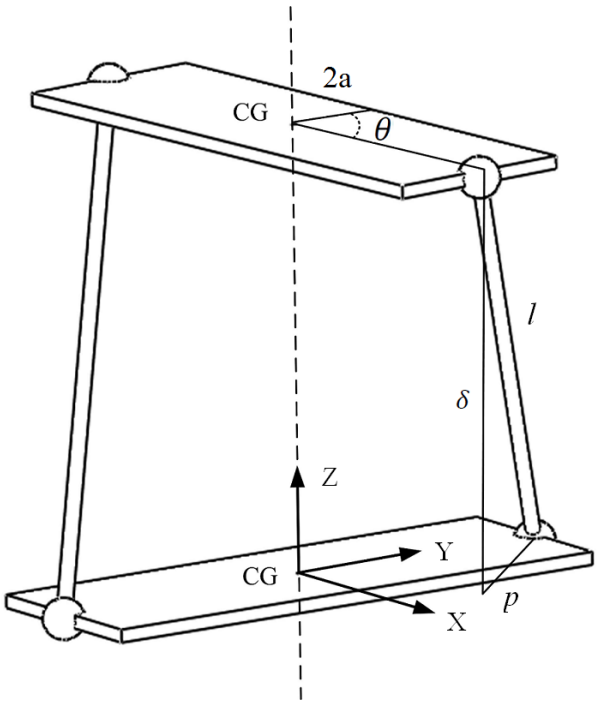

Figure 4.2: Schematic diagram of the two-leg mechanism.

4.2 Kinematic Analysis of the Two-Leg Mechanism

The two-leg mechanism presented in this section converts translational motion due to vibrations into rotary motion. This kinematic mechanism consists of two rectangular plates, connected to each other via two legs, as shown in Figure 4.2.

Referring to Figure 4.2, let us obtain a formula describing the separation distance of plates, δ, as a function of the rotation angle, θ. From Figure 4.2, we have

$$l^2 = \delta^2 + p^2 \tag{4.1}$$

where δ is the projection of l on the Z axis and p is the projection of l on the XY plane. Furthermore, considering Figure 4.3, the projection of p on the X and Y axes as a function of the rectangle length, $2a$, and rotation angle θ are given by

$$p_X = asin\theta, \quad p_Y = a - acos\theta. \tag{4.2}$$

Utilizing the geometrical relationship $p^2 = p_X^2 + p_Y^2$ results in

$$p^2 = 2a^2(1 - cos\theta). \tag{4.3}$$

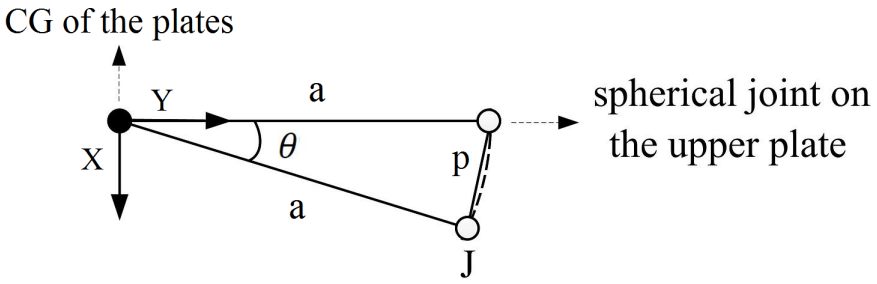

Figure 4.3: Projections of p on X and Y axes.

Substituting (4.3) in (4.1) yields

$$\delta = \sqrt{l^2 - 2a^2(1 - cos\theta)}. \tag{4.4}$$

From (4.4), when $\theta = 0$ the two-leg mechanism is fully extended and δ reaches its maximum value.

Since the force applied by a linear shock absorber is proportional to the speed between two sides of the shock absorber, and the two-leg mechanism is used as a linear-to-rotary converter in the suggested regenerative shock absorber, it is necessary to obtain the relationship between the translation and rotary speeds of the two plates of the two-leg mechanism. This relationship will be used in Section 4.3 and explained in details. To this end, taking a derivative of (4.4) and performing some algebraic manipulations, yield

$$\dot{\delta} = -\frac{a^2 sin\theta}{\sqrt{l^2 - 2a^2(1 - cos\theta)}}\dot{\theta}. \tag{4.5}$$

Equation 4.5 describes a nonlinear kinematic relationship between the translational and rotary speeds of the two plates in the two-leg mechanism.

Let us define the relative linear and rotary motions by $\tilde{\delta}$ and $\tilde{\theta}$, respectively, as follows

$$\delta - \delta_0 = \tilde{\delta} \tag{4.6}$$

$$\theta - \theta_0 = \tilde{\theta} \tag{4.7}$$

where δ_0 and θ_0 are the static equilibrium points of δ and θ, respectively. Substituting (4.6) and (4.7) into (4.4), linearization about θ_0, and taking a derivative result in

$$\dot{\delta} = -c\dot{\theta} \tag{4.8}$$

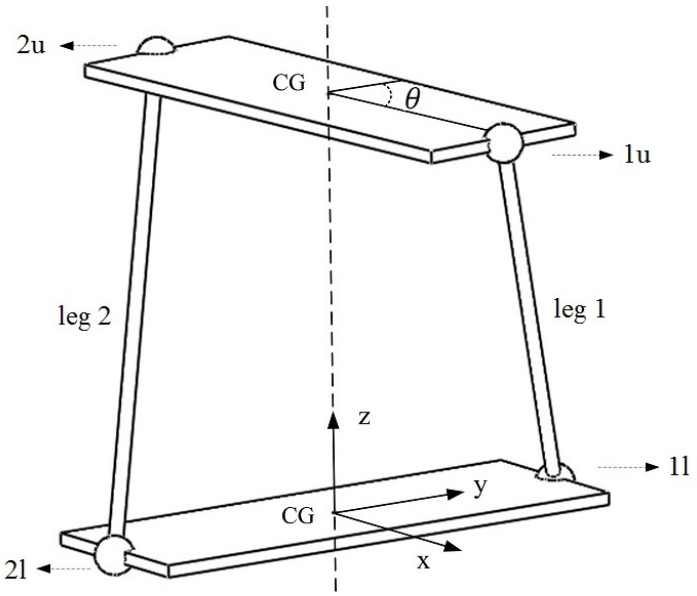

Figure 4.4: Schematic diagram of the two-leg mechanism to analyze collision.

where c is the slope of the nonlinear relationship between $\dot{\delta}$ and $\dot{\theta}$ given by

$$c = \frac{a^2 sin\theta_0}{\delta_0}. \tag{4.9}$$

The process of linearization and taking derivative of (4.4) is presented in Appendix B.

Equations 4.5 and 4.8 will be utilized in Section 4.3 to obtain the formula describing the linear damping coefficient provided by the regenerative shock absorber.

4.2.1 Collision between legs of two-leg mechanism

To find the collision angle, a coordinate system is attached to the centroid of the lower plate of the two-leg mechanism shown in Figure 4.4, then the coordinates of midpoints of the legs are obtained in this coordinate system, the angle in which these two midpoints become coincident is the collision angle, θ_c. In Figure 4.4 the legs of the two-leg mechanism and their spherical joints are shown. The notations used in this figure and their meanings are as follows:

1u : Spherical joint of the leg **1** on the **upper** plate

1l : Spherical joint of the leg **1** on the **lower** plate

2u : Spherical joint of the leg **2** on the **upper** plate

2l : Spherical joint of the leg **2** on the **lower** plate

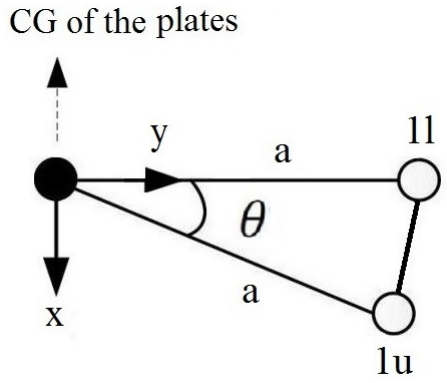

Figure 4.5: Projection of leg 1 on xy plane, and its relationship with the length of the rectangular plates and rotation angle.

Projection of leg 1 on xy plane, and its relationship with the length of the rectangular plates and rotation angle are shown in Figure 4.5. Considering Figure 4.4 and Figure 4.5, for the spherical joints 1l and 1u we have

$$x_{1l} = 0$$
$$y_{1l} = a$$
$$z_{1l} = 0$$

$$x_{1u} = asin\theta$$
$$y_{1u} = acos\theta$$
$$z_{1u} = \delta$$

Then, the coordinate of the midpoint of leg 1 is calculated as follows

$$x_{1m} = \frac{x_{1l} + x_{1u}}{2} = \frac{a}{2}sin\theta$$
$$y_{1m} = \frac{y_{1l} + y_{1u}}{2} = \frac{a}{2} + \frac{a}{2}cos\theta$$
$$z_{1m} = \frac{z_{1l} + z_{1u}}{2} = \frac{\delta}{2}$$

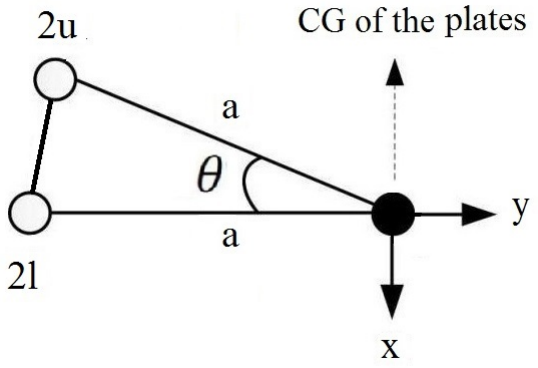

Figure 4.6: Projection of leg 2 on xy plane, and its relationship with the length of rectangular plates and rotation angle.

Projection of leg 2 on xy plane, and its relationship with the length of the rectangular plates and rotation angle are shown in Figure 4.6. Considering Figure 4.4 and Figure 4.6, for the spherical joints 2l and 2u we have

$$x_{2l} = 0$$
$$y_{2l} = -a$$
$$z_{2l} = 0$$

$$x_{2u} = -asin\theta$$
$$y_{2u} = -acos\theta$$
$$z_{2u} = \delta$$

Then, the coordinate of the midpoint of leg 2 is calculated as follows

$$x_{2m} = \frac{x_{2l} + x_{2u}}{2} = -\frac{a}{2}sin\theta$$
$$y_{2m} = \frac{y_{2l} + y_{2u}}{2} = -\frac{a}{2} - \frac{a}{2}cos\theta$$
$$z_{2m} = \frac{z_{2l} + z_{2u}}{2} = \frac{\delta}{2}$$

Finally, by equalizing the the coordinates of midpoints of leg 1 and leg 2 the collision angle is obtained as follows

$$x_{1m} = x_{2m} \Rightarrow \theta_c = 180$$
$$y_{1m} = y_{2m} \Rightarrow \theta_c = 180$$
$$z_{1m} = z_{2m} \Rightarrow \theta_c = anyangle$$

As it can be seen the collision angle is $\theta_c = 180$. It should be noted that in our analysis to calculate the collision angle, the diameter of each leg was assumed to be zero. Therefore the obtained collision angle, $\theta_c = 180$, is the theoretical collision angle. To avoid collision between legs in practical applications of the two-leg mechanism, first the theoretical collision angle should be used as the criterion, then by considering the diameter of legs and manufacturing limits the practical collision angle can obtained.

As mentioned before, the collision angle between each two adjacent legs of the algebraic screw is 120, while the collision angle between legs of two-leg mechanism is 180. The bigger rotation angle for a fixed translational motion helps the regenerative shock absorber to have a higher efficiency; this point will be explained in details in Section 4.3.

4.3 Dynamics of the Regenerative Shock Absorber

The main functionality of a shock absorber in a suspension system is to provide a damping force to the system characterized by linear damping coefficient. In this section, an analytical expression describing the linear damping coefficient provided by the regenerative shock absorber is derived. It should be noted that, the obtained linear damping coefficient in this section includes the effect of electrical part of the shock absorber and friction of different parts of the shock absorber together.

One method of evaluating the functionality of a shock absorber is to excite it by a sinusoidal displacement and obtain the force-displacement loops [91]. In this section, performance of the suggested regenerative shock absorber under sinusoidal excitation is discussed, then obtained analytical results will be used to verify the experimental results obtained in Section 4.6.

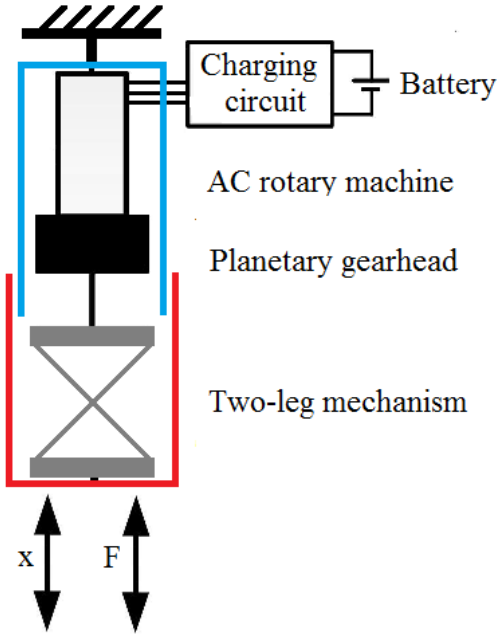

Figure 4.7: The regenerative shock absorber under sinusoidal excitation.

4.3.1 Linear Damping Coefficient Provided by the Regenerative Shock Absorber

To obtain the linear damping coefficient, B_L, of the device, consider Figure 4.7 which depicts the regenerative shock absorber excited by displacement x from equilibrium point. The input power to the shock absorber, P_{input}, is given by

$$P_{input} = B_L \dot{x}^2 \tag{4.10}$$

where $\dot{x}$ is the excitation speed. The input power is split into two parts as follows. The term $P_{lost(f)}$ is the power loss due to friction in the two-leg mechanism, planetary gearhead and rotary machine; and the term P_E is the power at the AC generator connected to the charging circuit. Therefore, we have

$$\eta_{tl}\eta_{gh}\eta_g P_{input} = P_E \tag{4.11}$$

where η_{tl} is the efficiency of the two-leg mechanism, η_{gh} is the efficiency of the gearhead, and η_g is the efficiency of the generator. It should be noted that, as the casting and two-leg mechanism work together to provide motion conversion, the friction effect of the casting is considered in two-leg mechanism efficiency.

Substituting (4.10) and (2.21) into (4.11) results in

$$\eta_{tl}\eta_{gh}\eta_g B_L \dot{x}^2 = B_R \dot{\gamma}^2. \tag{4.12}$$

The relationship between $\dot{\gamma}$ and $\dot{\theta}$ is given by

$$\dot{\gamma} = n\dot{\theta} \tag{4.13}$$

where n is the gear ratio of the planetary gearhead. Since the displacement x is measured from equilibrium point, we have

$$x = \delta - \delta_0. \tag{4.14}$$

Differentiating (4.14) with respect to time results in

$$\dot{x} = \dot{\delta}\cdot \tag{4.15}$$

Substituting (4.5) into (4.15) yields

$$\dot{x} = -\frac{a^2 sin\theta}{\sqrt{l^2 - 2a^2(1 - cos\theta)}}\dot{\theta}\cdot \tag{4.16}$$

Substituting (4.13) and (4.16) in (4.12) and performing some algebraic manipulations result in

$$B_L = \frac{[l^2 - 2a^2(1 - cos\theta)]n^2 B_R}{\eta_{tl}\eta_{gh}\eta_g a^4 sin^2\theta}. \tag{4.17}$$

Using the linear approximation given by (4.8) we have

$$B_L = \frac{n^2 B_R}{\eta_{tl}\eta_{gh}\eta_g c^2}. \tag{4.18}$$

Substituting (2.22) in (4.18) yields

$$B_L = \frac{1.5 \times n^2 {k_t}^2}{\eta_{tl}\eta_{gh}\eta_g c^2 (R + r)}. \tag{4.19}$$

Equation 4.19 describes the linear damping coefficient, B_L, provided by the shock absorber. According to (4.19), c and η_{tl} are the parameters related to the two-leg mechanism; n and η_{gh} are the effects of gearhead; k_t, r, and η_g are generator parameters; and R is the effect of the charging circuit.

It should be noted that, the difference between Equation 4.19 and Equation 3.29 is the friction effect of two-leg mechanism, gearhead, and generator on linear damping coefficient which is covered by term $\eta_{tl}\eta_{gh}\eta_g$ in Equation 4.19.

4.3.2 Regenerative Shock Absorber Under Sinusoidal Vibration

In this section, the kinematics and dynamics of the proposed system under sinusoidal displacement are presented; and the obtained results will be utilized to analyze experimental data reported in Section 4.6. Referring to Figure 4.7 and using the Lagrangian formulation, the equation of motion for the system is obtained as follows

$$\frac{d}{dt}(\frac{\partial T}{\partial \dot{x}}) - (\frac{\partial T}{\partial x}) + \frac{\partial U}{\partial x} + \frac{\partial R_D}{\partial \dot{x}} = F \tag{4.20}$$

where x is the displacement, F is the force provided by the shaker, and T, R_D are the energies due to kinetic and damping effects, respectively. The term T is given by

$$T = \frac{1}{2}m_c\dot{x}^2 + \frac{1}{2}m_t\dot{x}^2 + \frac{1}{2}I_t\dot{\theta}^2 + \frac{1}{2}I_g\dot{\theta}^2 + \frac{1}{2}I_r\dot{\gamma}^2 \tag{4.21}$$

where m_c is the mass of the casting; m_t and I_t are the mass and moment of inertia of the two-leg mechanism, respectively; and I_g, I_r are the moments of inertia of the gearhead and the rotary machine, respectively. Rearranging (4.16) and substituting (4.13) and (4.16) in (4.21) leads to

$$T = \frac{1}{2}(m_c + m_t)\dot{x}^2 + (I_t + I_g + n^2I_r)\frac{l^2 - 2a^2(1-\cos\theta)}{a^4 sin^2\theta}\dot{x}^2. \tag{4.22}$$

Using the linear approximation given by (4.8) results in

$$T = \frac{1}{2}(m_c + m_t + \frac{I_t + I_g + n^2I_r}{c^2})\dot{x}^2. \tag{4.23}$$

Let us define m_{eq} as

$$m_{eq} = (m_c + m_t + \frac{I_t + I_g + n^2I_r}{c^2}). \tag{4.24}$$

Substituting (4.24) in (4.23) yields

$$T = \frac{1}{2}m_{eq}\dot{x}^2. \tag{4.25}$$

The damping effect R_D is given by

$$R_D = \frac{1}{2}B_L\dot{x}^2. \tag{4.26}$$

Hence, substituting (4.25) and (4.26) in (4.20) leads to

$$m_{eq}\ddot{x} + B_L\dot{x} = F. \tag{4.27}$$

By considering the displacement function as follows

$$x = X \sin \omega t \tag{4.28}$$

the acceleration is obtained as

$$\ddot{x} = -\omega^2 X \sin \omega t = -\omega^2 x \tag{4.29}$$

Hence, substituting (4.29) in (4.27) yields

$$-m_{eq}\omega^2 x + B_L \dot{x} = F \tag{4.30}$$

Equation 4.30 describes the motion of the shock absorber under sinusoidal base excitation. In this equation, the coefficient of x is the equivalent stiffness defined by

$$K_{eq} = -m_{eq}\omega^2 \tag{4.31}$$

Referring to (4.31), the mass and inertia of moving parts of the shock absorber, represented by m_{eq}, result in a frequency dependent equivalent stiffness term given by K_{eq}. This phenomenon is observed in experimental results presented in Section 4.6.

4.4 Power and Efficiency Analysis

The objective of this section is to investigate the influence of system parameters on the power output and efficiency of the system. The amount of input power of the shock absorber is given by

$$P_{input} = B_L \dot{x}^2. \tag{4.32}$$

The portion of input power that is lost due to friction in the two-leg mechanism, gearhead, and generator is given by

$$P_{lost(f)} = (1 - \eta_{tl}\eta_{gh}\eta_g)P_{input}. \tag{4.33}$$

By defining the mechanical efficiency as

$$\eta_{Mech} = \eta_{tl}\eta_{gh}\eta_g \tag{4.34}$$

and substituting (4.34) into (4.33) we have

$$P_{lost(f)} = (1 - \eta_{Mech})P_{input}. \tag{4.35}$$

The remaining component of input power, i.e., electrical power, that reaches the generator and charging circuit is obtained as follows

$$P_E = \eta_{Mech} P_{input}. \tag{4.36}$$

The electrical power is split into two parts. One part is lost in the internal resistance of the generator and the other part is captured by the charging circuit. Therefore, we have

$$P_E = P_{captured(R)} + P_{lost(r)}. \tag{4.37}$$

Referring to Figure 2.2, the portion of power captured in the charging circuit is calculated as follows

$$P_{captured(R)} = Ri_1^2 + Ri_2^2 + Ri_3^2 \tag{4.38}$$

in which

$$\begin{aligned} i_1 &= I_m \cos(\omega_e t - 120) \\ i_2 &= I_m \cos(\omega_e t) \\ i_3 &= I_m \cos(\omega_e t + 120) \end{aligned} \tag{4.39}$$

where I_m is the amplitude of the current. Substituting (4.39) into (4.38) results in

$$P_{captured(R)} = 1.5 \times RI_m^2. \tag{4.40}$$

Using the same procedure, the power lost in the internal resistance of the generator is calculated as

$$P_{lost(r)} = 1.5 \times rI_m^2. \tag{4.41}$$

Therefore, the electrical efficiency of the shock absorber is obtained as follows

$$\eta_{Elec} = \frac{P_{captured(R)}}{P_{captured(R)} + P_{lost(r)}} = \frac{R}{R+r}. \tag{4.42}$$

Considering the mechanical efficiency η_{Mech} and electrical efficiency η_{Elec}, the total efficiency of the regenerative shock absorber is obtained as follows

$$\eta_{RSA} = \eta_{Mech}\eta_{Elec}. \tag{4.43}$$

The obtained results in this section will be used in Section 4.6 to pick appropriate parts for the suggested regenerative shock absorber and to evaluate the experimental results.

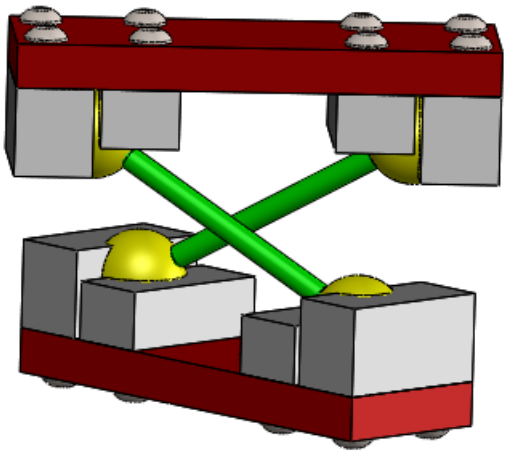

Figure 4.8: Designed prototype of the two-leg mechanism.

4.5 Simulation Results

The purpose of this section is to evaluate the functionality of the suggested regenerative shock absorber as a part of a quarter car with the parameters shown in Table 3.2. To this end, a Simulink model of a quarter car shown in Figure 3.6 was developed using the SimMechanics toolbox of MATLAB. The procedure of developing the Simulink model is similar to the procedure explained in Section 3.4 with the following differences.

To avoid collision between legs, by utilizing theoretical collision angle which is 180 degrees (discussed in Section 4.2.1) and considering the manufacturing limits and diameter of each leg, the practical rotation angle between the two-leg mechanism plates is obtained to be 150 degrees.

By utilizing Equation 4.4, and considering the working and safety areas (explained in Section 3.4), the two-leg mechanism is designed to convert 3 cm of peak-to-peak translational motion (2×1.5 cm of stroke) into 150 degrees of rotation, providing a motion range of $\delta_1 = 1.5$ cm to $\delta_2 = 4.5$ cm. Table 4.1 shows the dimensions of the designed two-leg mechanism.

For the above motion range of two-leg mechanism, the static operating point is calculated as $\delta_0 = \frac{1.5+4.5}{2} = 3$ cm. By using Equation 4.4, the corresponding rotation angle to the static operating point is calculated equal to $\theta_0 = 105$ degrees. Figure 4.9 illustrates the nonlinear mapping and its linearized approximation around the operating point in the working and safety areas of the device.

By substituting parameters of the two-leg mechanism shown in Table 4.1, and information of static equilibrium point of the two-leg mechanism in Equation 4.9, the slope of the nonlinear

Table 4.1: Dimensions of the designed two-leg mechanism.

Parameter	Value
Two-leg mechanism leg length, l	4.5 cm
Two-leg mechanism rectangle length , $2a$	4.3 cm

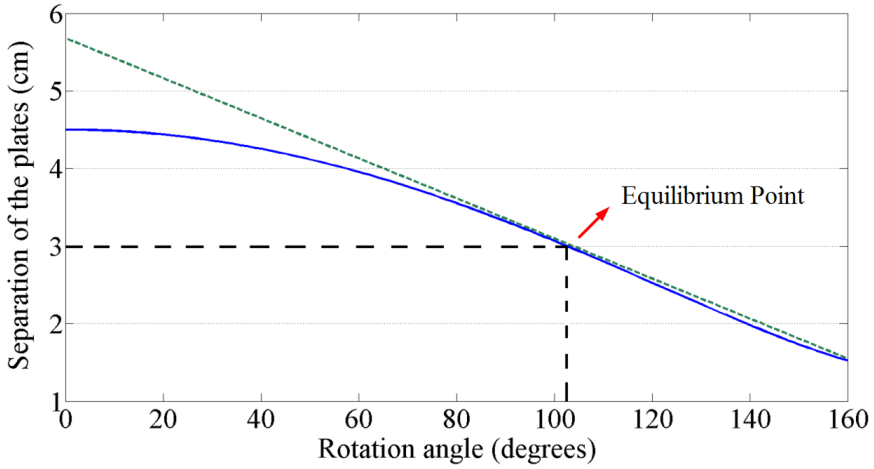

Figure 4.9: Nonlinear and linear mapping around the operating point describing the separation of the two-leg mechanism plates, δ, versus rotation angle, θ.

relationship between $\dot{\delta}$ and $\dot{\theta}$ is calculated as follows

$$c = \frac{a^2 sin\theta_0}{\delta_0} = \frac{0.0215^2 \times sin105}{0.03} = 0.0148cm$$

This parameter will be used to calculate the linear damping coefficient provided by the shock absorber.

By utilizing the dimensions of the designed two-leg mechanism provided in Table 4.1, a Simulink model of this device was developed. To complete the Simulink model of the regenerative shock absorber, a gearhead with a gearing ratio of 26:1 and a rotary damper with rotary damping coefficient of $B_R = 0.000486N.m.s$ (instead of the rotary machine connected to the charging circuit discussed in Section 2.3) was added to the model. Using Equation 4.18 and by ignoring the friction in the system which means $\eta_{tl}\eta_{gh}\eta_g = 1$, the linear damping coefficient provided by the model is calculated as follows

$$B_L = \frac{26^2 \times 0.000486}{0.0148^2} = 1500N.s/m$$

At the end, by adding the mass ($m_m = 450kg$) and the spring ($K = 30000N/m$) the one-degree-of-freedom (1-DOF) model of a quarter was completed.

By applying different base excitation profiles, the Simulink model was evaluated in working and safety areas and the results are shown in Figure 4.10 to Figure 4.13. In these figures, modeling refers to a quarter car system in which a linear shock absorber with a fixed damping coefficient of $B = 1500N.s/m$ was used and simulation refers to the explained Simulink model of the quarter car in which the suggested regenerative shock absorber was used.

As it can be seen in Figures 4.10 and 4.11, modeling and simulation results of force-displacement loops do not match, which is due to nonlinearity of the two-leg mechanism. However, as explained before, our main focus would be on the results of relative displacement. Figure 4.12 shows that the modeling and simulation results completely agree. Considering that in both systems, mass, stiffness coefficient, and base excitation profile are the same, it can be concluded that the suggested regenerative shock absorber can work properly in working area. By considering Figure 4.13, showing the system in the safety area, it is noticed that simulation results show smaller relative displacements compare to the modeling results at the positive stroke. One should consider two points: First, the Simulink model of the regenerative shock absorber utilizing the designed prototype shown in Figure 4.8, includes nonlinearity of the two-leg mechanism but the modeling is based on the linear approximation provided by Equation 4.9. Hence, the difference between simulation and modeling results is due to the difference between nonlinear and linear mappings shown in Figure 4.9. Secondly, this difference means error=$\frac{12.5-11.7}{12.5} \times 100 = 6.5\%$ for the stroke of 12.5 mm and error=$\frac{15-13.5}{15} \times 100 = 10\%$ for the stroke of 15 mm; considering that a shock absorber rarely works in safety area and these errors are small enough, they can be ignored for the application of usual passenger cars.

Regarding the simulation results, it should be noted that, in the quarter car the proposed shock absorber works along with a mass and a spring. Since the mass and spring are linear parts, they eliminate some of the nonlinear terms of the damping force originated from the two-leg mechanism. Thus, the obtained results are correct only for the combination of mass, stiffness coefficient and damping coefficient shown in Table 3.2. For any other combination simulation should be repeated.

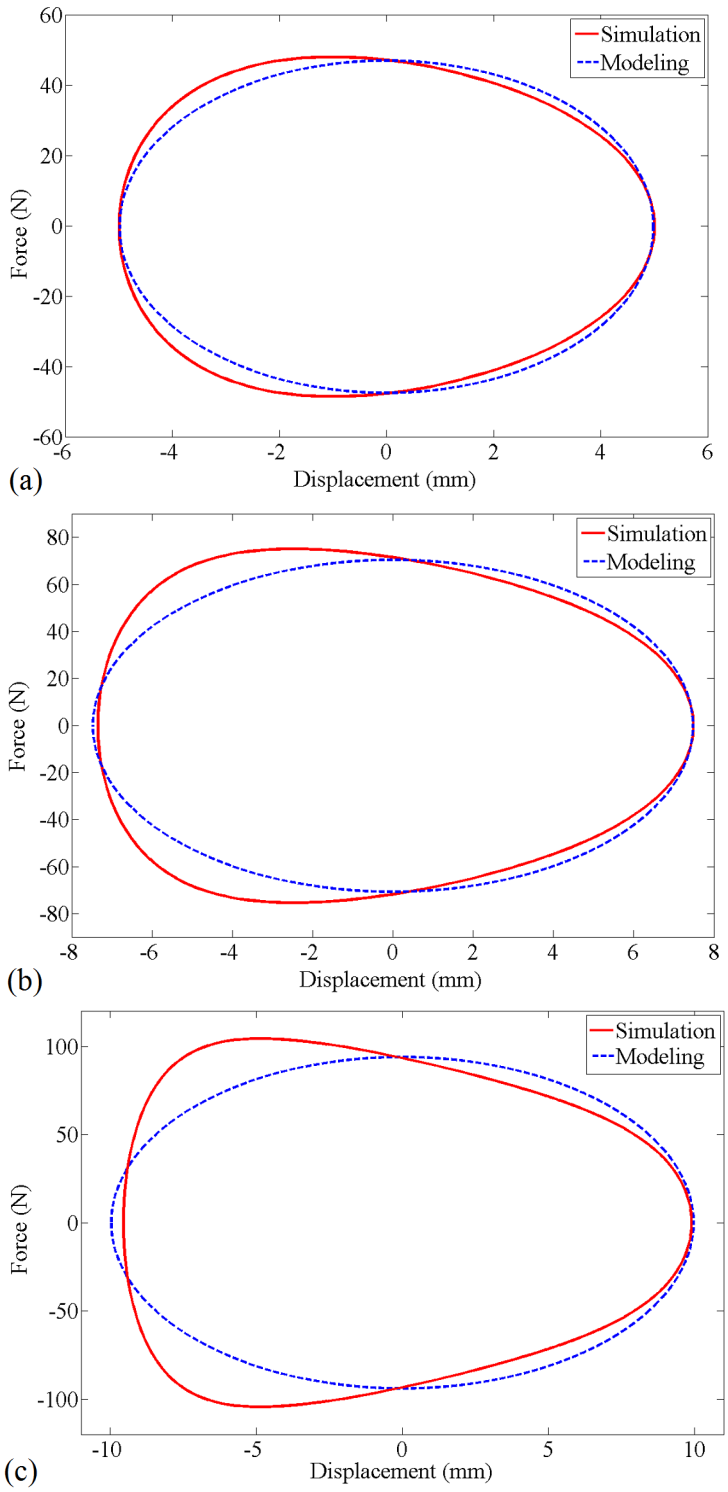

Figure 4.10: Simulation and modeling results of the force-displacement loops for the amplitude of (a) 5 mm, (b) 7.5 mm, (c) 10 mm.

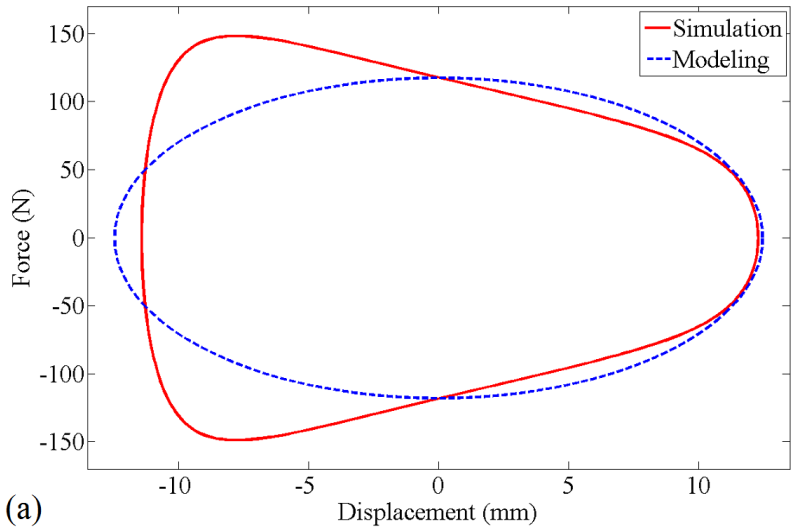

Figure 4.11: Simulation and modeling results of the force-displacement loops for the amplitude of (a) 12.5 mm, (b) 15 mm.

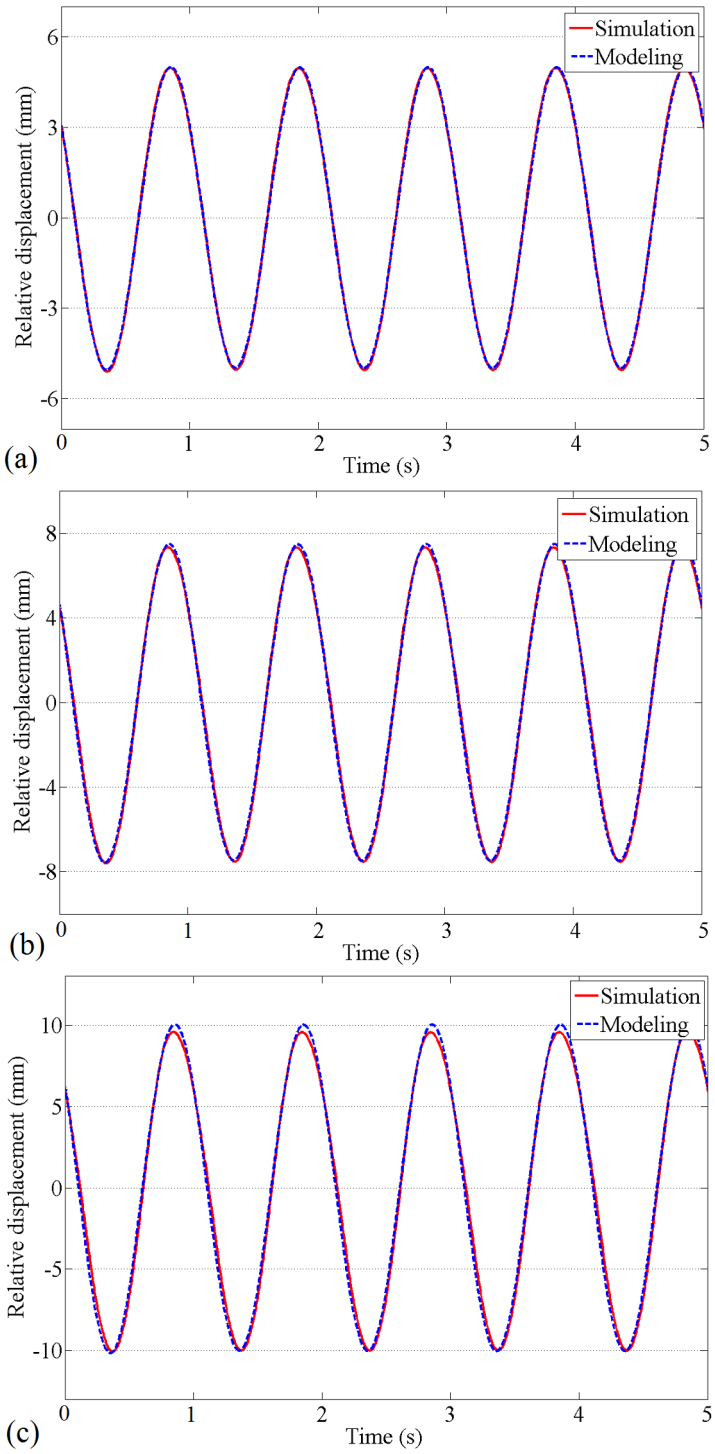

Figure 4.12: Simulation and modeling results in working area for the relative displacement of (a) 5 mm, (b) 7.5 mm, (c) 10 mm.

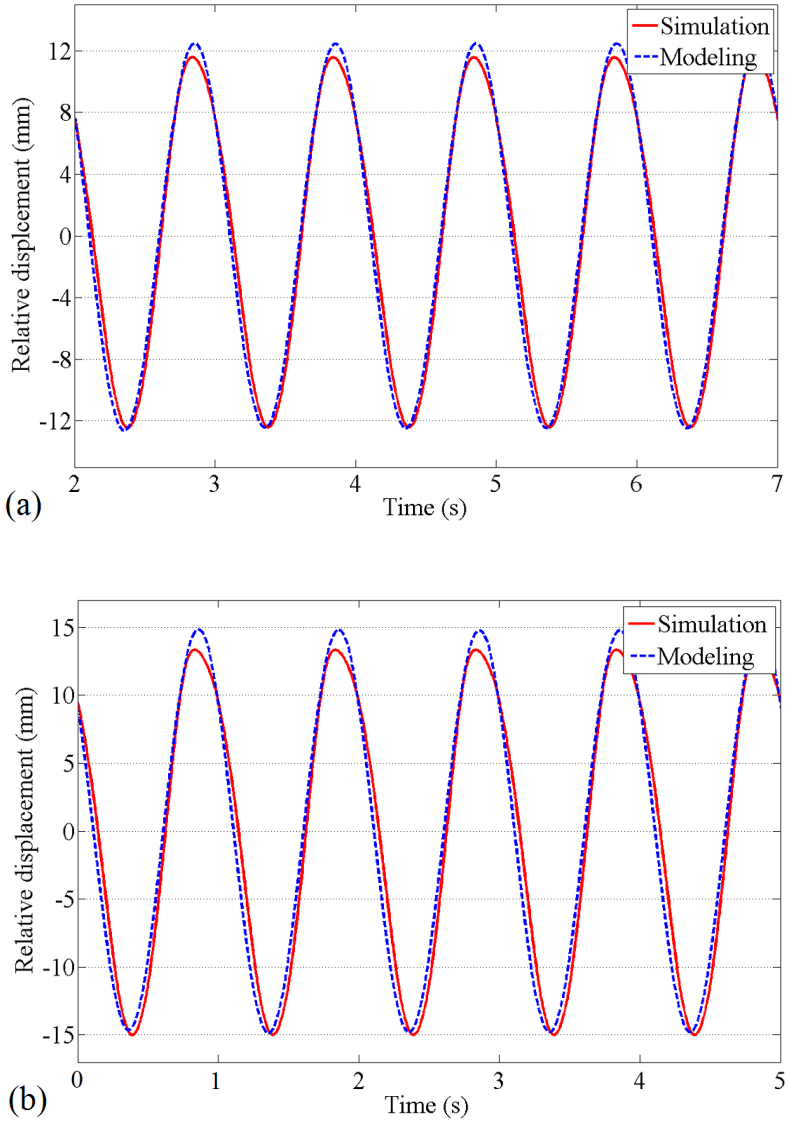

Figure 4.13: Simulation and modeling results in safety area for the relative displacement of (a) 12.5 mm, (b) 15 mm.

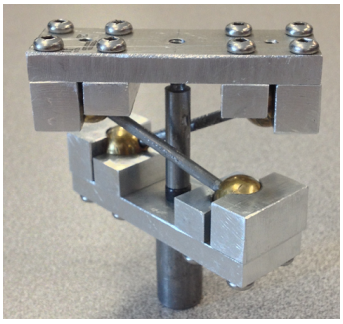

Figure 4.14: Physical model of the two-leg mechanism.

4.6 Experimental Setup and Results

To evaluate performance of the system shown in Figure 4.1, first the two-leg mechanism designed in Section 4.5 and shown in Figure 4.8 was manufactured. The physical model of the two-leg mechanism is shown in Figure 4.14. Then considering (4.19) and (4.43), a prototype regenerative shock absorber was manufactured. The prototype shown in Figure 4.15 has a diameter of 7.6 cm and includes the mentioned two-leg mechanism, a planetary gearhead (Maxon GP52C223087), and a rotary permanent-magnet (PM) brushless machine (Maxon ECmax40-369146). Table 4.2 shows the parameters of this prototype.

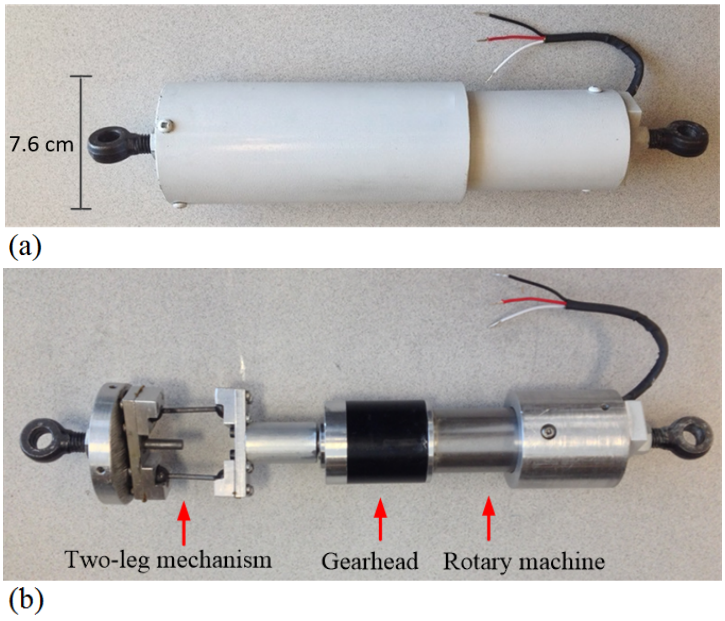

Figure 4.15: Developed damper prototype: (a) With casting, (b) Without casting.

Table 4.2: Parameters of the prototype.

Parameter	**Value**
Internal resistance of the rotary machine, r	0.124 Ohm
Torque constant of the rotary machine, k_t	0.0145 Nm/A
Rotor inertia of the rotary machine, I_r	$53.8 \times 10^{-7} kg.m^2$
Gearing ratio of the gearhead, n	26
Inertia of the gearhead, I_g	$9.1 \times 10^{-7} kg.m^2$
Two-leg mechanism leg length, l	4.5 cm
Two-leg mechanism rectangle length , $2a$	4.3 cm
Inertia of the two-leg mechanism plate, I_t	$4.5 \times 10^{-5} kg.m^2$
Mass of the two-leg mechanism plate, m_t	0.1 kg
Mass of the casting, m_c	0.4 kg

The experimental setup for evaluating the performance of the shock absorber is shown in Figure 4.16. In this setup, a hexapod (Mikrolar P2000) was used to excite the shock absorber. The force and displacement signals were measured with a load cell (L204-200 from Omega) and a displacement sensor (MLT Series 101.6 mm from Honeywell), respectively. A dSPACE 1104 real-time board along with a host computer system is used for data acquisition and analysis.

Using (4.19), the damping coefficient provided by the shock absorber can be calculated. All of the parameters of this equation can be obtained by using (4.9), Figure 3.8, and Table 4.2, except mechanical efficiency of the system which will be obtained through measurements. Referring to (4.34) the mechanical efficiency of the shock absorber is comprised of the mechanical efficiency of the rotary machine, the gearhead, and the two-leg mechanism.

Using data sheets of the rotary machine and gearhead, one can estimate the mechanical efficiency of these parts. In addition, by considering the efficiency of the ball joints of the two-leg mechanism the mechanical efficiency of the two-leg mechanism can be estimated [81]. Finally, using (4.34) the mechanical efficiency of the shock absorber is estimated to be equal to 0.9.

Next, three external resistors of R = 0.6 Ω were connected to the rotary machine similar to the pattern shown in Figure 2.2. Using (4.19), the linear damping coefficient provided by the shock absorber is calculated as follows

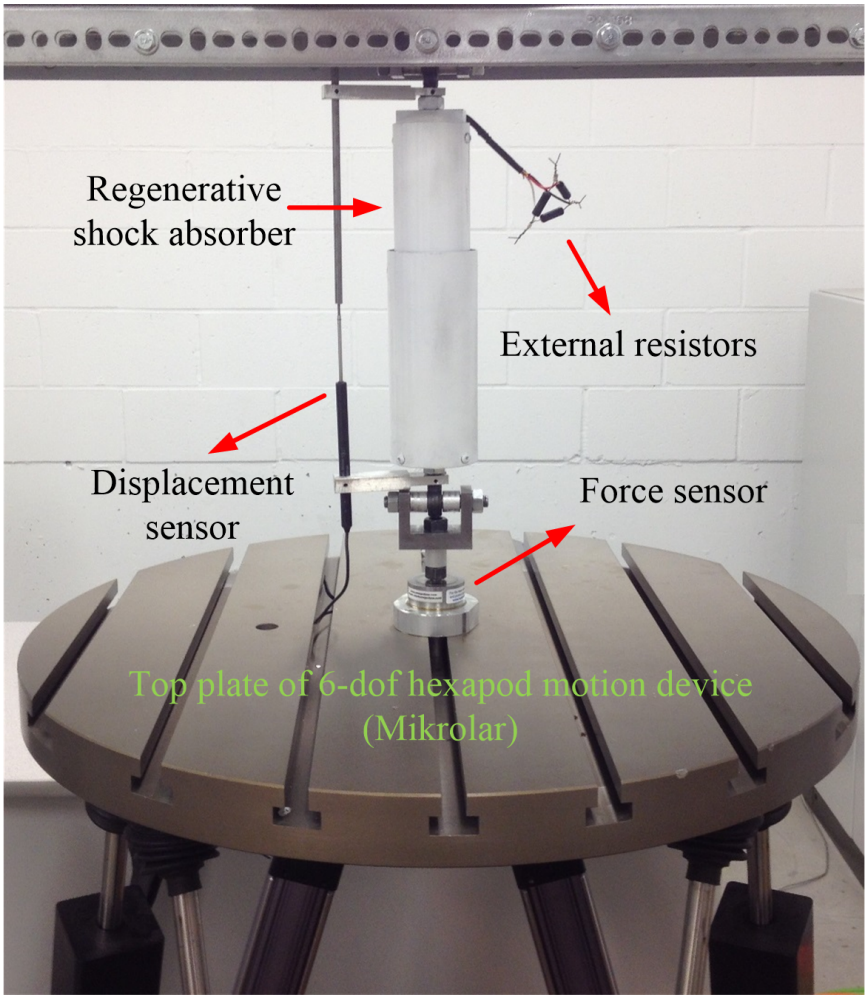

Figure 4.16: Experimental setup.

$$B_L = \frac{1.5 \times n^2 {k_t}^2}{\eta_{tl}\eta_{gh}\eta_g c^2 (R+r)} = \frac{1.5 \times 26^2 \times 0.0145^2}{0.9 \times 0.0148^2 \times (0.6+0.124)} = 1500 N.s/m$$

The provided linear damping coefficient by the shock absorber (B_L = 1500 N.s/m) is close to the damping coefficient of a typical passenger car.

Based on [27], [73], [95], when a passenger car travels on a regular road with a speed higher than 30 km/hr, the amplitude of excitation is mostly between 5 mm to 10 mm with an excitation frequency above than 1 Hz. Therefore, the prototype was tested with sinusoidal displacement inputs for different amplitudes and frequencies in the above ranges.

4.6.1 Linear Damping Coefficient

If a shock absorber is excited under a sinusoidal displacement profile, the force-displacement loop is an ellipse [91]. This concept is used in this work, to evaluate the functionality of the shock absorber from damping perspective.

Figure 4.17 shows the force-displacement loops of the suggested regenerative shock absorber for different amplitudes and frequencies when a sinusoidal excitation is used. The area of each loop represents mechanical work ΔW in one cycle. Hence, the linear damping coefficient can be calculated as follows

$$B_L = \frac{\Delta W}{\pi \omega X^2} \tag{4.44}$$

Using (4.44) for different loops shown in Figure 4.17, the experimental average linear damping coefficient is obtained as $B_{L_E} = 1720 N.s/m$. The reason of difference between calculated linear damping coefficient ($1500 N.s/m$) and obtained one from experiments ($1720 N.s/m$) is as follows. To calculate the linear damping coefficient provided by the shock absorber, the mechanical efficiency of the shock absorber was estimated as 0.9, resulting in a linear damping coefficient of $1500 N.s/m$. However, the average mechanical efficiency obtained from experiments is about 0.78 (as discussed in 4.6.2), which results in a linear damping coefficient of $1720 N.s/m$. It should be noted that by changing the external resistors, R, the average experimental damping coefficient can be regulated.

Next, let us study the inertial effect of the moving parts of the damper as evidenced by (4.24). Considering the numerical data given in Table 4.2, we obtain $m_{eq} = 17$kg, which is relatively small when compared to the quarter mass of a vehicle (e.g., about 400kg for a small car). Thus one interpretation of the effect of m_{eq} is adding to the sprung mass of the vehicle. In this work, the effect of m_{eq} is interpreted as producing a negative stiffness term shown in equation (4.31), which corresponds to the non-zero diagonal slopes in the force-displacement curves in Figure 4.17.

Due to certain limitations in materials used and manufacturing imperfections, there was a clearance of $0.5mm$ inside the housing of ball joints in the manufactured two-leg mechanism. This clearance resulted in fluctuations at each end of the force-displacement loops. This problem can be solved of by using better materials and more precise manufacturing methods.

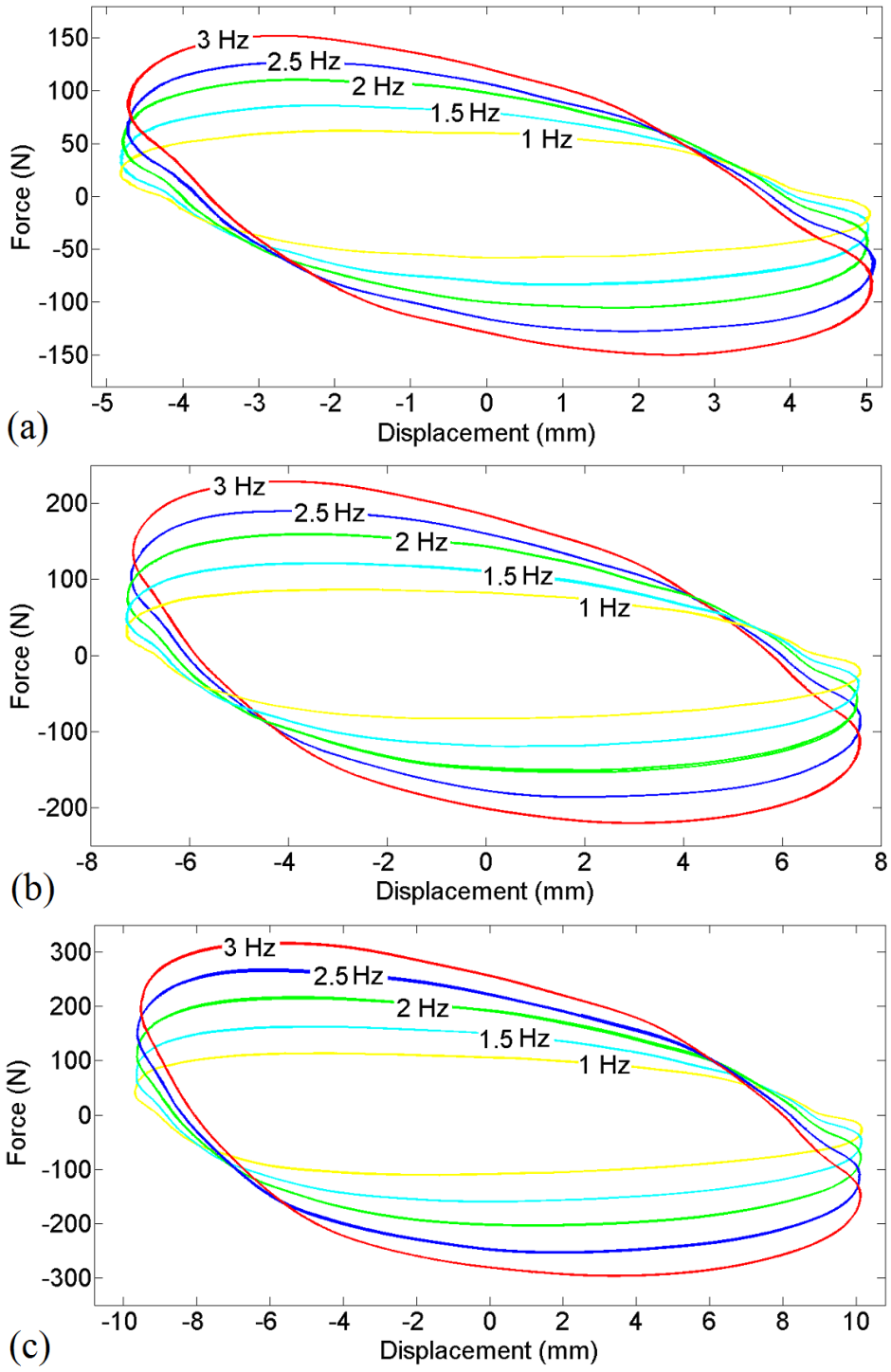

Figure 4.17: Force-displacement loops for amplitudes of (a) 5 mm, (b) 7.5 mm, and (c) 10 mm at different frequencies.

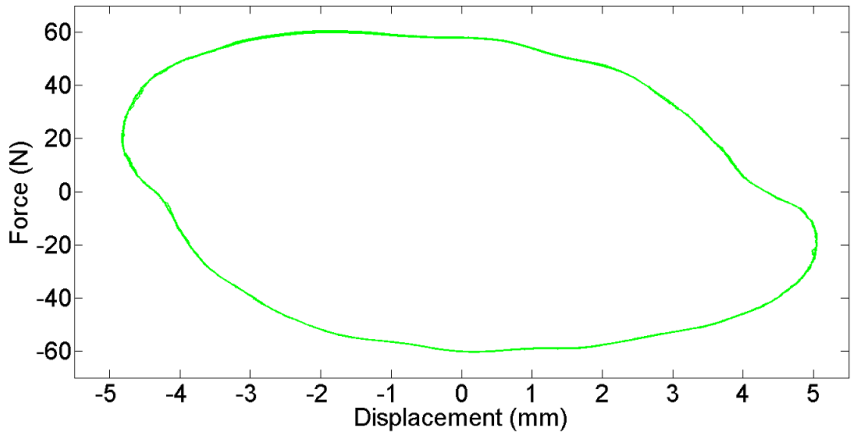

Figure 4.18: Force-displacement loop at a frequency of 1 Hz with an amplitude of 5 mm.

4.6.2 Efficiency of the Regenerative Shock Absorber

Referring to (4.42) the electrical efficiency of the system is simply obtained as follows

$$\eta_{Elec} = \frac{0.6}{0.6 + 0.124} = 0.83.$$

But to evaluate the mechanical efficiency of the shock absorber experimentally, a two- step procedure is needed as follows. First, the total efficiency is calculated as

$$\eta_{RSA} = \frac{P_{out(ave)}}{P_{input(ave)}} \tag{4.45}$$

where $P_{out(ave)}$ is the average of output electrical power and $P_{input(ave)}$ is the average of input mechanical power in one cycle. Then by rearranging (4.43) the mechanical efficiency is given by

$$\eta_{Mech} = \frac{\eta_{RSA}}{\eta_{Elec}}. \tag{4.46}$$

Regarding $P_{input(ave)}$ in (4.45) it can be said that, the area of each force-displacement loop is the input mechanical work ΔW in one cycle, hence the average of input mechanical power in one cycle is given by

$$P_{input(ave)} = \frac{\Delta W}{T} \tag{4.47}$$

where T is the period of excitation.

Figure 4.18 shows the force-displacement loop at a frequency of 1 Hz with an amplitude of 5 mm. Utilizing (4.47) in Figure 4.18, we have $P_{input(ave)} = 0.91W$.

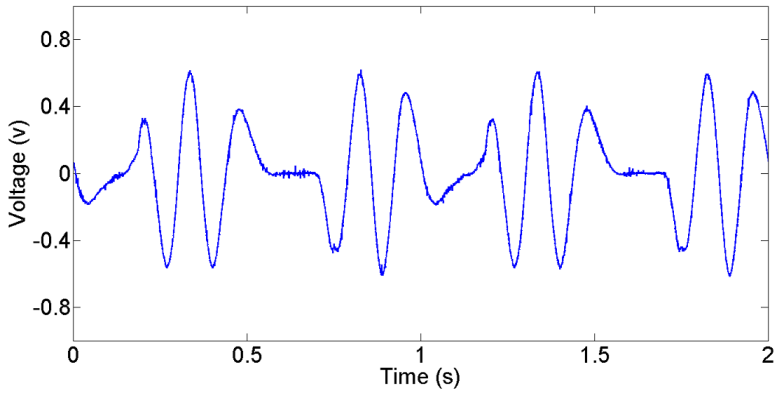

Figure 4.19: Instant voltage of each external resistor at a frequency of 1 Hz with an amplitude of 5 mm.

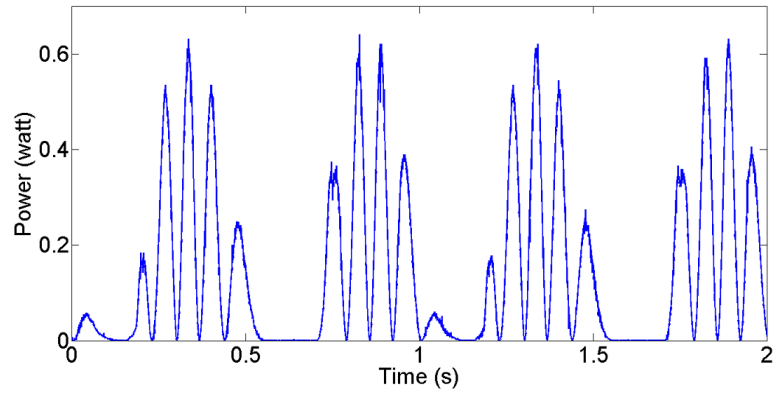

Figure 4.20: Instant electrical power in each external resistor at a frequency of 1 Hz with an amplitude of 5 mm.

To calculate $P_{out(ave)}$, first the instant electrical power in each external resistor is calculated based on the recorded voltage and resistor value as follows:

$$P_{instant} = \frac{V^2}{R} \tag{4.48}$$

where V is the instant voltage. Then the average of output electrical power in three external resistors is given by

$$P_{output(ave)} = 3 \times \frac{\int_0^T \mathrm{P}_{instant}\,\mathrm{d}t}{T}. \tag{4.49}$$

Figure 4.19 and Figure 4.20 show the instant voltage and instant electrical power of each external resistor at a frequency of 1 Hz with an amplitude of 5 mm, respectively. Utilizing (4.49) in Figure (4.20), we have $P_{out(ave)} = 0.54W$.

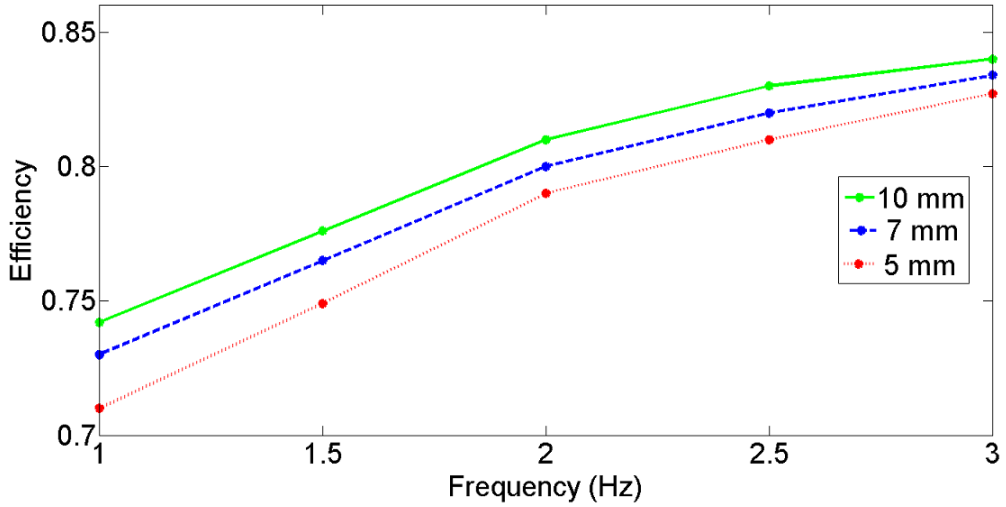

Figure 4.21: Mechanical efficiency of the shock absorber for different amplitudes.

Utilizing (4.45) the total efficiency of the shock absorber at a frequency of 1 Hz with an amplitude of 5 mm is calculated as $\eta_{RSA} = \frac{0.54}{0.91} = 0.59$. As mentioned before, the electrical efficiency of the system is 0.83, thus using (4.46) the mechanical efficiency of the shock absorber at a frequency of 1 Hz with an amplitude of 5 mm is calculated as $\eta_{Mech} = \frac{0.59}{0.83} = 0.71$.

By using the same procedure the mechanical efficiency for different amplitudes and frequencies was calculated and the results are shown in Figure 4.21. As it can be seen in this figure, $0.71 < \eta_{Mech} < 0.84$ with an average value of 0.78.

There are several works about regenerative shock absorbers in the literature, but among all of them mechanical efficiency was only studied in [73]. Based on this study the mechanical efficiency ranges from 0.33 to 0.63 with different vibration frequencies with an amplitude of 10 mm and a damping coefficient of 1800 N.s/m.

Referring to Figure 4.21 the mechanical efficiency is increased as a result of increasing the amplitude and excitation frequency; the reason of this fact can be explained by studying the mechanical efficiency as a function of friction. To this end, first the mechanical efficiency of the shock absorber is described by

$$\eta_{Mech} = \frac{P_{input(ave)} - P_{f(ave)}}{P_{input(ave)}} \tag{4.50}$$

where $P_{f(ave)}$ is the average of lost power due to friction in one cycle. Then dependency of $P_{input(ave)}$ and $P_{f(ave)}$ to the amplitude and excitation frequency are investigated as follows.

Dependency of the average of input mechanical power, $P_{input(ave)}$, to the amplitude and excitation frequency is explained as follows. Since the shock absorber is tested under sinusoidal displacement excitation, any increase in the amplitude and excitation frequency increases the speed between two sides of the shock absorber. In addition the net damping force is given by $F_D = B_L\dot{x}$ where B_L is the linear damping coefficient and $\dot{x}$ is the speed between two sides of the shock absorber. Therefore the net damping force, representing the average of input mechanical power, is increased proportional to the excitation amplitude and frequency increase.

Dependency of the average of lost power due to friction, $P_{f(ave)}$, to the amplitude and excitation frequency is explained as follows. The kinetic friction force is given by $F_f = \mu_k N$ where μ_k is the coefficient of kinetic friction and N is the normal force between surfaces. Considering the structure of the shock absorber shown in Figure 4.1, the normal force in the spherical joints and bearing of the gearhead are increased as the amplitude and excitation frequency is increased. However, the normal force between castings of the shock absorber and the normal forces in the generator parts are not frequency dependent and would remain constant. Therefore, it can be said that the friction force representing the average of lost power due to friction does not increase proportional to the excitation amplitude and frequency increase.

From the two previous paragraphs we can conclude that, by increasing the amplitude and frequency excitation the ratio of lost power due to friction to the input power is decreased; then by considering Equation (4.50) resulting in increased mechanical efficiency.

4.7 Summary and Conclusion

In this chapter, the design and implementation of a novel regenerative shock absorber for a passenger-sized car were studied. First, appropriate performance of the shock absorber as a part of a suspension system, was demonstrated through simulation. Then, A prototype shock absorber was manufactured and its performance was evaluated on a test-bench under sinusoidal displacement. The results demonstrate that the regenerative shock absorber can provide the same level of damping for a passenger-sized car while meeting the size requirement. Furthermore, vibration energy is harvested with a mechanical efficiency measured between 0.71 and 0.84.

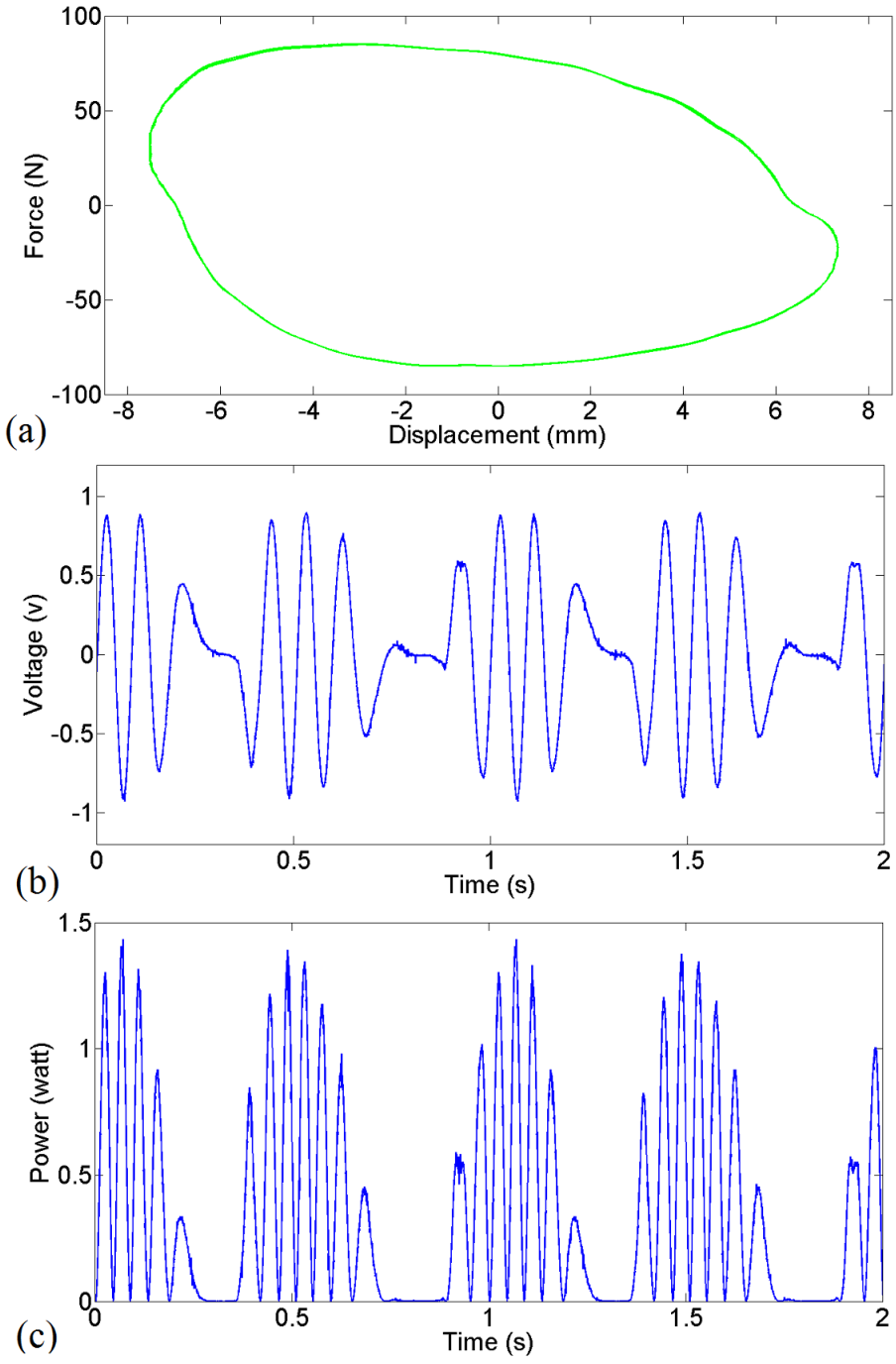

Figure 4.22: (a) Force-displacement loop, (b) Instant voltage of each external resistor, (c) Instant electrical power in each external resistor at a frequency of 1 Hz with an amplitude of 7.5 mm.

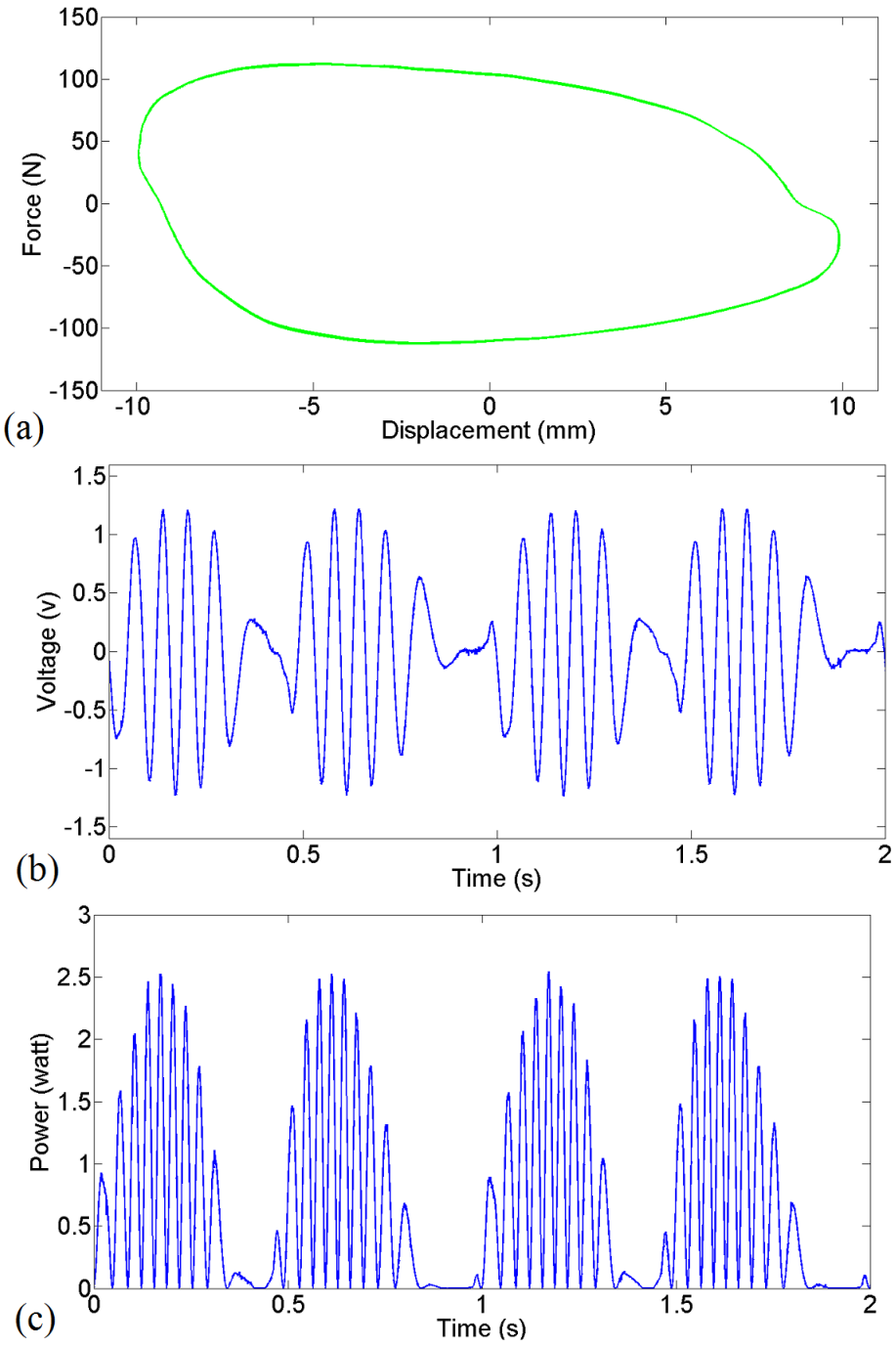

Figure 4.23: (a) Force-displacement loop, (b) Instant voltage of each external resistor, (c) Instant electrical power in each external resistor at a frequency of 1 Hz with an amplitude of 10 mm.

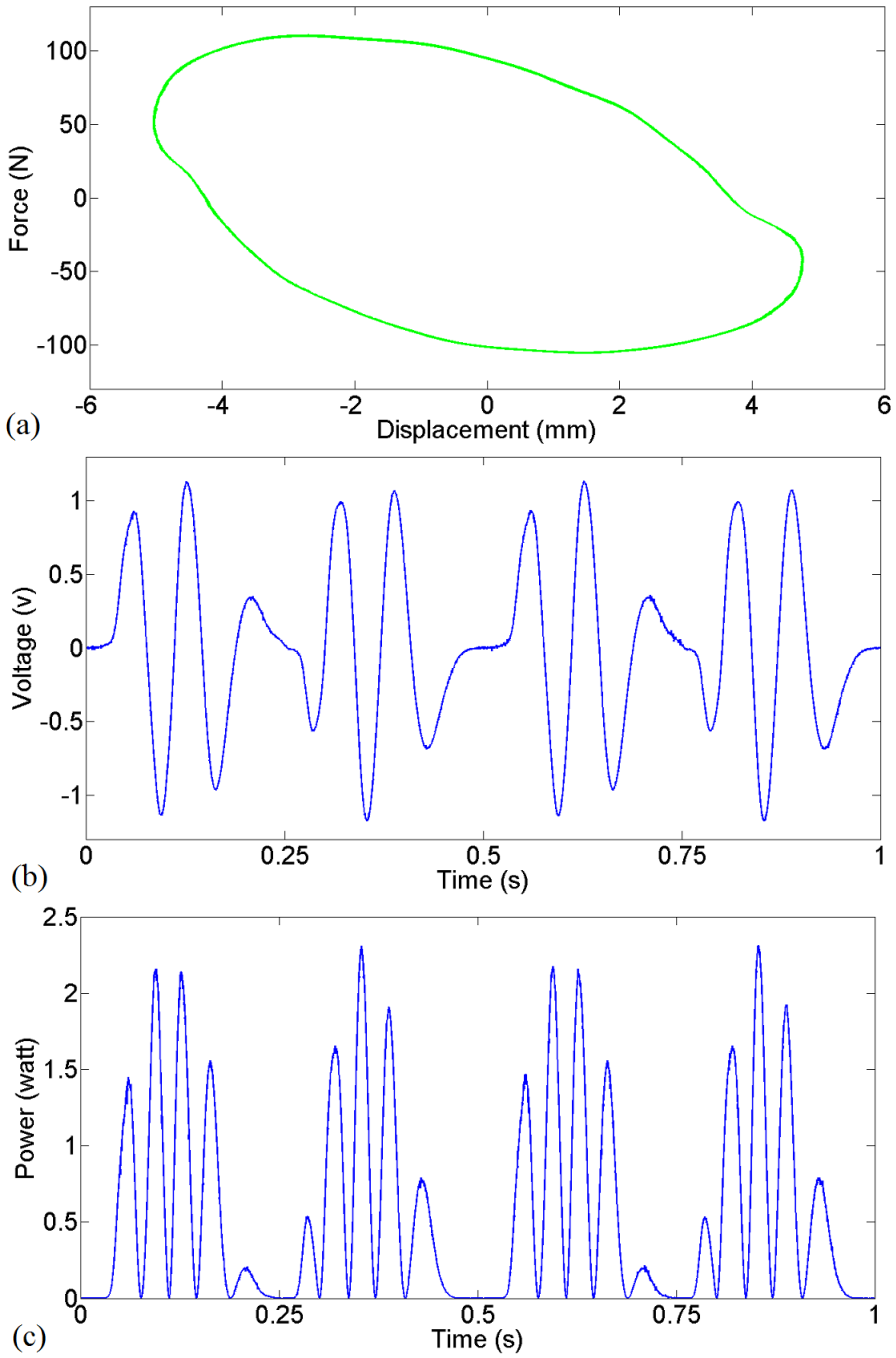

Figure 4.24: (a) Force-displacement loop, (b) Instant voltage of each external resistor, (c) Instant electrical power in each external resistor at a frequency of 2 Hz with an amplitude of 5 mm.

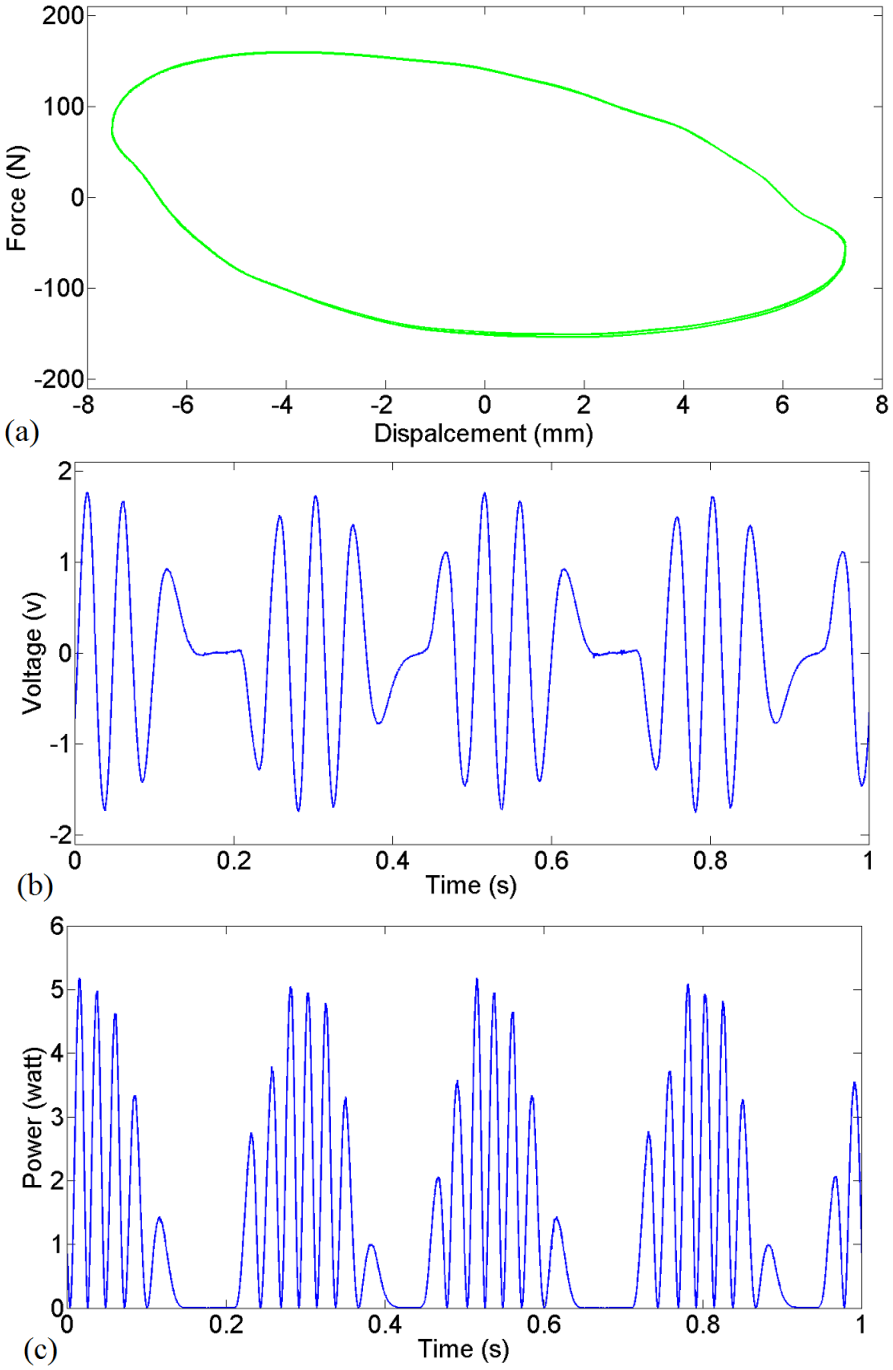

Figure 4.25: (a) Force-displacement loop, (b) Instant voltage of each external resistor, (c) Instant electrical power in each external resistor at a frequency of 2 Hz with an amplitude of 7.5 mm.

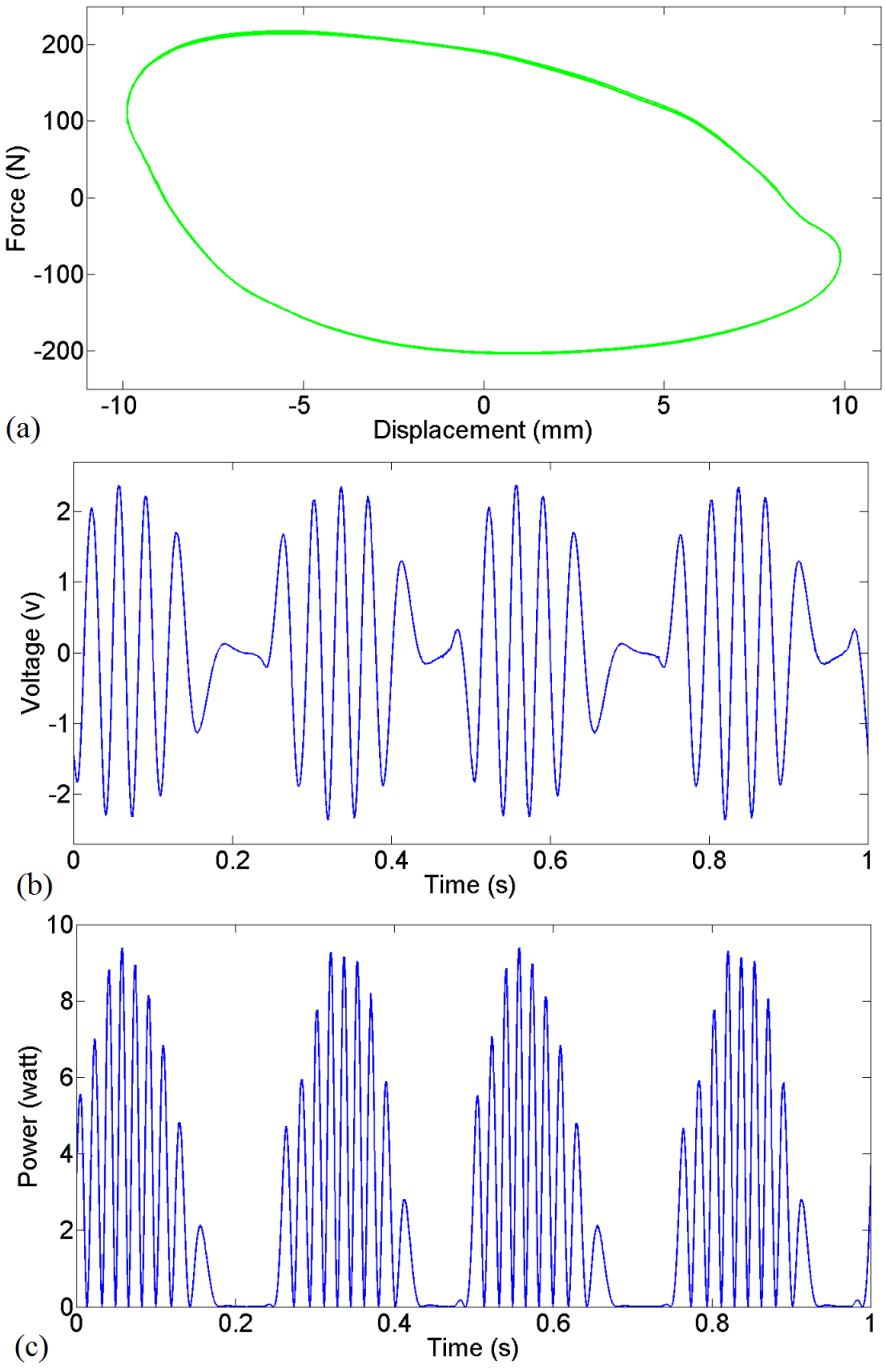

Figure 4.26: (a) Force-displacement loop, (b) Instant voltage of each external resistor, (c) Instant electrical power in each external resistor at a frequency of 2 Hz with an amplitude of 10 mm.

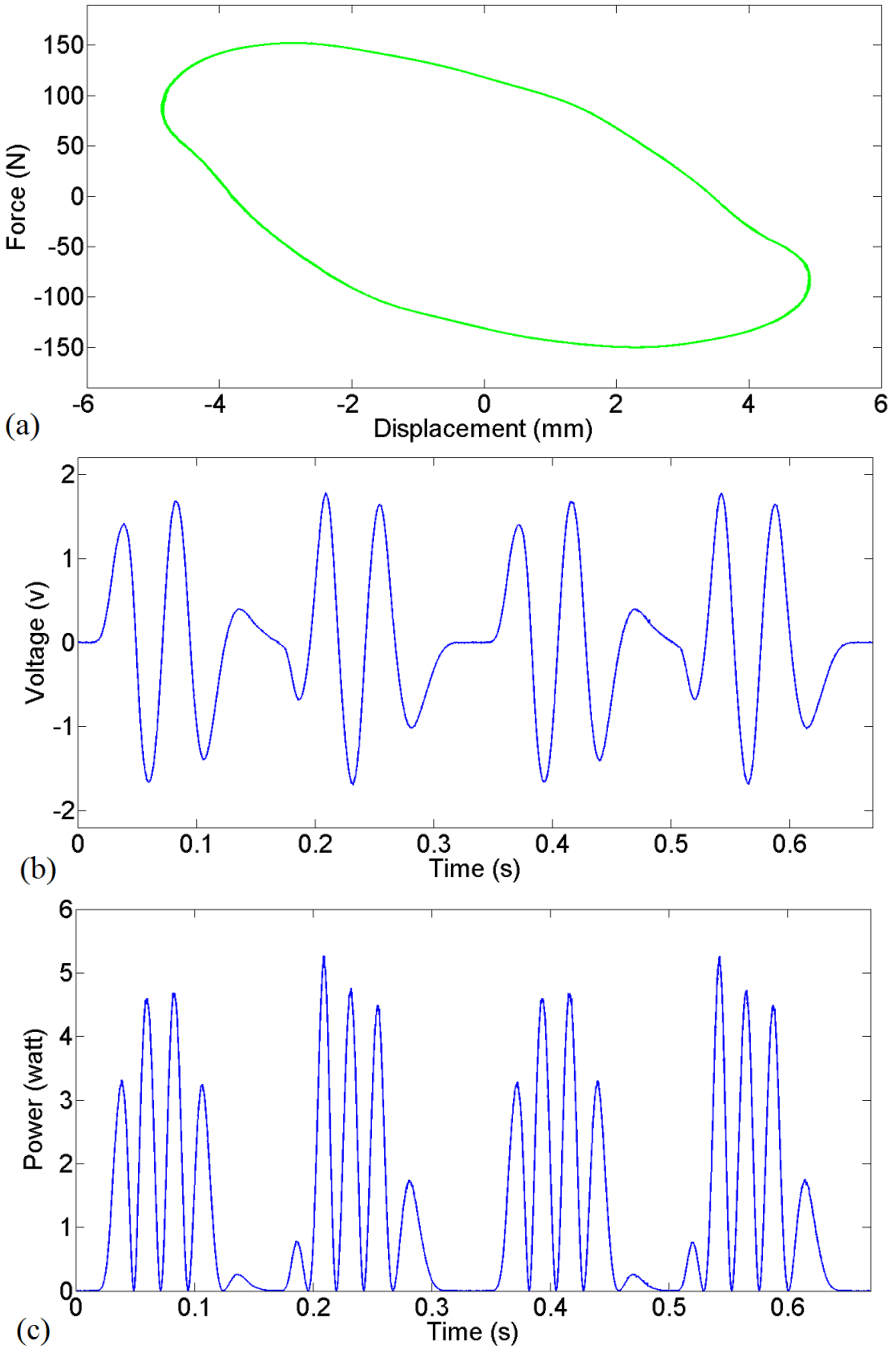

Figure 4.27: (a) Force-displacement loop, (b) Instant voltage of each external resistor, (c) Instant electrical power in each external resistor at a frequency of 3 Hz with an amplitude of 5 mm.

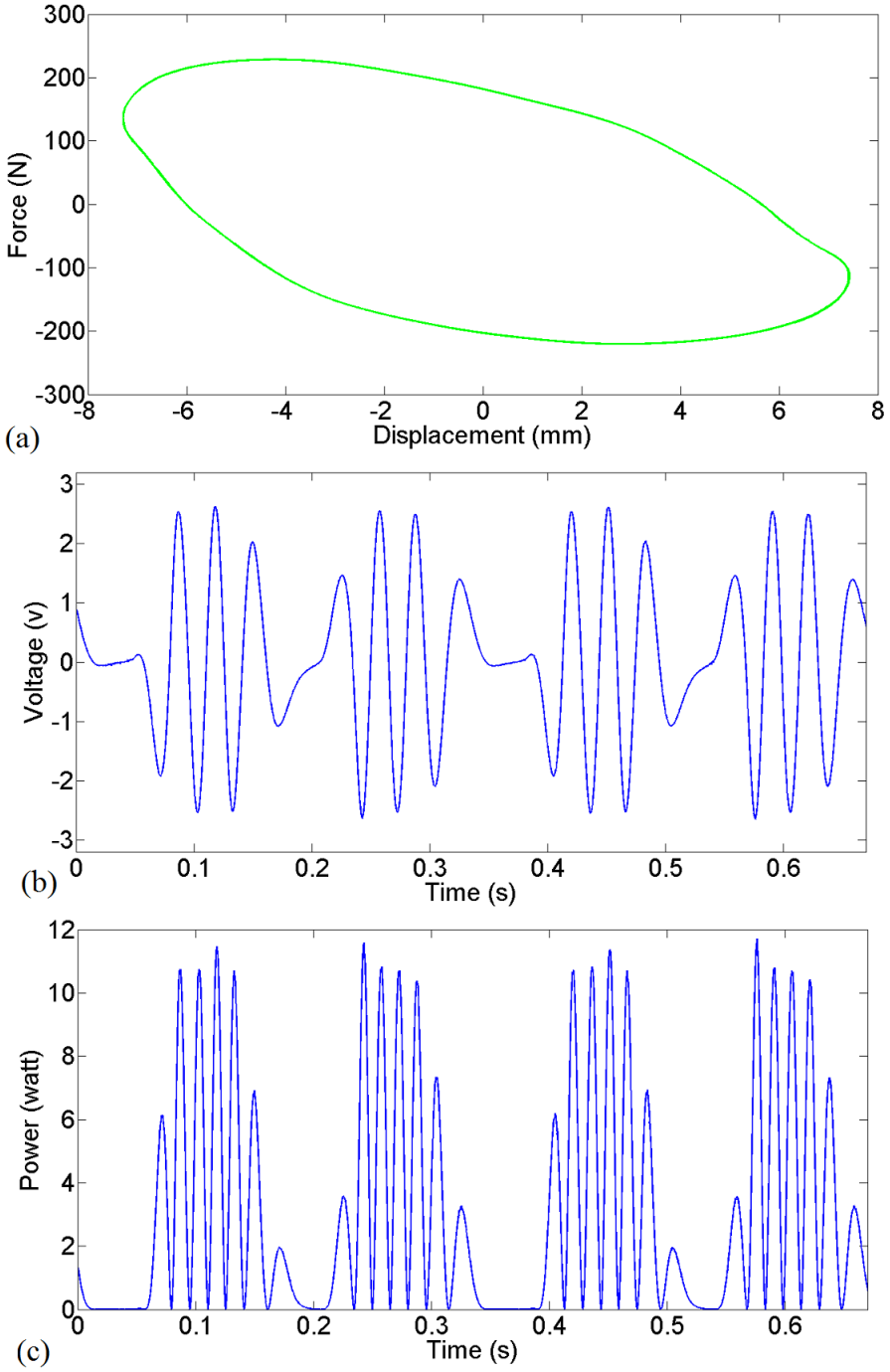

Figure 4.28: (a) Force-displacement loop, (b) Instant voltage of each external resistor, (c) Instant electrical power in each external resistor at a frequency of 3 Hz with an amplitude of 7.5 mm.

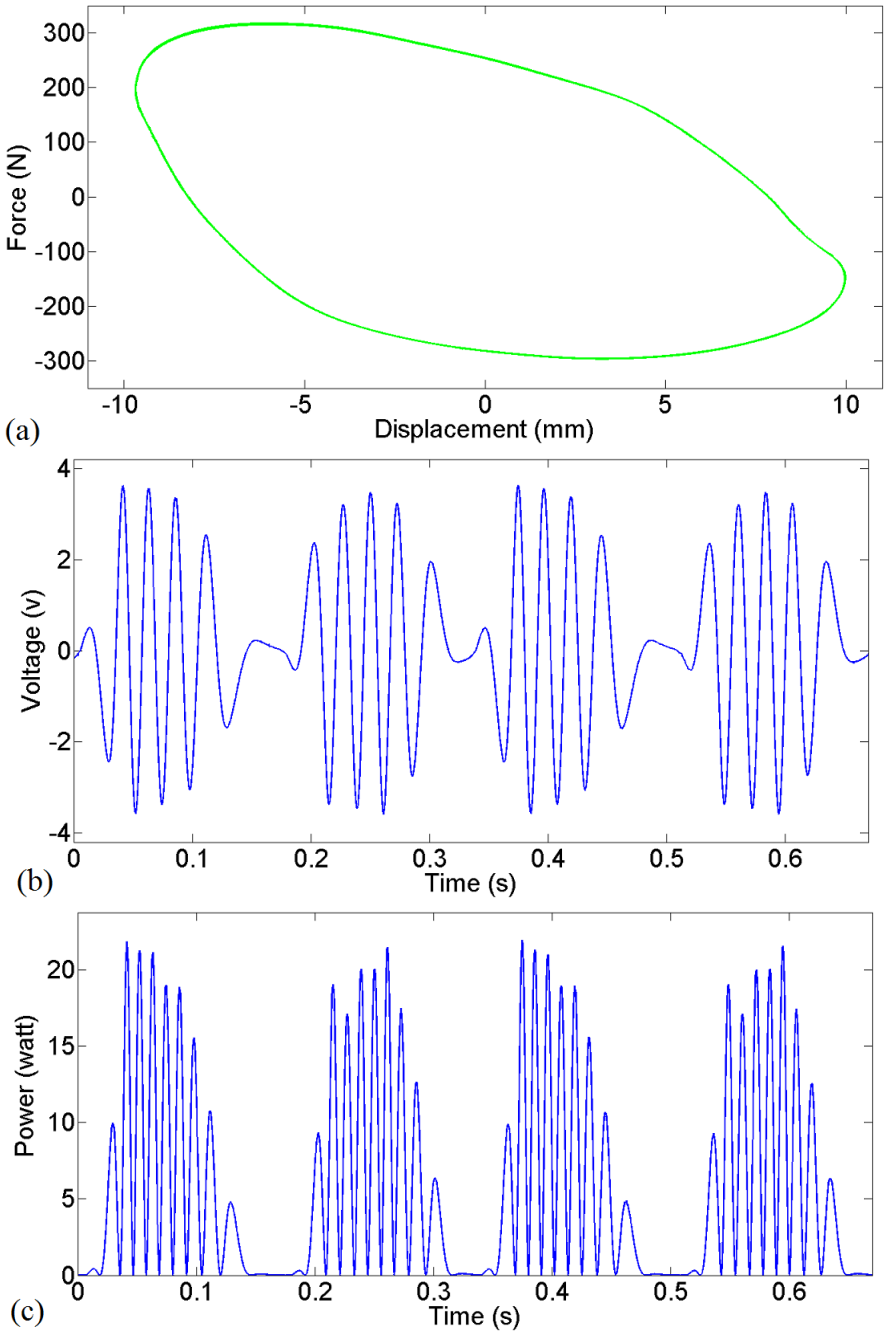

Figure 4.29: (a) Force-displacement loop, (b) Instant voltage of each external resistor, (c) Instant electrical power in each external resistor at a frequency of 3 Hz with an amplitude of 10 mm.

Chapter 5

A Case Study About Nonlinear Terms of the Two-Leg Mechanism

5.1 Introduction

As mentioned in Chapter 4, the linear damping coefficient provided by the proposed shock absorber is not a constant, which is due to nonlinear terms of the two-leg mechanism. The effect of two-leg mechanism nonlinearity was discussed in Section 4.5. It was noticed that the maximum error of the relative displacement, due to nonlinearity of the two-leg mechanism, is about 10% which can be ignored in the application of usual passenger cars.

However, there are some applications for the proposed regenerative shock absorber such as suspension system of luxury passenger cars, suspension system of trucks, and suspension system of driver's seat of tracks, in which the variable linear damping coefficient provided by the shock absorber could not be applicable. In this chapter, we study compensating the effect of the two-leg mechanism nonlinear terms on linear damping coefficient, by utilizing a variable external resistance provided by the charging circuit through appropriate control.

5.2 Nonlinear Terms Analysis

Let us see how the nonlinear terms of the two-leg mechanism affects the linear damping coefficient, and as a result the damping force applied by the presented regenerative shock absorber. To this end, consider Figure 5.1 showing the force-displacement loops at a frequency of 1 Hz

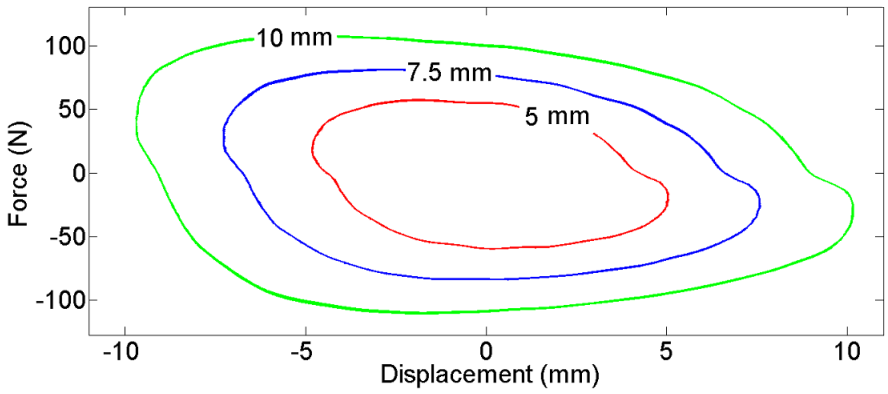

Figure 5.1: Force-displacement loops at a frequency of 1 Hz for different amplitudes by utilizing fixed external resistance.

for different amplitudes, where the external resistance is constant (These loops are from experimental results explained in the previous chapter). From this figure, the force-displacement loop is symmetric for an amplitude of 5 mm. However, by increasing the amplitude, the vertical diameter of the loops are shifted to the left which is due to the nonlinear relationship given by (4.4). Referring to Figure 4.9, for the amplitude up to 5 mm from the equilibrium point, the nonlinear and linear mapping are very close; therefore the linear damping coefficient is almost a constant, and as a result the force-displacement loop is symmetric. But by increasing the amplitude, the nonlinear mapping becomes separated from the linear mapping, which means the linear damping coefficient is a variable. As a result the damping force applied by the shock absorber is not symmetric and the vertical diameter of the loops are shifted to the left.

The objective of this section, is to compensate the nonlinear terms of the two-leg mechanism by a variable external resistance sent from charging circuit. As a result, the linear damping coefficient provided by the shock absorber would be constant, and the force-displacement loops would be symmetric. To this end, consider Equation 4.17, in which the nonlinear kinematic relationship between the translational and rotary speeds of the plates in the two-leg mechanism is utilized. By substituting (2.22) in (4.17) we have

$$B_L = \frac{1.5n^2k_t^2[l^2 - 2a^2(1 - cos\theta)]}{\eta_{tl}\eta_{gh}\eta_g a^4 sin^2\theta(R + r)}. \tag{5.1}$$

Referring to (5.1) by controlling the external resistance, the amount of linear damping coefficient can be controlled. Solving (5.1) in terms of R results in

$$R = \frac{1.5n^2k_t^2\,[l^2 - 2a^2(1 - cos\theta)]}{B_L\eta_{tl}\eta_{gh}\eta_g a^4 sin^2\theta} - r \tag{5.2}$$

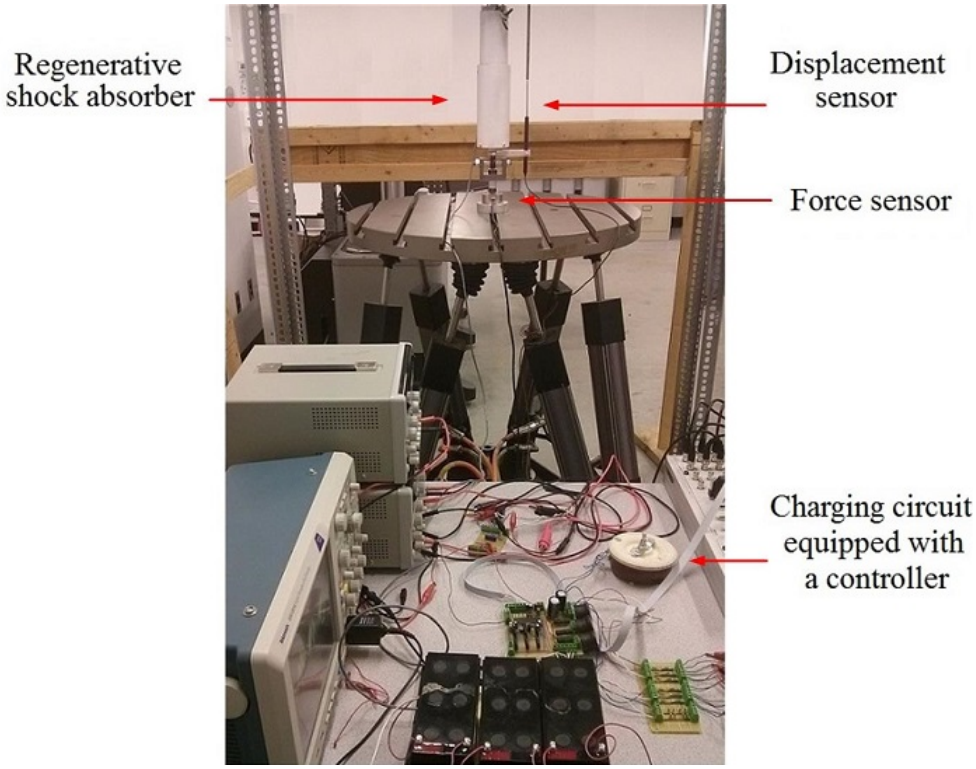

Figure 5.2: Experimental setup.

As the displacement measurement is more common and easier compared to the measurement of angular position, (5.2) can be further simplified by performing some algebraic manipulations and utilizing (4.4) and (4.14) as follows

$$R = \frac{n^2 k_t^2}{B_L \eta_{tl} \eta_{gh} \eta_g} \times \frac{6(x+\delta_0)^2}{4a^2[l^2-(x+\delta_0)^2]-[l^2-(x+\delta_0)^2]^2} - r \tag{5.3}$$

Equation 5.3 demonstrates the relationship between the external resistance sent from the charging circuit and linear displacement. Utilizing this relationship, for any desired linear damping coefficient, B_L, an appropriate resistance, R, at each position, x, can be calculated.

5.3 Experimental Setup and Results

To evaluate the mentioned theory, the manufactured shock absorber was connected to a charging circuit equipped with a controller, and tested in the setup shown in Figure 5.2 under sinusoidal displacement.

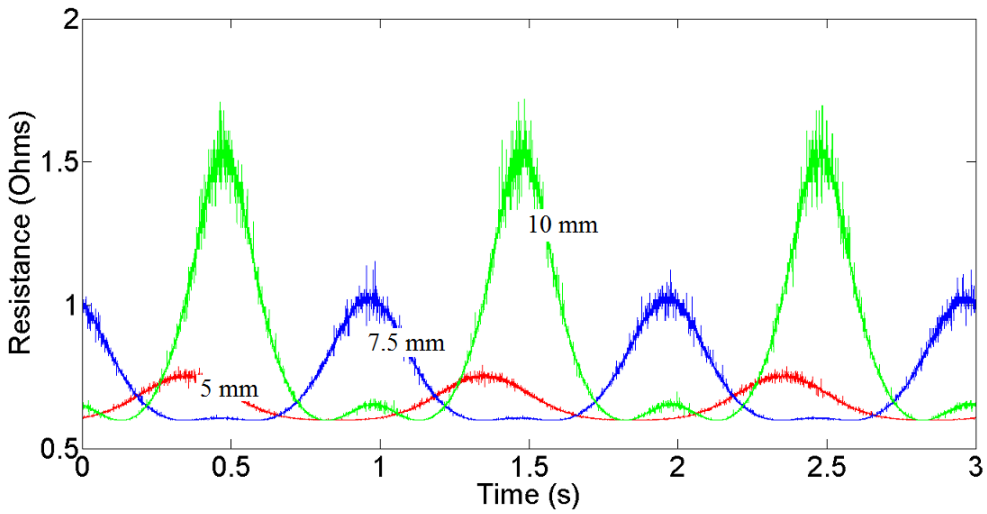

Figure 5.3: Variable external resistance for constant linear damping coefficient under different base excitation amplitudes.

In this setup, displacement is measured by the displacement sensor and sent to the charging circuit, then the charging circuit applies the corresponding external resistance to each displacement, based on Equation 5.3.

In the experiments, the desired linear damping coefficient was 1720 N.s/m, and the mechanical efficiency of the system was considered equal to 0.78 which is the average of mechanical efficiency presented in Section 4.6.2. Results of these experiments are shown in Figure 5.3 and Figure 5.4 as follows.

Figure 5.3 shows the amount of external resistance for different amplitudes. As it can be seen in this figure, for the amplitude of 5 mm the external resistance fluctuations are very small, which is due to the closeness between linear and nonlinear mapping up to 5 mm from equilibrium point. However, by increasing the amplitude, the nonlinear mapping becomes separated from linear mapping, therefore the external resistance, fluctuates more to compensate the nonlinear effects of the two-leg mechanism.

Figure 5.4 shows the force-displacement loops for different amplitudes. Compare to the loops shown in Figure 5.1, the vertical diameter of the loops for the amplitudes of 7.5 mm and 10 mm have been shifted to the right and the loops are symmetric. This change proves that the nonlinear terms of two-leg mechanism have been compensated by the variable external resistance, therefore the linear damping coefficient provided by the shock absorber is constant.

It should be noted that, this chapter was accomplished in collaboration with a colleague

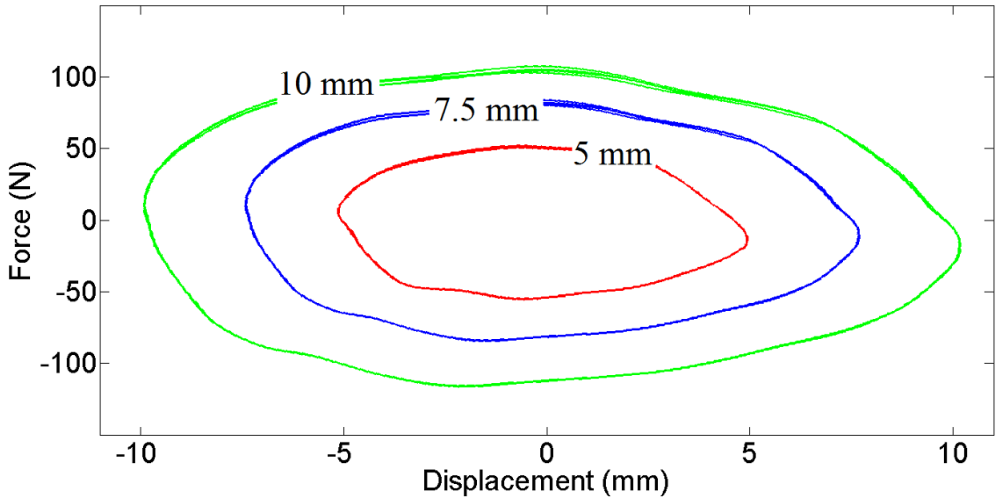

Figure 5.4: Force-displacement loops at a frequency of 1 Hz for different amplitudes by utilizing variable external resistance.

with electrical engineering background. In this collaboration my colleague was in charge of electrical engineering materials specially the charging circuit equipped with a controller and I was in charge of mechanical engineering materials as explained. Therefore in this dissertation, only the mechanical engineering materials were explained in details.

5.4 Summary and Conclusion

In this chapter, the effect of two-leg mechanism nonlinear terms, on linear damping coefficient provided by the presented regenerative shock absorber, was studied and it was noticed that these terms make the linear damping coefficient variable. Then the theory of using a variable external resistance, provided by the charging circuit, to compensate the two-leg mechanism nonlinear terms was presented; and at the end the accuracy of this theory was verified through some experiments.

Chapter 6

Summary, Conclusions, and Suggestions for Future Work

6.1 Summary and Conclusions

In this thesis, the idea of a novel regenerative shock absorber for a passenger car was presented. To this end, first rotary damping coefficients provided by DC and AC rotary machines connected to appropriate charging circuits were studied. An AC rotary machine connected to external resistors (to simulate charging circuit) was evaluated in a dynamo system, experimentally. The experimental results show a good match with theoretical results. Then, a proof of concept regenerative shock absorber using algebraic screw was introduced, and analytical expression describing linear damping coefficient provided by this system was derived. The prototype of this system was developed and evaluated in a mass-spring setup. The experimental results demonstrate accuracy of theoretical results. Furthermore, the design and implementation of a novel simple regenerative shock absorber for a passenger-sized car was studied. A prototype shock absorber was manufactured and its performance in terms of damping coefficient and mechanical efficiency was evaluated on a test-bench under sinusoidal displacement. The results demonstrate that the regenerative shock absorber can provide damping and a physical size that are commensurate with those of a passenger car. Meanwhile, vibration energy can be regenerated with a measured mechanical efficiency between 0.71 and 0.84.

6.2 Future Research

Based on the experience gained and results obtained in the course of this research, the following activities may be considered for future work.

6.2.1 Strength of Materials Analysis

The scope and contribution of current work was investigation of the kinematics and dynamics of the proposed regenerative shock absorber. However to utilize this system in real applications, a comprehensive analysis concerning strength of materials issues such as stress, buckling, and fatigue in different parts of the system is needed and would be worthwhile studying in any future developments.

6.2.2 Manufacturing Improvement

Among the parts utilized to manufacture the presented shock absorber, generator and gearhead were bought off the shelves. These parts have high efficiencies; and they are compact and light enough. However, the two-leg mechanism and the casting were built in an academic machineshop, thus there are some imperfections in these parts which cause the mechanical efficiency to be decreased. Moreover these parts are bulky and heavy. By utilizing better materials, optimized sizes and more precise manufacturing methods, a better version of the presented regenerative shock absorber in terms of mechanical efficiency, weight, and size can be manufactured. Thus, manufacturing improvement could be a topic of future work.

6.2.3 Two-leg mechanism Modification

Based on the theory presented in this work, bigger rotation angle of motion converter, causes a smaller need in gearing ratio; and smaller gearing ratio results in higher mechanical efficiency in the regenerative shock absorber. One way of having bigger rotation angle in two-leg mechanism is using a bended legs in this system, however in this situation a special spherical joint to lead each leg in a special path is needed. A study about bended legs and corresponding spherical joints is worth to be a subject of a future work.

6.2.4 Other Vehicular Applications

In this work a comprehensive study about damping and efficiency of a novel regenerative shock absorber was presented. Although the obtained results were used to design and manufacture a shock absorber for a passenger car, they can be used as a solid ground for other applications such as suspension system of trucks, suspension system of driver's seat of trucks, and suspension system of driver's seat of boats. Each of the mentioned applications is worth a topic for future work.

6.2.5 Ocean Wave Converter

The subject of this study is capturing energy from a car shock absorber motion, which is a one dimensional vibration. Considering that the ocean waves are modeled as three dimensional vibrations, this system can be extended to three dimensions and be used as a ocean wave energy coveter.

Bibliography

[1] U.S. Energy Information Administration [Online].
Available: http://www.eia.gov/energyexplained/index.cfm?page=us_energy_home#tab3

[2] National Energy Board [Online].
Available: http://www.neb-one.gc.ca/clf-nsi/rnrgynfmtn/nrgyrprt/nrgyftr/2013/nrgftr2013-eng.html#s4_1

[3] Environment Canada [Online].
Available: http://www.ec.gc.ca/ges-ghg/985F05FB-4744-4269-8C1A-D443F8A86814/1001-Canada's%20Emissions%20Trends%202013_e.pdf

[4] U.S. Department of energy [Online].
Available: http://www.fueleconomy.gov/FEG/atv.shtml

[5] X. Nian, F. Peng, and H. Zhang, "Regenerative Braking System of Electric Vehicle Driven by Brushless DC Motor," *IEEE Transactions on Industrial Electronics,* vol. 61, no. 10, pp. 5798-5808, 2014.

[6] S. Lu, P. Weston, S. Hillmansen, H. B. Gooi, and C. Roberts, "Increasing the Regenerative Braking Energy for Railway Vehicles," *IEEE Transactions on Intelligent Transportation Systems,* vol. 15, no. 6, pp. 2506-2515, 2014.

[7] J. N. Bae, Y.E. Kim, and C.S. Jin, "Design and Analysis of a Regenerative Electromagnetic Brake," *IEEE Transactions on Intelligent Transportation Systems,* vol. 50, no. 11, Paper ID : 8103204, 2014.

[8] J. N. Bae, Y.E. Kim, and C.S. Jin, "Design and Analysis of a Regenerative Electromagnetic Brake," *IEEE Transactions on Intelligent Transportation Systems,* vol. 50, no. 11, Paper ID : 8103204, 2014.

[9] A.M.C. Odhams,R. L. Roebuck,Y. J. Lee, S. W. Hunt, and D. Cebon, "Factors influencing the energy consumption of road freight transport," *IEEE Transactions on Intelligent Transportation Systems,* vol. 224, no.9, pp. 1995-2010, 2009.

[10] J. N. Bae, Y.E. Kim, and C.S. Jin, "Potential for Regenerative Braking Systems as Applied to Automobiles," *Journal of Vibration and Acoustics,* vol. 105, no.3, pp. 300-304, 1981.

[11] D, Adhikary, M, Z, Rahman, M. M. Nahin, and M. S. Abdullah, "Design and Implementation of Regenerative Braking System," *Proceedings of ASME 2013 Conference on Smart Materials, Adaptive Structures and Intelligent Systems,* Snowbird, Utah, USA, September 1618, 2013,

[12] Y, Yang, J, Zou, Y. Yang, and D, Qin, "Design and Simulation of Pressure Coordinated Control System for Hybrid Vehicle Regenerative Braking System," *Journal of Dynamic Systems, Measurement, and Control,* vol. 136, Paper ID : 051019, 8 pages, 2014.

[13] W. J. Midgley, and D. Cebon, "Comparison of regenerative braking technologies for heavy goods vehicles in urban environments," *Journal of Automobile Engineering,* vol. 226, no. 7, pp. 957-970, 2011.

[14] W. Midgley, H. Cathcart, and D. Cebon, "Modelling of hydraulic regenerative braking systems for heavy vehicles," *Journal of Automobile Engineering,* vol. 227, no. 7, pp. 1072-1084, 2012.

[15] X. Huang, and J. Wang, "Model predictive regenerative braking control for lightweight electric vehicles with in-wheel motors," *Journal of Automobile Engineering,* vol. 229, no. 6, pp. 1220-1232, 2012.

[16] www.bmw.com

[17] www.mazda.ca

[18] www.toyota.ca

[19] L. Segel, and L.X. Pei, "Vehicular Resistance to Motion as Influenced by Road roughness and Highway Alignment," *Australian Road Research,* vol. 12, no 4, pp. 211-222, 1982.

[20] D. Karnopp, "Permanent Magnet Linear Motors Used as Variable Mechanical Dampers for Vehicle Suspensions," *Vehicle System Dynamics,* 18, pp. 187200.

[21] P. Hsu, "Power Recovery Property of Electrical Active Suspension Systems," *Proceedings of the 31st Intersociety Energy Conversion Engineering Conference,* pp. 18991904, Washington, DC, 1996.

[22] A. Abouelnour, and N. Hammad, "Electric Utilization of Vehicle Damper Dissipated Energy," *Al-Azhar Engineering Seventh International Conference,* Cairo, Egypt, 2003.

[23] A. Abouelnour, and N. Hammad, "A Preliminary Study of Energy Recovery in Vehicles by Using Regenerative Magnetic Shock Absorbers," *SAE Technical Paper Series,* Paper No. 2001-01-2071.

[24] Y. Kawamoto, Y. Suda, H. Inoue, and T. Kondo, "Modeling of electromagnetic damper for automobile suspension," *Journal of System Design and Dynamics,* vol. 1, no. 3, pp. 524-35, 2007.

[25] Y. Zhang, K. Huang, F. Yu, Y. Gu, and D. Li, "Experimental verification of energy-regenerative feasibility for an automotive electrical suspension system," *IEEE International Conference on Vehicular Electronics and Safety,* pp. 1-5, 2007.

[26] Z. Li, L. Zuo, G. Luhrs, L. Lin, and Y. Qin, "Electromagnetic Energy-Harvesting Shock Absorbers: Design, Modeling, and Road Tests," *IEEE Transactions on Vehicular Technology,* vol. 62, no. 3, pp. 1065-1074, 2013.

[27] L. Zuo, and P. Zhang, "Energy Harvesting, Ride Comfort, and Road Handling of Regenerative Vehicle Suspensions," *Journal of Vibration and Acoustics,* vol. 135, issue 1, Paper ID : 011002, 8 pages, 2013.

[28] R. B. GmbH, *Automotive Handbook,* 1996.

[29] Energy Density [Online].
Available: http://en.wikipedia.org/wiki/Engine-efficiency

[30] Energy Density [Online].
Available: http://en.wikipedia.org/wiki/Energy-density

[31] C. Squatriglia, "High-tech shocks tum bumps into power," 2009,
http://www.Levantpower.com.

[32] X. Tang, T. Lin, and L. Zuo "Design and Optimization of a Tubular Linear Electromagnetic Vibration Energy Harvester," *IEEE/ASME Transactions on Mechatronics,* vol. 19, no. 2, pp. 615 - 622, 2014.

[33] I. Martins, J. Esteves, G. D. Marques, and F. P. da Silva, "Permanent-magnets linear actuator applicability in automobile active suspensions," *IEEE Transactiosn on vehicular technology.,* vol. 55, no. 1, pp. 86-94, 2006.

[34] L. Zuo, B. Scully, J. Shestani and Y. Zhou, "Design and characterization of an electromagnetic energy harvester for vehicle suspensions," *Journal of smart materials and structures,* vol. 19, no. 2, pp. 1 - 10, 2010.

[35] B. L. J. Gysen, J. L. G. Janssen, J. J. H. Paulides. , and E. A. Lomonova, "Design Aspects of an Active Electromagnetic Suspension System for Automotive Applications," *IEEE Transactions on Industry Applications,* vol. 45, no. 5, pp.1589-1597, 2009.

[36] B. L. J. Gysen, T. P. J. van der Sande, J. J. H. Paulides. , and E. A. Lomonova, "Efficiency of a Regenerative Direct-Drive Electromagnetic Active Suspension," *IEEE Transactions on Vehicular Technology,* vol. 60, no. 4, pp.1384-1393, 2011.

[37] R. Sabzehgar and M. Moallem, "A boost-type power converter for energy regenerative damping," *IEEE/ASME Transactions on Mechatronics,* vol. 18, no. 2, pp. 725-732, 2013.

[38] A. Kim and Y. Okada, "Variable resistance type energy regenerative damper using pulse width modulated step-up chopper," *ASME Journal of Vibration and Acoustics,* vol. 124, pp. 110-115, 2002.

[39] A. Stribrsky, K. Hyniova, J. Honcu and A. Kruczeka, "Energy Recuperation in Automotive Active Suspension Systems with Linear Electric Motor," *ASME Journal of Vibration and Acoustics,* pp. 1-5, Athens, Greece, 2007.

[40] Y. Okada and H. Harada, "Regenerative Control of Active Vibration Damper and Suspension Systems," *35th Annual IEEE Decision and Control Conference,* Kobe, Japan, 1996.

[41] R. U. Patil, and S. S. Gawade "Design and Static Magnet Analysis of Electromagnet Regenerative Shock Absorber," *International Journal of Advanced Engineering Technology,* E-ISSN 0976-3945, 2012.

[42] Z. Longxin, and W. Xiaogang, "Structure and Performance Analysis of Regenerative Electromagnetic Shock Absorber," *Journal of Networks,* vol. 5, no. 12, pp. 1467-1474, 2010.

[43] N. V. Satpute, S. Singh, and S.M. Sawant, "Energy Harvesting Shock Absorber with Electromagnetic and Fluid Damping," *Journal of Networks,* vol. 5, no. 12, pp. 1467-1474, 2010.

[44] B. Ebrahimi, M. B. Khamesee, and F. Golnaraghi, "Permanent magnet configuration in design of an eddy current damper," *Microsystem Technologies,* vol. 16, no. 12, pp. 1924, 2010.

[45] L. Zuo, X. Chen, and S. Nayfeh, "Design and Analysis of a New Type of Electromagnetic Damper With Increased Energy Density," *ASME Journal of Vibration and Acoustics,* vol. 133, 041006, 2011.

[46] A. Tonoli and N. Amati, "Dynamic Modeling and Experimental Validation of Eddy Current Dampers and Couplers," *ASME Journal of Vibration and Acoustics,* vol. 130, 021011, 2008.

[47] Z. Hong and S. H. zhi, "Research of the orthoscopic permanent magnet eddy current damper in magnetic stage," *International Conference on Computer Application and System Modeling (ICCASM) ,* pp. 354-356, China, 2010.

[48] N. D. Ngoc, D. Zhaoxiang, and C. Youqiang, "Direct current linear actuator using in the active suspension system of automobile," *International Conference on Electric Information and Control Engineering ,* pp. 58555860, Wuhan, China, 2011.

[49] M. F. Ismail and Y. M. Sami, "A Control Performance of Linear Model and the MacPherson Model for Active Suspension System Using Composite Nonlinear Feedback," *International Conference on Control System, Computing and Engineering,* pp. 227233, Penang, Malaysia, 2012.

[50] M. F. Ismail and Y. M. Sami, "Design and experimental validation of a linear robust controller for an active suspension of a quarter car," *Proceeding of the 2004 American Control Conference,* pp. 14811486, Boston, Massachusetts, USA, 2004.

[51] S. Lee, and W.j. Kim, 'Active Suspension ControlWith Direct-Drive Tubular Linear Brushless Permanent-Magnet Motor," *IEEE Transactions on Control Systems Technology,* vol. 18, no. 4, pp. 859870, 2010.

[52] J. Wang, W. Wang, and K. Atallah, 'A Linear Permanent-Magnet Motor for Active Vehicle Suspensionr," *IEEE Transactions on Vehicular Technology,* vol. 60, no. 1, pp. 5563, 2011.

[53] J. Wang and W. Wang, "A Control Performance of Linear Model and the MacPherson Model for Active Suspension System Using Composite Nonlinear Feedback," *International Conference on Electrical Machines and Systems,* pp. 17,Beijing, China, 2011.

[54] J. Wang, W. Wang, K. Atallah and D. Howe "Comparative Studies of Linear Permanent Magnet Motor Topologies for Active Vehicle Suspension," *IEEE Vehicle Power and Propulsion Conference,* Harbin, China, 2008.

[55] J. Prudell, M. Stoddard, E. Amon, T. K. A. Brekken, and A. von Jouanne, "A permanent-magnet tubular linear generator for ocean wave energy conversion," *IEEE Transactions on Industrial Applications,* vol. 46, no. 6, pp. 23922400, 2010.

[56] CENTROID Servo Motor Dimensions. (2013, Jun.). [Online]. Available: www.centroidcnc.com/servo-dimensions.htm

[57] C. Squatriglia, "High-tech shocks tum bumps into power," 2009, *http://www.Levantpower.com.*

[58] X. Lin and G. Xuexun, "Hydraulic transmission electromagnetic energy-regenerative active suspension and its working principle," *Int. Workshop on Intelligent Systems and Applications,* pp. 1-5, 2010.

[59] Z. Fang, X. Guo, L. Xu, and H. Zhang, "Experimental Study of Damping and Energy Regeneration Characteristics of a Hydraulic Electromagnetic Shock Absorber," *Advances in Mechanical Engineering ,* vol. 2013, Article ID 943528, 9 pages.

[60] X. Lin, Y. Bo, G. Xuexun, and Y. Jun, "Simulation and Performance Evaluation of Hydraulic Transmission Electromagnetic Energy-regenerative Active Suspension," *Second WRI Global Congress on Intelligent Systems,* pp. 5861, Washington, DC, USA, 2010.

[61] X. Guo and L. Xu, "Structure Designs and Evaluation of Performance Simulation of Hydraulic Transmission Electromagnetic Energy-Regenerative Active Suspension," *SAE Technical paper,* 2011-01-0760, 2011.

[62] Avadhany S, Abel P, Tarasov V and Anderson Z, " Regenerative shock absorber," *US Patent Specification 0260935,*

[63] L. Hao, and C. Namuduri, "Electromechanical Regenerative Actuator With Fault-Tolerance Capability for Automotive Chassis Applications," *IEEE Transactions on industry applications,* vol. 49, no. 1, pp. 84-91, 2013.

[64] Y. Zhang, K. Huang, F. Yu, Y. Gu, and D. Li, "Experimental verification of energy-regenerative feasibility for an automotive electrical suspension system," *IEEE International Conference on Vehicular Electronics and Safety,* pp. 1-5, 2007.

[65] Y. Kawamoto, Y. Suda, H. Inoue, and T. Kondo, "Modeling of electromagnetic damper for automobile suspension," *Journal of System Design and Dynamics,* vol. 1, no. 3, pp. 524-35, 2007.

[66] K. Singal and R. Rajamani, "Simulation Study of a Novel Self-Powered Active Suspension System for Automobiles," *American Control Conference,* pp. 33323337, San Francisco, CA, USA, 2011.

[67] S. Liu, H. Wei, and W. Wang, "Investigation on some key issues of regenerative damper with rotary motor for automobile suspension," *International Conference on Electronic and Mechanical Engineering and Information Technology,* pp. 14351439, Harbin, Heilongjiang, China, 2011.

[68] N. Amati, A. Canova, F. Cavalli, S. Carabelli, A. Festini, A. Tonoli and G. Caviasso, " Electromagnetic shock absorbers for automotive suspensions: electromechanical design," *8th Biennial ASME Conf. on Engineering Systems Design and Analysis,* pp. 131140, Torino, Italy, 2006.

[69] Song X and Li Z, " Regenerative damping method and apparatus ," *US Patent Specification 6920951,*

[70] Song X, Li Z and Edmonson J, " Regenerative passive and semi-active suspension ," *US Patent Specification 7087342,*

[71] P. C. Lemor, "The roller screw, an efficient and reliable mechanical component of electromechanical actuators," *Energy Conversion Engineering Conference,* pp. 215220, Washington, DC, USA, 1996.

[72] M. H. Jones, and S. A. Velinsky, "Kinematics and Efficiency Analysis of the Planetary Roller Screw Mechanism," *ASME Journal of Mechanical Design,* vol. 131, issue 6, Paper ID : 011016, 8 pages, 2009.

[73] Z. Li, L. Zuo, G. Luhrs, L. Lin, and Y. Qin, "Electromagnetic Energy-Harvesting Shock Absorbers: Design, Modeling, and Road Tests," *IEEE Transactions on Vehicular Technology,* vol. 62, no. 3, pp. 1065-1074, 2013.

[74] S.B. Choi, M.S. Seong, and K.S. Kim, "Vibration control of an electrorheological fluid-based suspension system with an energy regenerative mechanism," *Journal of Automobile Engineering,* vol. 223, no. D, pp. 459-69, 2009.

[75] Z. Li, L. Zuo, J. Kuang, and G. Luhrs, "Energy-harvesting shock absorber with a mechanical motion rectifier," *Journal of Smart Materials and Structures,* vol. 22, no. 2, 025008, 2013.

[76] Z. Li, Z. Brindak, and L. Zuo, "Modeling of an electromagnetic vibration energy harvester with motion magnification," *in Proc. ASME Int. Mech. Eng. Congr.,* Denver, CO, 2011, pp. 285293.

[77] Zhang, P. S., "Design of Electromagnetic Shock Absorber for Energy Harvesting from Vehicle Suspensions," *MS thesis, Advisor L. Zuo, Stony Brook University, Stony Brook, NY.*

[78] E. Lefeuvre, D. Audigier, C. Richard, and D. Guyomar, " Buck-Boost Converter for Sensorless Power Optimization of Piezoelectric Energy Harvester," *IEEE Transaction on Power Electronics,* Vol. 22, no. 5, pp. 2018-2025, 2007.

[79] X. Tang and L. Zuo, " Simultaneous Energy Harvesting and Vibration Control of Structures with Tuned Mass Dampers," *Journal of Intelligent Materials Systems and Structures,* in print 2012.

[80] R. Sabzehgar and M. Moallem, "A boost-type power converter for energy regenerative damping," *IEEE/ASME Transactions on Mechatronics,* vol. 18, no. 2, pp. 725-732, 2013.

[81] R. Sabzehgar, Amir Maravandi, and M. Moallem, "Energy Regenerative Suspension Using an Algebraic Screw Linkage Mechanism," *IEEE/ASME Transactions on Mechatronics,* vol. 19, no. 4, pp. 1251-1259, 2014

[82] http://www.maxonmotor.com/

[83] http://en.wikipedia.org/wiki/Brushless-electric-motor

[84] http://www.popularmechanics.com/home/reviews/news/whats-so-great-about-brushless-motor-power-tools

[85] http://blog.toolup.com/brushless-technology/

[86] M. Husty and A. Karger, "Self-motions of Griffis-Duffy type parallel m-Manipulators," *IEEE Int. Conf. on Robotics and Autom.,* vol. 1, pp. 7-12, San Francisco, CA, 2000.

[87] J.D. Robinson and M.J.D. Hayes, "The dynamics of a single algebraic screw pair," *Transactions of the Canadian Society for Mechanical Engineering,* vol. 35, no. 4, pp. 491-503, 2011.

[88] J.D. Robinson and M.J.D. Hayes, "Reachable Workspace Comparison of Revolute Pair Jointed and Algebraic Screw Pair Jointed Kinematic Chains," *Proceedings of The Canadian Society for Mechanical Engineering Forum 2010,* June 7-9, 2010, Victoria, British Columbia, Canada.

[89] J.D. Robinson and M.J.D. Hayes, "THE KINEMATICS OF A-PAIR JOINTED SERIAL LINKAGES," *Proceedings of the ASME 2010 International Design Engineering Technical Conferences and Computers and Information in Engineering Conference,* August 15-18, 2010, Montreal, Quebec, Canada.

[90] A. Karger and M. Husty, "Classification of all self-motions of the original Stewart-Gough platform," *Journal of Computer-Aided Design,* vol. 30, No. 3. pp. 205-215, 1999.

[91] D.J. Inman, *Engineering Vibration,* Prentice Hall, 2nd edition, NJ, USA, 2001.

[92] S. Rao, *Mechanical Vibrations,* Fifth edition, 2010.

[93] W. Thomson, *Theory of Vibration with Applications,* Fifth edition, 1997.

[94] L. Zuo, and P. Zhang, "Energy Harvesting, Ride Comfort, and Road Handling of Regenerative Vehicle Suspensions," *Journal of Vibration and Acoustics,* vol. 135, issue 1, Paper ID : 011002, 8 pages, 2013.

[95] D. Kowalski, M. D. Rao, J. Blough, S. Gruenberg, and D. Griffiths, " The Effects of Different Input Excitation on the Dynamic Characterization of an Automotive Shock Absorber," *SAE 2001 Noise and Vibration Conference and Exposition,* Grand Traverse, Michigan, United States, 12 pages, 2001.

Appendix A

Equation A.1 describes the separation of the algebraic screw plates, δ, as a function of the rotation angle between plates, θ.

$$\delta = \sqrt{l^2 - \frac{a^2}{12}(5 - 4cos\theta)}\cdot \tag{A.1}$$

Let us define the relative linear and rotary motions by $\tilde{\delta}$ and $\tilde{\theta}$, respectively, as follows

$$\delta - \delta_0 = \tilde{\delta} \tag{A.2}$$

$$\theta - \theta_0 = \tilde{\theta} \tag{A.3}$$

where δ_0 and θ_0 are the static equilibrium points of δ and θ, respectively.

To linearize (A.1) around θ_0, the first order of Taylor series of δ at θ_0 is utilized as follows

$$\delta = \delta_0 + \frac{d\delta}{d\theta}_{(\theta=\theta_0)}(\theta - \theta_0) \tag{A.4}$$

where

$$\delta_0 = \sqrt{l^2 - \frac{a^2}{12}(5 - 4cos\theta_0)} \tag{A.5}$$

$$\frac{d\delta}{d\theta}_{(\theta=\theta_0)} = -\frac{a^2 sin\theta_0}{6\sqrt{l^2 - \frac{a^2}{12}(5 - 4cos\theta_0)}} = -\frac{a^2 sin\theta_0}{6\delta_0}. \tag{A.6}$$

Substituting (A.6) into (A.4) and performing some algebraic manipulations results in

$$\delta = \delta_0 + \frac{a^2 sin\theta_0}{6\delta_0}\theta_0 - \frac{a^2 sin\theta_0}{6\delta_0}\theta. \tag{A.7}$$

Equation (A.7) is the linear approximation of (A.1) around θ_0. Taking a derivative from (A.7) results in

$$\dot{\delta} = -c\dot{\theta} \tag{A.8}$$

where c is the slope of the nonlinear relationship between $\dot{\delta}$ and $\dot{\theta}$ given by

$$c = \frac{a^2 sin\theta_0}{6\delta_0}. \tag{A.9}$$

Appendix B

Equation B.1 describes the separation of the two-leg mechanism plates, δ, as a function of the rotation angle between plates, θ.

$$\delta = \sqrt{l^2 - 2a^2(1 - cos\theta)} \tag{B.1}$$

Let us define the relative linear and rotary motions by $\tilde{\delta}$ and $\tilde{\theta}$, respectively, as follows

$$\delta - \delta_0 = \tilde{\delta} \tag{B.2}$$

$$\theta - \theta_0 = \tilde{\theta} \tag{B.3}$$

where δ_0 and θ_0 are the static equilibrium points of δ and θ, respectively.

To linearize (B.1) around θ_0, the first order of Taylor series of δ at θ_0 is utilized as follows

$$\delta = \delta_0 + \frac{d\delta}{d\theta}_{(\theta=\theta_0)}(\theta - \theta_0) \tag{B.4}$$

where

$$\delta_0 = \sqrt{l^2 - 2a^2(1 - cos\theta_0)} \tag{B.5}$$

$$\frac{d\delta}{d\theta}_{(\theta=\theta_0)} = -\frac{a^2 sin\theta_0}{\sqrt{l^2 - 2a^2(1 - cos\theta_0)}} = -\frac{a^2 sin\theta_0}{\delta_0}. \tag{B.6}$$

Substituting (B.6) into (B.4) and performing some algebraic manipulations results in

$$\delta = \delta_0 + \frac{a^2 sin\theta_0}{\delta_0}\theta_0 - \frac{a^2 sin\theta_0}{\delta_0}\theta. \tag{B.7}$$

Equation (B.7) is the linear approximation of (B.1) around θ_0. Taking a derivative from (B.7) results in

$$\dot{\delta} = -c\dot{\theta} \tag{B.8}$$

where c is the slope of the nonlinear relationship between $\dot{\delta}$ and $\dot{\theta}$ given by

$$c = \frac{a^2 sin\theta_0}{\delta_0}. \tag{B.9}$$